The layering of polar firn

Investigations of the climatic impact on polar firn structure using high resolution density measurements and 3D-X-ray-microfocus-computer-tomography

Maria Hörhold

Alfred-Wegener-Institut for Polar and Marine Research

Columbusstrasse

27568 Bremerhaven

Germany

Universität Bremen

Fachbereich Geowissenschaften (FB5)

Bibliotheksstrasse 1

28359 Bremen

Germany

Gutachter

Prof. Dr. H. Miller

Prof. Dr. K. Huhn

Prüfer

Prof. Dr. S. Kasemann

Prof. Dr. F. Wilhelms

Promotionskolloquium

3. November 2010

Erklärung

Hiermit versichere ich, dass:

- ich die beiliegende Arbeit ohne Hilfe Dritter
- und ohne Benutzung anderer als der angegebenen Quellen und Hilfsmittel angefertigt
- und die den benutzten Quellen wörtlich oder inhaltlich entnommenen Stellen als solche kenntlich gemacht habe.

Contents

1 Summary

The polar firn structure is investigated in terms of layering using high resolution density measurements of 19 firn cores and X-ray-microfocus-computer-tomography image analysis of 6 surface firn cores. The impact of local climate conditions such as annual mean temperature and accumulation rate on the generation, structure and evolution of the layering is studied. We find at all sites a high variability in density and microstructure due to the layered character of the firn. The standard deviation of the measured physical properties is used as a proxy to parameterize the layering and to compare the degree of layering at different sites. Main results are:

1. The different sites can be distinguished by the degree of layering, i.e. variability in density and microstructure. The variability in grain size increases with decreasing annual mean temperature, accumulation rate and maximum temperature gradient. Sites with lower accumulation rate and annual mean temperature show higher variability and thus a higher degree in layering in the upper firn column than sites with higher accumulation rate and annual mean temperature. This means, that a site from the high East Antarctic Plateau can be expected to show higher layering compared to sites from coastal regions of Antarctica.

2. The layers seem to be created randomly at the surface. In this study a seasonal variability with constant frequency in density could not be detected within the presented data. Possible reasons can be a high variation in accumulation rate, that can superpose a seasonality in deposition, or large horizontal discontinuity, which means, that a punctual firn core site would not capture all layers. However,

with the data investigated in this study it can be hypothesized, that surface firn stratigraphy does not show a seasonal layering.

3. The density variability is not continuously decreasing with depth, but shows a rather rapid drop in the upper 10-20 meter depth, which is followed by a second maximum in density variability. This leads to increased density variability at the depth interval of the firn-ice-transition.

4. The frequency and amplitude of the density variability is changing with depth. Even though there is no seasonal signature within the near-surface variability, in the depth interval of the second density variability maximum, the density fluctuations show a seasonal frequency at medium to high accumulation rate sites.

5. The density variability develops a correlation with the concentration of the calcium ion with depth. At the surface no correlation is evident. At the depth-interval of the second density variability maximum the calcium concentration and the density variability show a remarkably high correlation. Together with the shift in frequency of the density variability, this indicates an impact of (seasonal varying) impurities on the densification of the firn.

6. The summary of the results 2-5 indicates, that the seasonal stratigraphy in ice core records, which is assumed to be formed by a continuous deposition at the surface and yields the basis of paleo-climate studies, is not necessarily formed at the surface by depositional mechanisms, but by densification and snow metamorphism deeper down in the firn column, influenced by impurities.

7. The layering is displayed in the microstructure, but shows a very complex pattern as the result of the combined effect of initial layering, sintering and short-term changes in local climate conditions:

    a) The layering is created randomly at the surface, initiating a certain combination of density and microstructure. Within each depth interval the layering

shows a linear correlation in density and grain size, so that the grain size could be parameterized via density. The trend of this correlation however, differs for the different sites and changes with depth.

b) The firn layers all undergo the rather gradual process of sintering - the increase in density and grain size, which is determined by the accumulation rate and annual mean temperature of a site. A long term trend in density and grain size is observed, describing the densification and grain growth of the firn with depth.

c) Short-term changes in local climate conditions, such as variations in accumulation rate or temperature gradient at the surface superpose the initial layering and the gradual sintering, by changes in the metamorphism of the snow. Increased or decreased exposure to near surface temperature gradients or wind-ventilation causes more or less coarsening or more or less pronounced anisotropy within the structure. The coarsening leads to a short-term increase in pore size or air permeability with depth until a maximum at 2-4 meter depths. This is observed especially at the firn cores from low accumulation rate sites in Antarctica and at the firn core from the Greenland site. Accordingly, the most coarsened structures in terms of pore size can be expected at sites with low accumulation rate. These findings imply, that ventilation of the uppermost firn layers can be expected to be largest at low accumulation rate sites.

8. The combination of initial layering, sintering and coarsening at the surface induces an overall diverse evolution of microstructure variability. The relations between density, microstructure and air transport properties are influenced by each of these conditions very differently. Whereas the firn layer show a negative, linear trend in the density-grain-size relationship, the sintering shows a linear trend as well. But the sintering shows a trend with opposite sign, and the coarsening shows a non-linear pattern, which is changing with depth. This leads to a

complex pattern of density-microstructure relationship. Therefore a simple parameterization of microstructural characteristics, such as specific surface area and grain size, or air permeability, with density is not straight forward in polar firn.

9. Nevertheless the microstructure from these very different sites and very diverse metamorphic states shows some surprisingly well defined relationships: the specific surface area of the firn samples, which can be determined by several methods, can be described bijective from the measured chord length (average intersection of the ice phase with a line). This strengthens the assumption, that optical properties of snow and firn can be described by an effective radius of spheres, showing the same specific surface area as the measured sample. For any applications where the effective ice-air-interface of the firn is important, (air-exchange, chemical interactions, interactions with optical properties, microwaves), the easy-to-measure-specific surface area is sufficient to obtain the effective radius of the firn structure. This radius can easily be included into grain growth models or grain size modeling from remote sensing surface observations such as the Moderate resolution Imaging Spectroradiometer (MODIS).

   Furthermore, a structure model index is calculated, which describes the relation of curvature and surface of the firn. This index seems to be a well defined function of porosity for all investigated firn samples of this study. This indicates, that despite the diverse pattern in original layered microstructure created at the surface, sintering and coarsening, topological similar structures develop during the whole firn metamorphism process.

2 Zusammenfassung

Die Struktur des polaren Firns als poröses geschichtetes Medium wird mit den Methoden der Gamma Absorption an 19 Firnkernen und bildgebenden Verfahren der Röntgen-Computer-Tomography an 6 Firnkernen untersucht. Dabei wird insbesondere der Einfluss der lokalen klimatischen Randbedingungen, wie Akkumulationsrate oder mittlere Jahrestemperatur auf die Entstehung, Struktur und Entwicklung von Schichtung erkundet. Die Standardabweichung der gemessenen Dichte und Korngröße wird genutzt, um die Schichtung zu parameterisieren und die Intensität der Schichtung an verschiedenen Lokationen zu vergleichen. Hauptergebnisse dieser Studie sind:

1. Die verschiedenen Lokationen unterscheiden sich deutlich in der Schichtungs-Ausprägung. Die Korngrößenvariabilität nimmt mit abnehmender Akkumulationsrate und mittlerer Jahrestemperatur zu. Lokationen mit geringer Akkumulationsrate und Jahresmitteltemperatur zeigen eine stärkere Schichtung in Dichte und Korngröße als Lokationen mit höherer Akkumulationsrate und Jahresmitteltemperatur. Demnach kann man erwarten, dass Firnkerne vom Ost-Antarktischen Plateau eine stärkere Schichtung aufzeigen, als Firnkerne von den Küsten-nahen Gebieten.

2. Die Schichtung scheint ohne Systematik aus dem Zusammenspiel von Wind, Temperatur, Sonneneinstrahlung und Schneefall an der Oberfläche zu entstehen. In den Daten der hier vorliegenden Studie konnte keine saisonale Frequenz in der Dichtevariabilität detektiert werden. Mögliche Ursache dafür könnte eine starke Variabilität in der Akkumulationsrate sein, die das Frequenzsignal ver-

wischt. Weiterhin könnte die Tatsache, dass die Schichten eine große horizontale Variabilität aufweisen, dazu führen, dass nicht alle lokal deponierten Schichten mit einem Firnkern erfasst werden. Die hier vorliegenden Daten deuten aber darauf hin, dass im Oberflächen-Firn einfach keine Saisonalität vorhanden ist und die Schichten irregular deponiert werden.

3. Die Variabilität in der Dichte nimmt nicht einfach kontinuierlich mit der Tiefe ab. Alle hier untersuchten Firnkerne zeigen vielmehr einen schnellen Abfall in der Dichtevariabilität bis zu einer Tiefe von 10-20 Metern. Darunter nimmt die Variabilität wieder zu und zeigt somit auch in Tiefen-Intervallen des Firn-Eis-Übergangs deutlich erhöhte Amplituden.

4. Die Amplitude und Frequenz der Dichtevariabilität ändert sich mit der Tiefe. Obwohl an der Oberfläche kein saisonales Signal detektiert wurde, zeigen Kerne mit einer mittleren bis hohen Akkumulationsrate ein deutliches Signal in der Frequenz der jeweiligen Akkumulationsrate in dem Tiefen-Intervall des zweiten Maximums der Dichtevariabilität.

5. Die Dichtevariabilität entwickelt eine Korrelation mit der Konzentration des Calcium-Ions mit der Tiefe. An der Oberfläche gibt es keine detektierbare Korrelation. In der Tiefe des zweiten Variabilitäts-Maximums ist eine signifikante Korrelation zwischen der Dichte und der Calcium Konzentration zu finden. Zusammen mit dem Herausbilden der Frequenz der Akkumulationsrate einer jeweiligen Lokation deutet das darauf hin, dass die Verdichtung von Firn von Verunreinigungen, die an der Oberfläche saisonal eingetragen werden, beeinflusst wird.

6. Zusammenfassend sind die Ergebnisse 2 -5 ein Hinweis darauf, dass die Saisonalität in der Schichtung in Eis-Bohrkernen, nicht wie angenommen durch einen kontinuierlichen Ablagerung von Material an der Oberfläche generiert wird. Vielmehr lassen die Ergebnisse erkennen, dass die Saisonalität in der Schichtung durch die Verdichtung und Metamorphose unter Einfluss von Verunreinigungen erst mit

der Tiefe ausgebildet wird.

7. Die Schichtung findet sich auch in der Mikrostruktur wieder, zeigt aber ein komplexes Verhalten. Der Grund ist eine Überlagerung von ursprünglicher, an der Oberfläche generierter Schichtung, Sinterung und kurzzeitigen Änderungen in den lokalen klimatischen Randbedingungen:

   a) Die Schichtung wird zufällig an der Oberfläche generiert, wodurch eine bestimmte Kombination von Dichte und Mikrostruktur festgelegt wird. Innerhalb eines Tiefen-Intervalls zeigt die Variabilität der Schichtung eine lineare Korrelation zwischen Dichte und Korngröße, so dass die Korngröße über die Dichte parameterisiert werden kann. Der Trend dieser Korrelation unterscheidet sich für die verschiedenen Lokationen und ändert sich mit der Tiefe.

   b) Alle Firnschichten unterliegen dem graduellen Sintern - das Ansteigen der Dichte und der Korngröße mit der Tiefe, was durch lokale Akkumulationsrate und Temperatur vorgegeben wird. Demnach kann ein langfristiger Trend in Dichte und Korngröße beobachtet werden, der diese Verdichtung und das Kornwachstum mit der Tiefe beschreibt. Dieser Trend, zeigt ein positives Vorzeichen (zunehmende Dichte korrespondiert mit zunehmender Korngröße), wohingegen der Trend innerhalb einzelner Tiefen-Intervalle ein negatives Vorzeichen hat (hohe Dichte korrespondiert mit kleiner Korngröße und umgekehrt).

   c) Kurzfristige Änderungen der lokalen klimatischen Randbedingungen, wie zum Beispiel Variationen der Akkumulationsrate, können die Schichtung und das Sintern durch eine veränderte Metamorphose überprägen. Durch erhöhte oder erniedrigte Exposition der Schichten in oberflächennahen Temperatur-Gradienten (durch Änderungen der Akkumulationsrate), kann die Struktur verstärkte oder abgeschwächte Vergröberung erfahren oder eine mehr oder weniger stark ausgeprägte Anisotropie. Diese Veränderungen beeinflussen

immer mehrere Schichten gleichzeitig und verändern deren Struktur. Die Vergröberung führt zu einem kurzfristigem Anstieg der Porengröße und Permeabilität mit der Tiefe zu Maxima in bis zu 2-4 Metern Tiefe. Das wurde vor allem für die Lokation mit niedriger Akkumulationsrate in der Antarktis und an dem einen Kern aus Grönland beobachtet. Die gröbsten und somit vermutlich am höchsten permeablen Strukturen in den oberen Firnschichten sind in den Niedrig-Akkumulationsgebieten der Antarktis und in Grönland zu erwarten.

8. Die Kombination von anfänglicher Schichtung, Sinterung und verstärkter Metamorphose an der Oberfläche induziert eine vielfältige Entwicklung der Variabilität der Mikrostruktur. Die Schichtung zeigt einen linearen Trend in Dichte und Korngröße. Auch die Sinterung zeigt einen linearen Trend, mit umgekehrten Vorzeichen. Änderungen in der oberflächennahen Metamorphose und somit in dem Grad der Vergröberung sind nicht linear. Diese drei Prozesse führen zu einem komplexen Verhältnis zwischen Dichte und Mikrostruktur. Aus diesem Grund kann es im polaren Firn keine einfache, direkte Parametrisierung von mikro-strukturellen Parametern wie spezifische Oberfläche, Korngröße oder Permeabilität geben.

9. Die Mikrostruktur der Firnkerne zeigt trotz der sehr unterschiedlichen Randbedingungen einige überraschend eindeutige Beziehungen: Die spezifische Oberfläche, welche mit den unterschiedlichsten Methoden im Firn ermittelt werden kann, kann ein-eindeutig anhand der mit dem Röntgen-Computer-Tomographen gemessenen Chord-Länge beschrieben werden. Die Chord-Länge ist ein Maß für die mittlere Ausdehnung der Eis-oder Porenphase in einer Richtung innerhalb einer Probe. Dieses Ergebnis unterstützt die Annahme, dass optische Eigenschaften von Schnee und Firn mit einem effektiven Radius als Korngrößen-Parameter beschrieben werden können. Der effektive Radius entspricht dem Radius von gleichgroßen Kugeln in einer Matrix, die die selbe spezifische Oberfläche haben

wie die Firnprobe. Für alle Anwendungen, in denen die effektive Eis-Luft-Fläche im Firn eine Rolle spielt (Luftaustausch, chemische Interaktion von Atmosphäre und Schnee, optische Interaktionen, Mikrowellen), ist die recht einfach zu bestimmende spezifische Oberfläche ausreichend, um einen effektiven Radius als Korngrößen-Parameter zu bestimmen. Dieser Radius kann wiederum in Kornwachstums-Modellen oder Anwendungen zur Bestimmung der Korngröße aus der Fernerkundung verwendet werden.

Weiterhin konnte ein Größen-invarianter Struktur-Parameter (Struktur-Modell-Index SMI) berechnet werden, der die Beziehung zwischen Krümmung und Oberfläche der Struktur beschreibt. Alle hier untersuchten Firnproben zeigen eine fast eindeutige Beziehung von Porosität und dem Struktur Model Index. Obgleich der enormen Vielfalt der an der Oberfläche generierten Schichtung, der Sinterung und dem Vergröbern, werden durch die Firn-Metamorphose überall topologisch ähnliche Strukturen ausgebildet.

3 List of Publications submitted for the Thesis

- Publication 1

  The densification of layered polar firn

  M. W. Hörhold, S. Kipfstuhl, F. Wilhelms, J. Freitag, A. Frenzel

  Submitted to Journal of Geophysical Research, Earth Surface, accepted.

- Publication 2

  From random deposition to a firn core record - on the impact of impurities on the densification of polar firn -a first approach

  M. W. Hörhold, T. Laepple, J. Freitag, S. Kipfstuhl, M. Bigler, H. Fischer

  In preparation.

- Publication 3

  Grain size of layered polar firn - evolution, variability and a new grain growth model

  M. W. Hörhold, S. Linow, W. Dierking, J. Freitag

  In preparation.

- Publication 4

  M. W. Hörhold, M. R. Albert, J. Freitag (2009)

  The impact of accumulation rate on the anisotropy and air permeability of polar firn at a high accumulation site

  Journal of Glaciology, Vol.55, No. 192, pp.625-631.

- Publication 5

  Z. Courville, M. Hörhold, M. Hopkins, M. Albert

  Lattice Boltzmann modeling of the air permeability of polar firn

  Submitted to Journal of Geophysical Research, Earth Surface, accepted.

  Own contributions:

  - permeability measurements of the Hercules Dome samples;
  - micro-CT measurements of all samples;
  - 3D-image analysis with MAVI of all samples;
  - modeling permeability using microstructure parameter;
  - discussion of the modeling results

4 Introduction and Objectives

4.1 Topic

This study deals with the internal structure and layering of polar firn. Snow, accumulating on top of the polar ice sheets, gradually compacts and sinters under its own weight to form first firn and then ice. The polar firn composes the upper 60-120 meter of the polar ice caps and is porous and permeable to the air (Figure 4.2). The firn column shows an alternation of very different layers characterized by a large variety of physical properties. These stratigraphic sequences are created at the surface by discontinuous snow accumulation, wind, seasonal, diurnal or faster changes in weather conditions. This results in layers of different particle composition with different grain size, shape, density or air permeability, which can be visually distinguished (Figure 4.1, left hand side). The stratigraphy of the firn is kept during the compaction and sintering and visible even within the ice core record (Figure 4.1 right hand side). The stratigraphy of a site is supposed to reflect the local climate conditions of this site and it has been often used as a dating tool in firn and ice core analysis.

In firn studies the processes of sintering, densification, coarsening and metamorphism are often discussed with different meaning. In the following we use sintering as a description of a material process, where grain size and density increase (Kang 2005) with depth of the firn column and time, as a function of the overload pressure due to the layers permanently accumulated on top. Densification is used as the term for the overall increase in density with depth from surface densities of snow of approximately

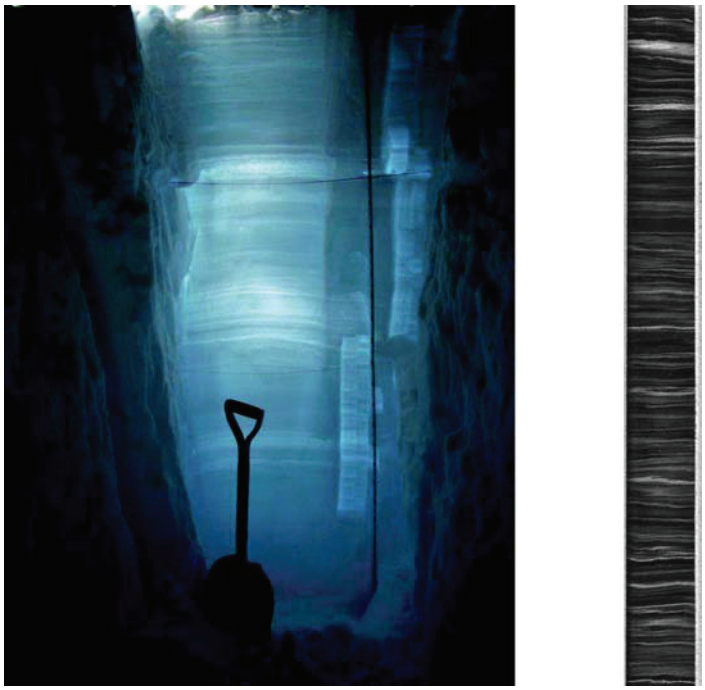

Figure 4.1: Left: Snow pit at Summit Station, Greenland. The three meter deep snow wall is illuminated by sun light through a second pit behind, so that the single snow layers are visible, picture by Z. Courville, June 2008. Right: Line-Scan of an ice core segment with transmitted light from 2700 m depth from the Greenland ice core NGRIP, unpublished data, picture by S. Kipfstuhl

300-500 kg/m^3 to the density of ice of 917 kg/m^3. The densification rate differs with accumulation rate and annual mean temperature at the different sites. Snow metamorphism is the umbrella term for the change of the snow structure after its deposition on the ground. The snow grains immediately change their structure and form bonds. A distinction is drawn between temperature gradient metamorphism, where enhanced mass flow along the temperature gradient distinctively changes the snow structure, and isothermal metamorphism, were the changes in the snow structure are driven by local water vapor gradients due to differences in curvature. Coarsening indicates a sintering process under temperature gradients with a simultaneous increase in grain size and pore size. The complete structure shifts from complex, small-scale structures to smooth, large-scale structures. This is observed to happen in the upper few meters of polar firn, due to temperature gradients altering the snow metamorphism.

4.2 Background

In many topics of polar research, the densification of the polar firn plays an important role. The densification is closely linked to the layering of the firn, since the layering induces a variability in density (Cuffey 2008). Research questions linked to density and layering are the convection of the surface firn and the air permeability, the densification of the firn at different sites and the entrapment of air bubbles into the ice as well as, regarding remote sensing techniques, the interaction of electromagnetic waves with the snow and firnpack.

The paleo-archive of polar ice sheets is unique as it directly records the atmospheric composition in the air bubbles of the ice (Blunier & Schwander 2000). But the firn forms a highly porous medium, where air convection and diffusion enable a distinct exchange with the atmosphere down to depths of several 10s of meter. This leads to an age difference between the air bubbles entrapped and the surrounding ice (delta age). In the uppermost part of the firn, the so called convection zone (Figure 4.2), the air is permanently exchanging with the atmosphere by convection and has therefore atmospheric

concentrations in aerosols (Figure 4.2). Below the convection zone, in the firn column with static air, gases mainly exchange by molecular diffusion and gravitational settling. Here the air experiences fractionation (Figure 4.2). Taking two gas components with a constant relationship in the atmosphere over time, any change in this relationship due to fractionation in the firn column can be used to calculate the height of the static-air firn column (Blunier & Schwander 2000) and thus estimate the close-off depth and the age of the enclosed air. The extend of the diffusive zone determines the main part of the age difference between ice and air bubbles. With fractionation models this age difference can be modeled, if the extend of the diffusive zone and the depth of close-off is known. The close-off depth is given as the sum of heights of the convection zone and the static-air firn column. An unknown extend of the convection zone induces an uncertainty in the close-off depth and therefore also in the calculation of the age difference of enclosed air and surrounding ice. Therefore measured data of the depth, until air ventilation of the snow and firn is possible, are very important for estimation of the delta age between ice and air bubbles in polar records.

The convection of the surface firn is possible due to the high air permeability of the snow structure. Air permeability of firn has been measured at several sites (Albert et al. 2000, 2004, Rick & Albert 2004, Courville et al. 2007) and an increase with depth, until a maximum at depths of 2-4 meter was found. Layering introduces a variability in the permeability profile, and single impermeable layers can decrease the air exchange of the whole underlying column, due to their specific microstructure. For example, wind- or sun crusts can reduce the air permeability in the firn column, as well as wind packed snow from storm events (Albert & Perron 2000). Thus the layering has a direct impact on the firn ventilation and the extension of the convection zone in the surface firn.

During the densification process the air of the pore space disintegrates into single air bubbles and encloses into the ice (Figure 4.2). The close-off depth is defined as the depth, where a critical density is reached (Landais et al. 2006) and the air gets enclosed (Figure 4.2), depending on the annual mean temperature of the site (Martinerie et al. 1992). Firn models systematically fail in predicting the close-off in glacial times,

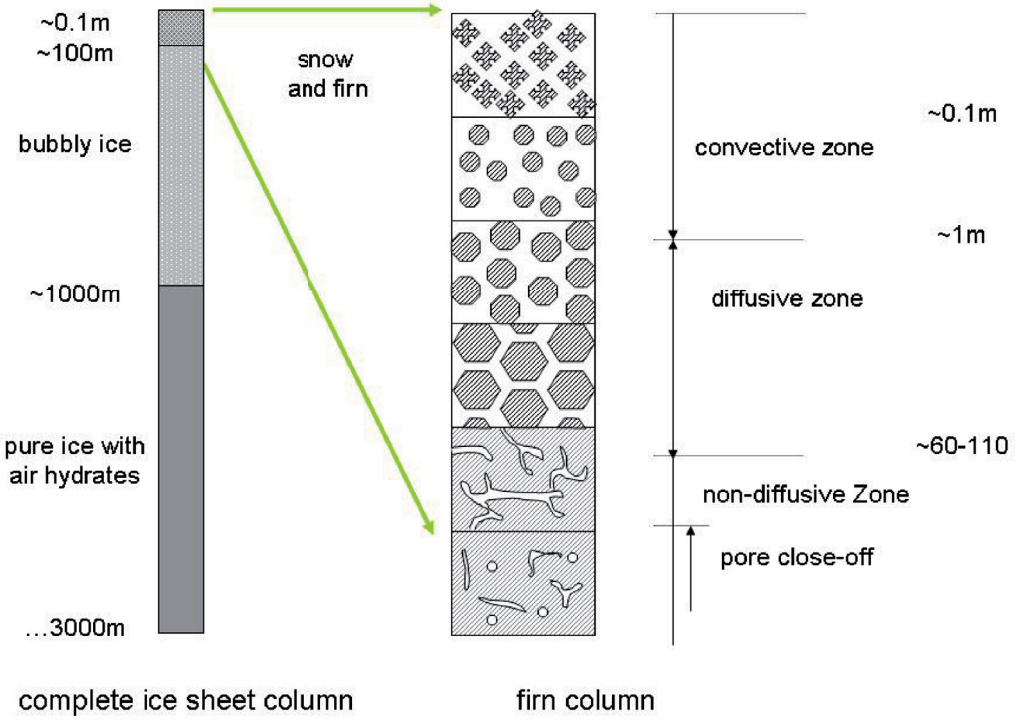

Figure 4.2: A scheme of a column from an ice sheet with the different depth intervals of snow (0.1m), firn, bubbly ice and pure ice (left hand side and a scheme of the upper approximately 100 meter of the ice sheet, representing the firn column. The different stages of air transport processes and enclosure are indicated.

because of the unknown extension of the convective zone and the poor estimation of the depth, where first high-density layers interrupt upwards exchange with the atmosphere - i.e. define the upper level of the so called lock-in zone, where the air enclosure is started. Early sealing of gases by horizontal impermeable layers (Severinghaus & Battle 2006), i.e. high density layers, can enhance fractionation, which alters the firn gas measurements. At sites with a very high variability in density the high-density layer close-off rather early, while other layers keep connected pores down to great

depths. Accordingly, a profound understanding of the layering and its evolution with depth down to the firn-ice-transition is crucial when understanding the process of air enclosure (Landais et al. 2006).

The densification of firn is usually described as a more or less continuous increase in density in dependence of the annual mean temperature and accumulation rate of a site (Herron & Langway 1980, Maeno & Ebinuma 1983, Arnaud et al. 2000, Goujon et al. 2003). Often mean density values are obtained from the field and the physical process of densification is connected to critical mean density and related microstructure changes. However, the layering of the firn induces a tremendous variability into the high resolution density profiles, and thus, defining a critical density and depth is actually not straight forward. Single layers reach these critical densities at different depths and the shift from one densification regime to another could be thought of a more or less gradual transition or even a layer-specific process.

The layering in density is not only important for the understanding of the density evolution with depth but also for the observation of the ice sheets with remote sensing techniques. The estimation of ice-sheet volume variations is one of the goals of satellite radar altimetry. The launch of the new satellite CryoSat2 in April 2010 has gained much attention, since its orbit is designed such, that it will scan the polar regions with a high time resolution, so that changes in ice sheet elevation can be detected seasonably (www.cryosat.de). However, a major obstacle to the correct interpretation of the data lies in the complex interaction with the reflecting snowpack (Legresy & Remy 1998, Cuffey 2008). The signal is reflected at the layer interfaces and scattered at the ice grains and matrix. Depending on the applied wavelengths the volume of interaction can be several centimeters down to several 10s of meters deep. Layering and grain size are supposed to play the most important roles in the backscatter behavior of electromagnetic waves (Rott et al. 1993, Surdyk & Fily 1993, Kärkäs et al. 2002). Analysis of the data obtained from remote sensing often contains the correction of the measured surface elevation by a density model of the upper firn column. The layering of the firn is included in these models, since the surface density seems to vary through the year

and seasonal variations in the density profile need to be considered, when calculating the elevation change.

For many applications the consideration of mean values, such as the one-meter mean density, might be sufficient. Nevertheless, the problems of air transport properties, air enclosure, densification and interpretation of remote sensing data cannot be solved without considering the stratigraphic layering of the firn. The ongoing improvement in measurement techniques and resolution enables a faster and more detailed observation of the polar firn structure (Marshall et al. 2007, Pielmeier & Schneebeli 2003). The integration of the variability into models is still a challenge. Parameterizing the variability in physical properties of the firn will improve the understanding and description of the firn structure and thus increase the scientific gain in both - the monitoring of the actual changes of the ice sheets as well as the interpretation of results from ice core records.

4.3 Main questions

Many detailed snow pit studies of layering are available from locally restricted areas. However, due to different methods applied and individual description and definition of layers or grain size, a comparative analysis is difficult to access. A systematic study is missing as well as a comparable objective measure of layering. Some of the main open questions are:

A What is layering? How to parameterize it?

B How is layering generated?

C How is layering evolving with depth and transferred to the firn-ice-transition?

D How is layering displayed in the microstructure and air permeability? Is there an explicit link between density and microstructure?

E Does variability differ for different sites? What is the impact of local climate on the

microstructure? Is there a regional variability, which is detectable with remote sensing, i.e. what creates the observed regions of similar backscatter behavior?

This study aims to start answering these questions and to give a contribution to the overall picture of polar firn structure and densification.

4.4 State of the art

In many snow pit studies the different layers are described by their visual appearance, which is mainly determined by grain size and density. Sequences of layers with a characteristic alternation of physical properties are often considered as annual deposition (Gow 1965, Palais J. M. 1982, Davis et al. 1996, Zwally & Jun 2002). High density layers are usually associated with winter deposition, whereas low density layers are often correlated to summer deposition (Gow 1965, Benson 1971, Alley 1988, Landais et al. 2006, Severinghaus & Battle 2006). The seasonal variability is linked to seasonally varying values in ion concentration or isotopic properties of the firn layers (Kreutz et al. 1999).

Alternating high and low density layers are created at the surface, reduce in amplitude with depth (Jun & Zwally 2002, Zwally & Jun 2002) and can still be distinguished at the depth of the firn ice transition. Higher-density winter layers become impermeable before lower-density summer layers (Martinerie et al. 1992, Landais et al. 2006, Severinghaus & Battle 2006). The layering is not only displayed in density but also in microstructure and air permeability. Quite often large grained firn layers are observed as low density and high permeability layers and vice versa. So with alternating density, these parameters also alternate in the firn column (Nakaya & Kuroiwa 1970). It is a common assumption, that these relationships, developed at the very surface of the ice sheet, are kept and transferred down to the firn-ice-transition. Any change in surface pattern due to accumulation rate changes, weather conditions or temperature will be directly transferred to the firn-ice-transition and stored in the ice, presuming they are

displayed in the layering of the firn.

Different local climate conditions will result in a different firn structure and layering. It is hypothesized that sites with high accumulation rate show a high variability in density, thus a more pronounced layering, since every single layer is buried rather fast under new snow accumulation. Moreover these sites are supposed to show no convection zone but a rather extended zone at the firn-ice-transition, were single layers are impermeable, while others are still open (Landais et al. 2006). Sites with low accumulation show no variability in density, because of vanished layering, a convective zone and heterogenous firn-ice-transition (Kawamura et al. 2006). The common idea is, that at low accumulation sites, the originally created stratigraphy will vanish. Due to the long exposure time at the surface, any difference in the layers will disappear and the firn shows a more or less homogenous structure. This in turn will result in less variability in density at the firn-ice-transition.

These different structures in layering and microstructure result in very different backscatter behavior of the firn column (Rott et al. 1993, Surdyk & Fily 1993). Satellite remote sensing can be used to study the firn structure on a much larger scale than ground based measurements would allow. Regions of similar backscatter were summarized to snow classes, which are supposed to show a similar structure (Rotschky et al. 2006, Tran et al. 2008). These snow class regions, display very well the known accumulation rate and temperature distributions as well as elevation and wind pattern. Accordingly, the firn structure is influenced by these local climate conditions differently at the various sites.

The summarized state of the art concerning the above stated questions (paragraph 4.3) is:

A Layering is displayed in the different physical properties of the firn, such as density and microstructure (Gow 1965, Benson 1971, Rundle 1971, Alley 1988), but published data are either restricted to a single site or lack objective and reproducible parameter for comparison. A comparative data base is missing and thus

a parameterization of the layering, with assimilable proxies, is still lacking.

B The layering is thought to be created at the surface due to seasonal varying snow deposition. At some sites winter deposition is reported to show high density and small grains, whereas summer deposition shows low density and large grains. At other sites this relation has been observed the other way around. All together the common assumption prevails, that a seasonal sequence of layers is created every year, which can be used to date the firn core (Martinerie et al. 1992, Jun & Zwally 2002, Li & Zwally 2004, Severinghaus & Battle 2006). However, reports of seasonality in snow pits from different sites are inconsistent and some studies on correlation of visible stratigraphy, seasonal varying ion chemistry, isotope measurements (Stenberg et al. 1999, Karlöf et al. 2006) question the image of a generalized annually resolved deposition history displayed in the stratigraphy of the firn.

C This structure of layering is kept during densification down to the firn-ice-transition. The amplitude of density variability is assumed to slowly decrease, until the density of ice is reached (Jun & Zwally 2002, Zwally & Jun 2002, Li & Zwally 2004, Landais et al. 2006). Nonetheless, first measurements with high resolution density data show a more complicated picture, either with increasing density variability (Gerland et al. 1999, Freitag et al. 2004) or with a change in correlation of density and backscatter behavior (Hawley & Morris 2006). Again a scarce data base is given to verify, whether these findings are the result of singular characteristics of the specific sites or if they indicate a more global behavior of firn densification.

D Layering is displayed in both - density and microstructure. At a single site grain size is linked to density. And as the density changes trough the seasons, the grain size does as well. This relation is kept and stored into the ice. Not many comparable data are available until now. From first measurements of grain size

and density of near surface samples and samples near the firn-ice-transition, a change in the relationship of grain size and density has been reported (Freitag et al. 2004, Fujita et al. 2009).

E High accumulation sites are expected to show high degrees of layering with large variability in density and low accumulation sites are expected to show low to zero degree in layering and only small variability in density or microstructure (Kawamura et al. 2006, Landais et al. 2006). However, no data are available to prove this, neither the variability of different sites at the surface nor at depths of the firn-ice-transition, where this difference in layering is supposed to influence the air enclosure, have been systematically investigated so far.

Not only the scarce data but also the contradictory observations as well as unexpected findings from sporadic high resolution data motivate this study. The aim is to generate a comparative data set, where the layering from surface down to the firn-ice-transition at different sites can be investigated.

5 Methods

5.1 Literature survey

Publications from the last 50 years were collected in order to summarize available observations of firn stratigraphy on the Antarctic ice sheet. The sites were collected in a data base and information about the occurrence of layering, hiatus or depth hoar were noted. Sometimes no layering was detected, sometimes seasonal sequences of layers were recorded. The results of this survey were plotted on a map, using ArcGis, in order to identify specific regions, probably in dependence on elevation, accumulation rate, wind field or annual mean temperature (Figure 6.8).

5.2 Firn cores

The studied firn cores cover a broad range in annual mean temperature and accumulation rate (Figure 5.1).

Firn cores from the Greenland ice sheet are all situated on the plateau, but differ distinctively in accumulation rate and temperature. The Antarctic firn cores originate not only from different sites of the plateau but also from coastal regions, such as B25 from Berkner Island or the PreIPICS cores B38, B39, DML95 and DML97 from near coastal Dronning Maud Land. With this collection of firn cores a very broad representation of firn structure and properties should be accessible. The two extreme sites are the B38 firn core with highest annual mean temperature of -18.1 °C and unusually high accumulation rate of 1.25 meter w.e. per year. The lower end in accumulation rate and annual

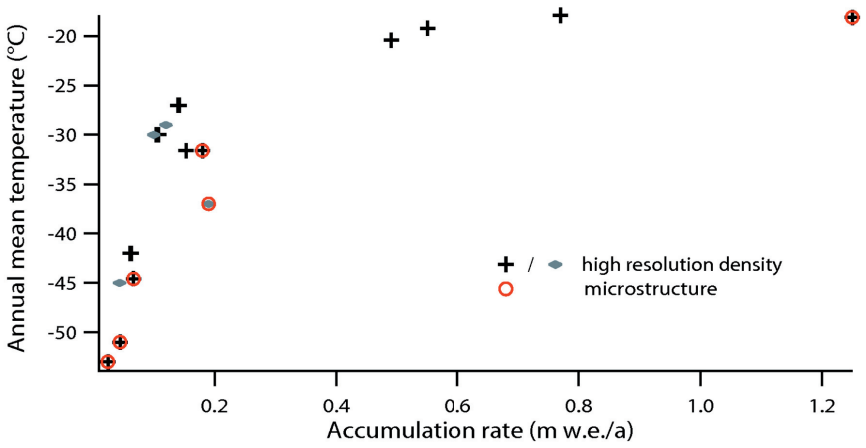

Figure 5.1: The annual mean temperature and accumulation rate of the studied firn core sites. Crosses mark positions, were temperature and accumulation rate was determined from measurements. Closed diamonds mark sites, were either the temperature or the accumulation rate was estimated from either nearby sites (DP7, B33) or from MODIS data (HD). At all firn cores high resolution density measurements were conducted, red circles mark firn core sites were additionally CT measurements were conducted.

mean temperature is represented by the Dome C area with -53 ℃ and 0.025 meter w.e. per year respectively. A detailed list of firn cores is shown in Table 1 of publication 1 and 2 for density measurements and Table 1 of publication 3 for CT-measurements, respectively.

5.3 High resolution gamma absorption method

High resolution density profiles, with a vertical resolution from 1 to 5 mm, were analyzed. Most firn core profiles of density raw data were available from previous measurement campaigns. To extend the range of local climate conditions, 8 firn cores were measured within this project. These are the EDC2 core and the FireTrack (FT) firn core from the Antarctic Dome C site, 4 firn cores from coastal Dronning Maud Land,

Antarctica (PreIPICS), the B36 firn core as the upwards extension of a previously measured firn core B37 near Kohnen Station in Dronning Maud Land, Antarctica, and the approximately 15 meter long firn core from site Depot700, provided by the Norwegian-American Troll-South-Pole traverse in 2007-2008.

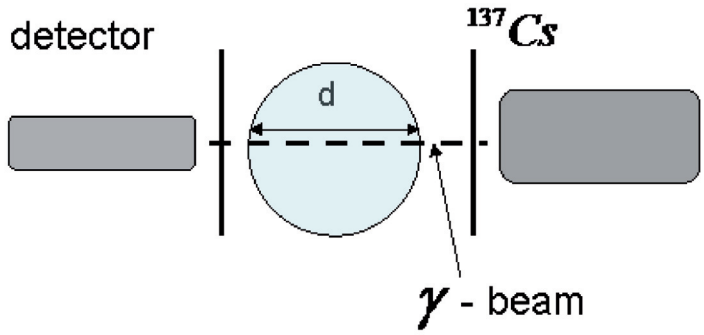

Figure 5.2: Measurement of high resolution density using gamma absorption method.

Density is measured by a non-destructive gamma-absorption method. The measured intensity of the attenuated gamma-beam trough the ice (Figure 5.2) is transferred into a density signal using Beer's law and the known mass absorption coefficient of ice, the intensity of the beam in air and the diameter of the firn core (Wilhelms 1996, 2000). The data are corrected for breaks and core catcher marks by linearly removing the outlier and interpolating over the gap.

5.3.1 Missing layers

The high resolution density measurement method enables a detailed study of the layered structure of the firn. However, in order to include all densities, occurring at a site, into the statistical analysis, all layers need to be captured in the measured firn core. But often firn cores break during the drilling procedure and also later, during the handling of the firn core pieces. Even more in many cases the upper 5-6 meter of firn core sites

are not sampled, due to the fragile texture of near surface firn. It is especially the low density layers, which consist of very loose snow and show a weak strength. During the processing of the density raw data, depth intervals, which show breaks or somehow disturbed data, are removed and interpolated. Therefore, low density layers might be underrepresented within the density analysis.

5.4 Permeability measurements

Permeability measurements were conducted using the device designed by the Cold Regions Research and Engineering Laboratory (Albert et al. 2000), based on Shimizu (1970). A flexible rubber membrane is inflated around the core sample to create an air-tight seal. Pressure and flow rates are measured through the sample. Ten measurements at incremental flow rates are conducted and it is ensured, that the pressure versus flow rate follows Darcy's law and is linear (Albert et al. 2000, Courville et al. 2007). Permeability was measured at two firn cores, the Hercules Dome firn core and the Depot 700 firn core, in cooperation with Dr. Zoe Courville, from the Cold Region Research and Engineering Laboratory, USA.

5.5 X-ray-microfocus-computer-tomography (CT)

The microstructure of firn samples was measured at -25℃ using a SkyScan 1074 X-ray-microfocus-computer-tomography-Scanner with a polychromatic X-ray beam with 40 kV and 1000 μA (Figure 5.3). The complete upper 1-2 m of each firn core, if available, were sampled. Otherwise approximately 40 cm were sampled every meter. From each depth interval firn core pieces are cut into 2.5 cm thick slices. From each slice a cylindric sample with a diameter of 2 cm is drilled with a bore hole saw. The sample is placed on a moveable turntable between X-ray-source and detector. During the scanning procedure the table rotates at intervals of 0.9°. A set of 400 shadow images is captured while the rotation completes a circle. With a digital convolution algorithm the

shadow images are transformed into a series of horizontal cross-section images which represent the 3-D structure of the firn sample, based on the locally different absorption of X-rays.

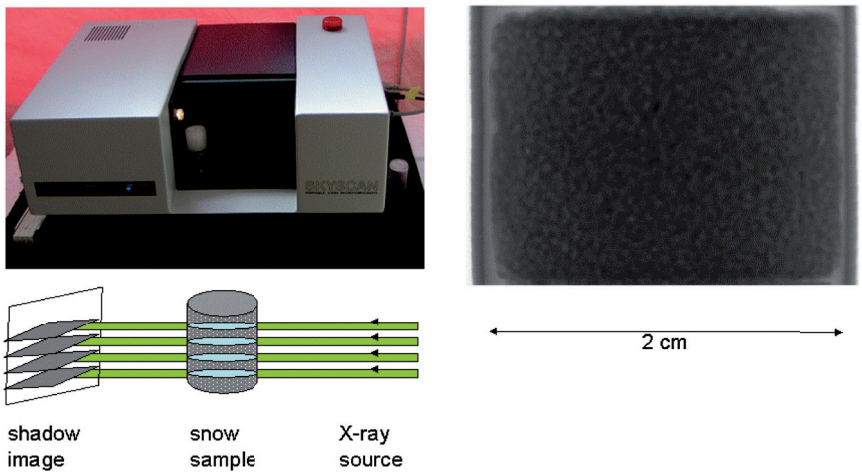

Figure 5.3: The Computer-Tomograph is operated in the cold room. Snow samples are placed on a table inside the tomograph. At every rotation step a shadow image is taken.

The resolution of the reconstructed images is 40 μm for the firn cores B26, B36, DP7, FT and HD and 15.7 μm for the firn core B38.

The X-ray-microfocus-computer-tomography-measurements deliver a coarser resolution than the density measurements. Values are averaged over a volume (vertical depth) of 1.6 cm side length. Further more discontinuous samples are taken, which restrict the amount of layers considered in each depth-interval.

5.6 Microstructural analysis using MAVI

The 3D analysis software MAVI was developed by the Fraunhofer Institute for the image analysis of 3D computer-tomography images. The grey value image stack is loaded into the software. For image analysis the samples are cropped to a cube of 1.6 x 1.6

x 1.6 cm side length (400 x 400 x 400 voxels). After applying a 3 x 3 x 3 median filter, the image is separated in voxels representing solid ice or air-filled voids. For this segmentation a global threshold value is determined from the bimodal grey-value histograms. Air and ice have a large difference in X-ray absorption and the mean grey levels of ice and air differ by as much as 100 units. Therefore a clear separation of the pore and ice phase is given, even though the global threshold offers a rather simple method of segmentation (Figure 5.4). On the resulting binarized 3-D image an object filter is applied, removing all voxels adding less than 1 % to the volume fraction of each phase.

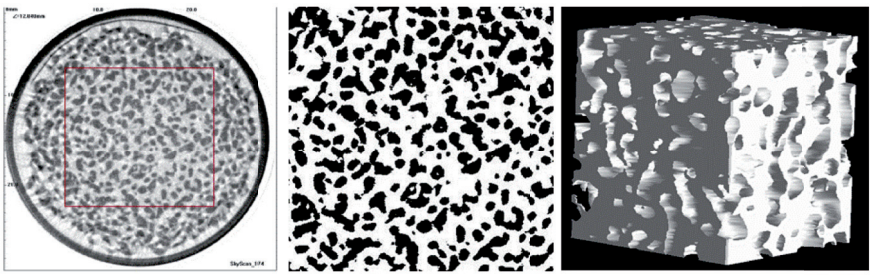

Figure 5.4: Image processing procedure: the cylindric sample is cropped to a cube (a) and binarized (b). The final image represents the complete 3D structure of the firn sample (c), 3-D image from Hercules Dome as an example, white: air space, voids: ice grains

More than 1400 binarized volume images were analyzed in the frame of this study for microstructural properties. Here the term microstructure is restricted to the following properties:

SSA The (optical) specific surface area is a measure of the size of the ice-air-interface in relation to the sample mass. It can also be obtained by other methods and therefore compared to observations in literature. Within this study it could be proved, that a bijective relationship between the size of the ice phase in terms of chord length and the surface area exists (Publication 3).

R_{eff} In order to assure a comparative measure of firn structure the optical specific surface area was calculated, which represents the ice-air interface accessible to gases per unit mass. From that the effective radius R_{eff} can be determined. It represents the radius of equal sized spheres with a similar specific surface area as the firn structure. With the firn samples from this study it is shown, that the representation of the firn structure by spheres is sufficient enough to describe the air-ice-interface accessible to gases or interaction with microwaves (Publication 3). This effective radius is taken as a measure of grain size, which can be obtained from several methods in the field and in the lab and thus can easily be compared to other measurements or used within grain size models (Publication 3). In the following the term grain size is always related to the effective radius.

l_{pore} The pore chord length l_{pore} (as well as grain chord length) is a measure of the average intersection lengths of a line with the air (or ice) phase. It can be determined for different directions. The chord length could be used as a grain size parameter, but in this study the grain chord length is explicitly not used as grain size parameter, but the above described effective radius.

anisotropy The anisotropy is calculated by the ratio of the fraction of surface normal vectors pointing into the horizontal direction and the fraction of surface normal vectors pointing into the vertical direction. If the ratio has values lower than one, more surface normal vectors point into the vertical section, i.e. the structure is horizontally elongated. A value of one indicates isotropic structures and values larger than one vertically elongated structures, i.e. vertical anisotropy (Publication 4).

SMI A size independent structure model index SMI has been developed in previous studies in order to compare structures, that are sufficiently similar like the ice phase from different depths in the firn column. It has been used in experiments with temperature gradient and equi-temperature metamorphism setups (Schneebeli & Sokratov 2004, Kaempfer & Schneebeli 2007). The index is determined by

the curvature of the ice phase and the surface area in relation to the volume of the firn. It enables a size independent comparison of structures and their curvatures (Ohser et al. 2009). Positive values indicate convex surfaces such as single ice grains. Values around 4 are obtained by spherical structures, values of 3 indicate cylindrical structures and values around zero represent flat surfaces (Ohser et al. 2009, Schneebeli & Sokratov 2004). Negative values indicate concave surfaces, the numbers equal in their meaning concerning the shape (i.e. -4, spherical enclosure, -3 cylindrical enclosure), but the sign of curvature is reversed.

6 Results and Discussion

6.1 Parameter of layering

The different layers of the firn column induce a variability in density. This is visualized by a light table image and the corresponding high resolution density profile (Figure 6.1). The light source is below the firn core piece. Layers with high density absorb more light and appear dark, layers with low density absorb less light and appear bright. The scattering of light is larger at layers with large grains and smaller at layers with fine-grained firn. The different appearance in brightness corresponds to different densities and grain sizes (Figure 6.1).

In order to parameterize this layering induced variability in the density profile, the mean density is subtracted from the measured density (Figure 6.2 a). From the residual signal the running mean of a sliding window of 1 meter length and the standard deviation of the mean (Figure 6.2 b) are calculated. This standard deviation is taken as the measure of variability in density due to the layering of the firn. In the following this standard deviation is used to study how the variability, and thus the layering, behaves with depth (Publication 1 and 2) and how it varies at different sites (Publication 1 and 3).

The layered induced variability is not only displayed in density but also in the microstructure. The CT measurements are conducted with a coarser resolution, nevertheless the variability is captured well (Figure 6.3 a and b, example from FT firn core). The density obtained from CT-measurements follows the fluctuation in density obtained with the gamma absorption method. This variability is displayed in the microstructure, such as is

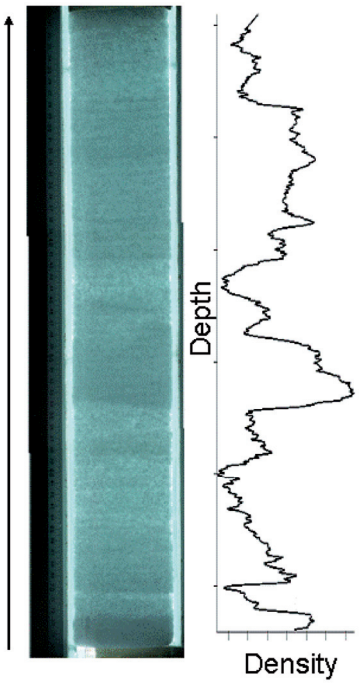

Figure 6.1: A 55 cm long firn core piece of the EDC firn core from 6.6 meter depth on a light table together with the high resolution density profile. Dark areas represent fine grained firn with high density values, bright areas coarse grained firn with low density values. The layering induces a variability in density.

the grain size, as well. In order to parameterize the variability in the microstructure, the mean and standard deviation of every depth interval was calculated (Figure 6.3 c). This means, that every set of samples from a one meter firn core piece (in most cases 16 samples) is considered as one depth interval. From this set the mean and the standard deviation are calculated (Figure 6.3 c). This standard deviation is taken as a parameter for the layering induced variability of the microstructure (Figure 6.3 d). It can be taken to compare the variability at different sites.

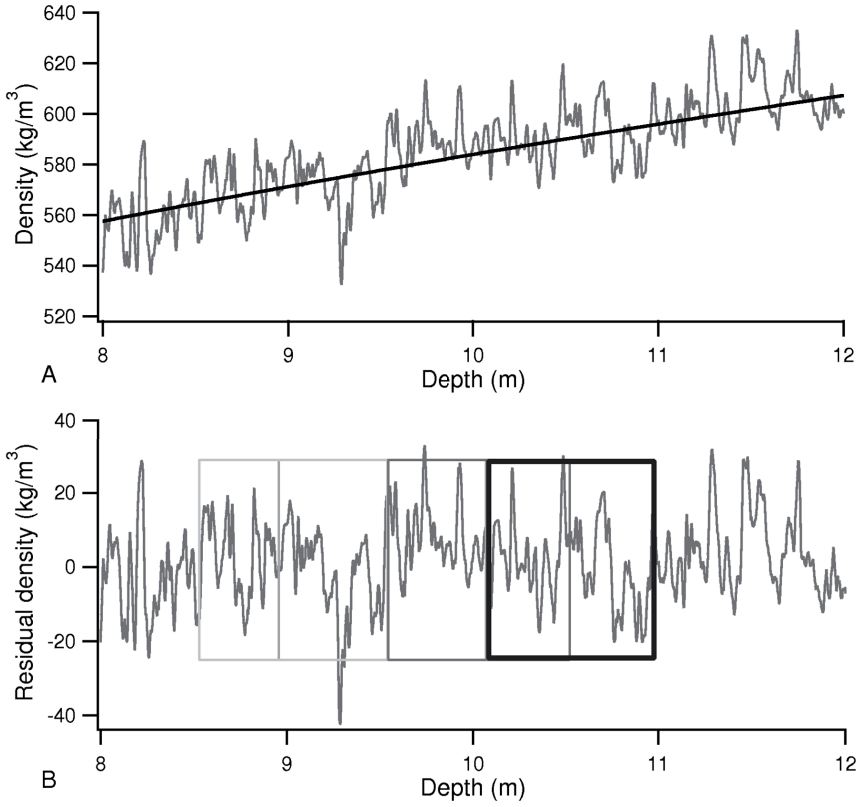

Figure 6.2: Detail from high resolution density profile (a) and the residual density after removing mean (b). The mean is subtracted from the measured profile. From the residual density the mean and the standard deviation are calculated with a sliding window.

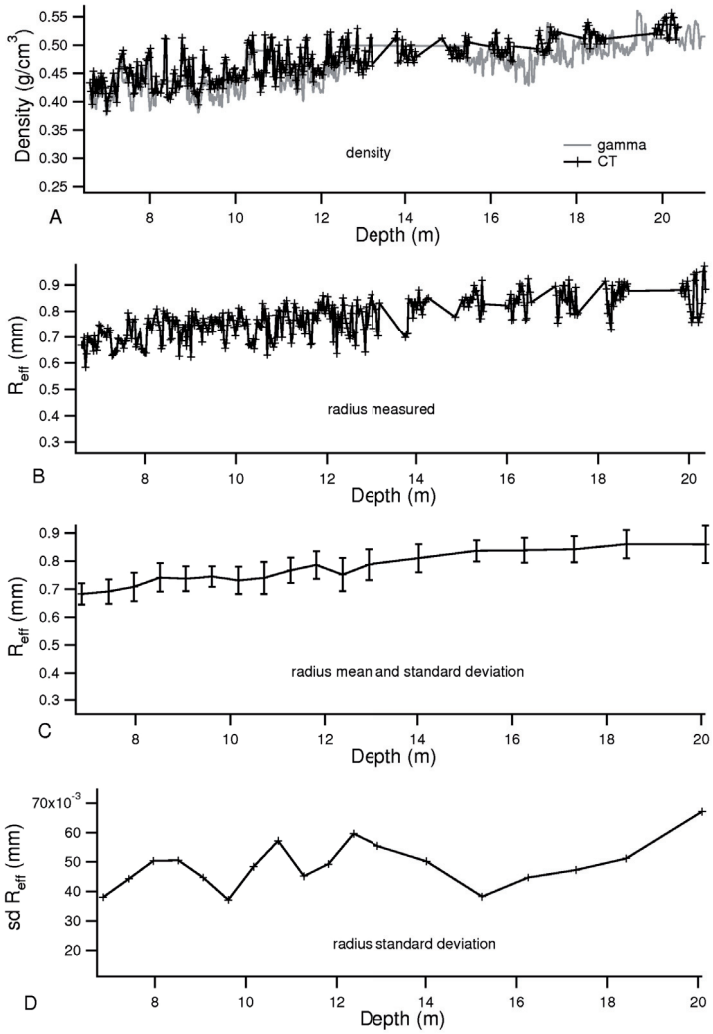

Figure 6.3: FT: High resolution density from gamma absorption method (a, grey line) together with the density values obtained by micro-CT (a, black crosse). The CT -measurements display the variability in density and microstructure due to the layering. Grain size shows large variability (b). The mean and the standard deviation sd of each depth interval is calculated (c) and can be used to compare variability at different sites (d).

The variability in microstructure within the different layers is visible in all parameters obtained by 3D analysis. Each layer shows a distinct combination of microstructural parameters, and each depth interval is characterized by different range in the microstruc-

ture properties. Especially grain size (here the effective radius) or specific surface area display the layering in their variability in the same manner as density. Sites showing a high density variability also show a high variability in grain size and vice versa. Parameters like pore chord length or anisotropy (Figure 6.4) display not only the variability due to layering but also the variability as the result of coarsening and densification.

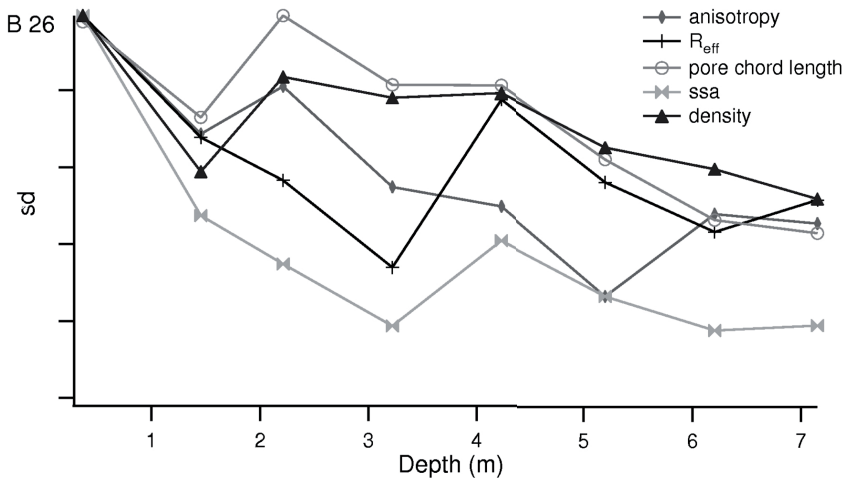

Figure 6.4: The standard deviation sd of density, effective radius, pore chord length, specific surface area ssa, density and anisotropy of the depth intervals at the B 26 site in Greenland obtained by CT-analysis.

Contribution Topic A: The different snow layers created at a site by single deposition events compose an inhomogeneous firn structure. The polar firn consists of single layers, each characterized by specific density and microstructure. As reported in literature density and grain size are the most clear and pronounced parameters, in which the layers differ significantly and which can be used to quantify the variability. This layering can be parameterized by the standard deviation of physical parameters of the firn layers, such as density or grain size (Publication 1 and 3).

6.2 Generation of layering

In order to test the common assumption, that the layering at the surface displays the alternating deposition of annual accumulation, the apparent frequencies in the density variability were investigated. For that the meter depth scale was transferred to meter water-equivalent depth. This removes the effect of thinning and enables a comparison of layers from different depth and sites. It also means, that if there is a seasonal frequency in the density variability, the frequency analysis should reveal a distinct peak in the frequency of the accumulation rate, because of the repetition of sequences of layers every year. For all 17 firn cores with high resolution density measurements reaching the depth-interval of the firn-ice-transition, this investigation in the frequency domain was conducted (Publication 2). In most cases we do not find a clear signature in accumulation rate frequency in the surface density variability, but a rather broad range in apparent frequencies. It seems, that with the high resolution density data a seasonal alternation of layers can not be detected. The layers seem to be created randomly at the surface.

Contribution Topic B: The common assumption in literature is, that the firn layers are the result of seasonally varying firn deposition and that density accordingly varies with a seasonal frequency. In this study, the analysis of high resolution density profiles did not reveal a seasonal frequency in layering in the surface firn. The layering of the firn seems to be created randomly at the surface (Publication 2).

6.3 Evolution of layering with depth

At all investigated sites the variability in density decreases with depth and then increases again (Publication 1). The minimum is obtained in a depth interval of 10 to 20 meter water equivalent (Figure 6.5). The following increase is smallest for the low accumulation sites such as EDC2 and B36/ B37 (Figure 6.5). The peak is highest for the

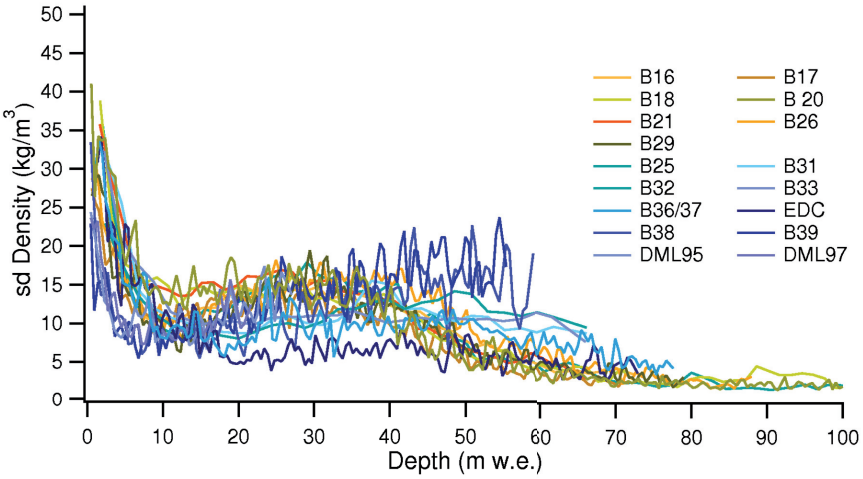

Figure 6.5: The standard deviation sd of density with meter water equivalent for the 17 firn core sites. Firn cores from Greenland are shown in yellow-brown colors, Antarctic sites in blue colors.

coastal sites B38 and B39. The depth of the maximum second peak and the decrease towards the density of ice differs for the different sites (Publication 1). Taking other observations into account, for example the finding of a flip in the density-backscatter-intensity relationship (Hawley & Morris 2006) or a flip in density-electrical conductivity relationship (Gerland et al. 1999) at a similar depth interval (Fujita et al. 2009), it occurs, that the original low density layers densify faster than the original high density layers. The former low density layers overcome the high density layers. This would explain the minimum in density variability (at the cross-over) and the following increase in variability. It furthermore would explain the flip in the above mentioned relationship. Because optical properties are linked to grain size, an originally large grained layer with low density has developed to a large grained layer with high density below the cross-over (Publication 1). However from comparison studies of high resolution density measurements to high resolution grain size measurements (unpublished data by Sepp Kipfstuhl) it seems, that this shift is not a continuous process, but that there are depth intervals, where the flip in grain-size and density can be observed, just next to depth-

intervals, where this is not the case. The increase in density variability seems to be the result of a more complex process in densification.

Looking at the evolution of the frequency of the density variability, a change in the intensities of the frequency domain with depth is detected. At the surface a broad signal is observed for most sites, at the depth of the variability minimum no distinct signal in the frequency domain can be detected. Below we find, that at mainly medium to high accumulation rate sites, the second peak in density variability shows the frequency of the accumulation rate (Publication 2).

The seasonality in density variability, which was not detectable at the surface, develops with depth. In this study Calcium concentration, as one ion species deposited within the snow and measured by continuous flow analysis, from 5 firn cores was investigated and linked to the density profile. A correlation analysis of density and Calcium concentration was conducted, which supports the above stated observation of a changing frequency in the density variability with depth. At the surface no correlation between Calcium concentration and density can be detected, but it increases to significant values and shows highest correlation in the depth interval of the second density variability maximum. The hypothesis is, that seasonally incorporated impurities into the snow layers at the surface, alter the densification of the single layers and thus reshape the layering of the firn down to depths of the firn-ice transition (Publication 2).

Contribution Topic C: In most publications and firn models using density variability a gradual decrease of variability with depth is assumed. The variability in density from the surface, such as high density winter layers and low density summer layers, is assumed to be kept during densification and still pronounced at depth of the firn-ice-transition. In this study it is found, that the layering induced variability is not linearly decreasing with depth, but rapidly decreases and then increases again (Publication 1). The variability further more changes the frequency and amplitude with depth. From a randomly created signal at the surface a variability with a seasonal frequency develops with depth

(Publication 2). It seems, that the layers are altered non-linearly by impurities or any other parameter, which are incorporated into the snow at the surface with a seasonal variability. Accordingly any composition of density and microstructure, created at the surface is changing non-linearly with depth, which would explain the change in the relationship of density and physical properties, as reported in literature.

6.4 Layering in microstructure and air permeability

Measured grain size profiles show a large layer-induced variability. In order to see the correlation to density, the trend of grain size in density was investigated (Figure 6.6). Within a single depth interval, the structural layering shows a linear negative correlation with density - the larger the grains the lower the density (grey lines in Figure 6.6). Such a linear trend in microstructure and density was found for all sites, even though the slope of the trend is increasing with increasing age (at a single site) and decreasing accumulation rate and temperature (comparing different sites). The warmest site B38 even shows a positive trend in grain size and microstructure as do the very surface samples at the B36 site. This indicates, that the relationship between density and grain size for fresh snow or firn from relatively warm sites, is a different one than the relationship of older, metamorphosed and colder firn. The overall trend of densification and sintering shows the opposite correlation (in sign) - an increase in grain size with increasing density (blue line in Figure 6.6). This relationship is sufficient to parameterize the long term behavior of average density and grain size at different local climate conditions, even though the relation within the single depth-intervals is very different.
Finally a third process can be observed, shaping the microstructure of the firn and superposing both - the initial layering and the sintering process. Short term changes in local weather conditions leave their imprint on the microstructure and superpose the long term trend of sintering. In the near-surface region down to 4-5 meter depth snow metamorphism and vertical mass transfer can be enhanced by temperature gradient effects. If the accumulation rate changes on a short-term time scale, certain layers spend

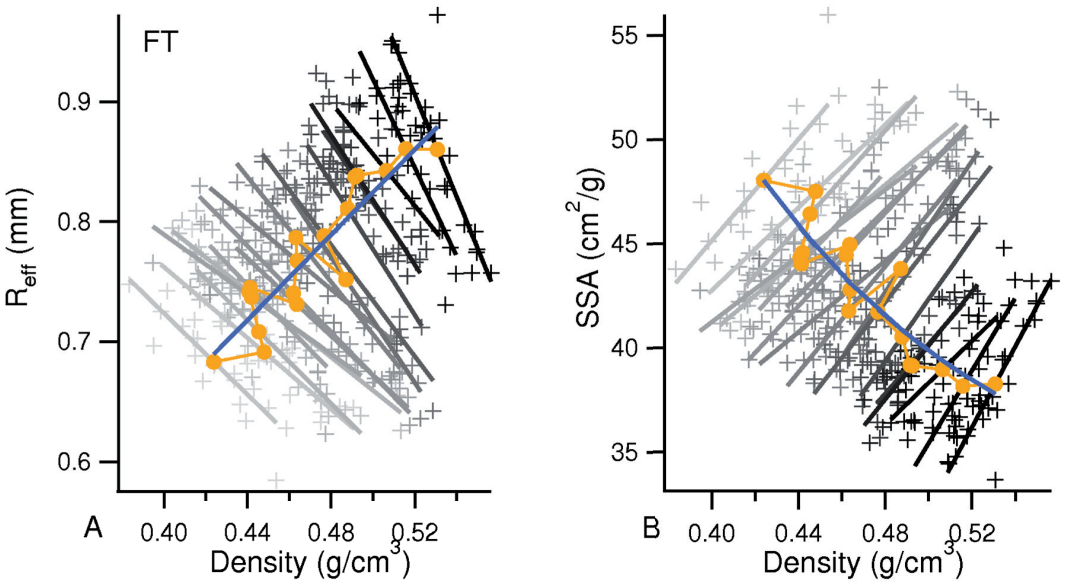

Figure 6.6: The grain size (a) and specific surface area (b) of the FT firn core with density. Grey lines indicate the single depth intervals, with increasing depth and age moving from light to dark grey. Orange points mark the mean value of each depth interval and the blue line the overall trend with increasing density.

longer time within this depth interval than others, experiencing enhanced temperature gradient metamorphism. This can be displayed in increased coarsening, anisotropy or air permeability, which is visible in both, low and high density layers (Publication 4). The coarsening is displayed in a temporary pore size increase with depth (Figure 6.7 a), which in turn favors increased permeability values (Figure 6.7 c and d). Larger pore channels and a coarse firn structure can provide an enhanced ventilation of the snow pack, even below a depth of some centimeters. Coarsening seems to occur down to a depth of 2-4 meter, until the weight of the overlying firn layers overcomes coarsening and densification takes over. The peak is displayed in a maximum in air permeability and in anisotropy in 2-4 meter depth.

To summarize, there are three different processes, determining the variability in mi-

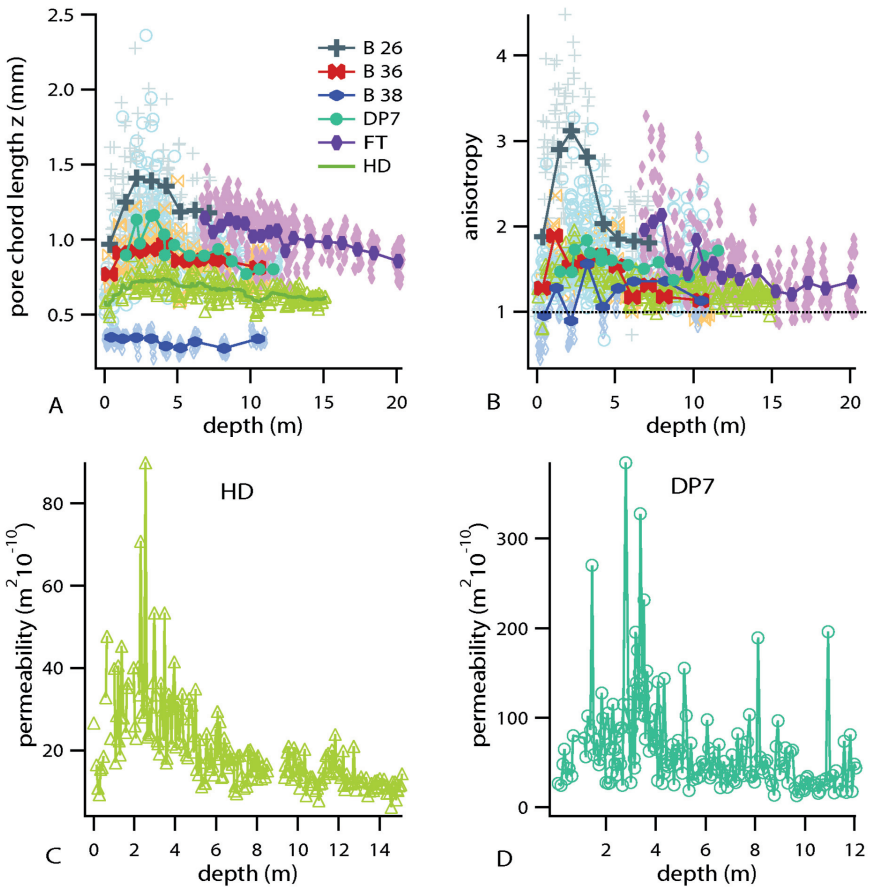

Figure 6.7: The evolution of pore chord length (a) and anisotropy (b) with depth at the different sites. The measured air permeability of the Hercules Dome site (c) and the Depot700 site (d, unpublished Data by Zoe Courville) with a maximum in 2.5 and 3 meter depth, respectively - note the different scale due to the large difference in permeability values.

crostructure and its relation to density variability: 1. The layering is randomly created at the surface, setting up a certain correlation in grain size and density. 2. The overall gradual sintering and densification increases grain size and density in equal rates. 3. Short term changes in exposure times (i.e. accumulation rate) of layer sequences lead to a coarsening of the structure, completely superposing the initial density-microstructure correlation and the linear increase with depth. A parametrization

of e.g. specific surface area in order to easily determine effective optical parameters from density measurements is not straight forward, because of the different impact of these three processes on the density-microstructure correlation in polar firn.

Contribution Topic D: In previous publications a systematic study of the link between density, density variability in terms of layering and microstructure has rarely been conducted. The common idea is, that correlations in density and microstructure are created at the surface and linearly transferred to ice. This would enable a parameterization of microstructure properties, such as grain size, from density, since a linear correlation is assumed. With the data obtained in this study, it appears, that microstructure displays variability in a manyfold way. First, the layering induces a correlation with density, so that grain size reflects the layering as it is expressed in density - low density corresponds to large grains and vice versa, except for the surface snow of B 36 and the firn core B 38. Second, the overall densification and grain growth result in a gradual increase in grain size with density, which can be parameterized and modeled for the different sites (Publication 3). And third, short term changes in accumulation rate can alter the time, certain layers are exposed to strong temperature gradients at the surface. This leads to increased coarsening of the structure and results in increased air permeability and anisotropy (Publication 4 and Publication 5). The effect is largest at the Greenland site B 26 and at the cold and low accumulation rate sites in Antarctica.

6.5 Layering at different sites

The literature survey did not yield a systematic picture of the occurrence of certain stratigraphic features in relation to local climate conditions. The individual description and different measurement methods are often very detailed and informative but do not always permit a comparative analysis (Figure 6.8). Even though some features might be detectable from the distribution of certain characteristics (Figure 6.8), an interpretation

is not possible: if the occurrence of for example signs for a hiatus in accumulation are not reported for a site, it does not mean, that there is no hiatus at this sites. It just indicates, that the authors did not notice, since the focus of the study and the observers was set to other topics.

The high resolution density measurements allow a comparison of the layering not only at the surface of the different sites, but also at the depth-interval of the firn-ice-transition. In this study the standard deviation is taken as a measure for the layering of a site and by that a comparison between different sites is possible in an objective and reproducible way. As proxy of the local climate conditions, the annual mean temperature, the accumulation rate, the maximum temperature gradients (end of summer) within 10 cm depth-intervals, as obtained from surface temperature observations, and the time, a layer spends within a 10 cm depth interval (determined from accumulation rate) are taken.

The surface density variability is decreasing with increasing annual mean temperature and accumulation rate (Publication 1), whereas the density variability at the firn-ice transition is increasing with increasing annual mean temperature and accumulation rate.

The diverse behavior of the standard deviation with depth indicates the different processes influencing the microstructure. Mainly the grain size is displaying the variability due to the layering similar than does the density. The surface trend in grain size variability is similar to the trend in density variability (Figure 6.9). Low accumulation (low temperature) sites show a higher variability in grain size, than high accumulation (temperature) sites (Figure 6.9). The increase in pores size (Figure 6.7 a) and pore size variability (Figure 6.10 a) with depth towards a maximum between 2 -4 meter depth, indicating the coarsening, can be observed at almost all firn core sites. Only the B38 core does not show any maximum in absolute values or an increase in variability. The pore chord length and anisotropy variability, as an example, are highest for the Greenland B26 site at the surface, followed by the cold Antarctic sites. However, to determine the layering and the resulting variability not all microstructure parameter seem to be useful. Grain size is suggested as a parameter, displaying the layering, as it is generated at the

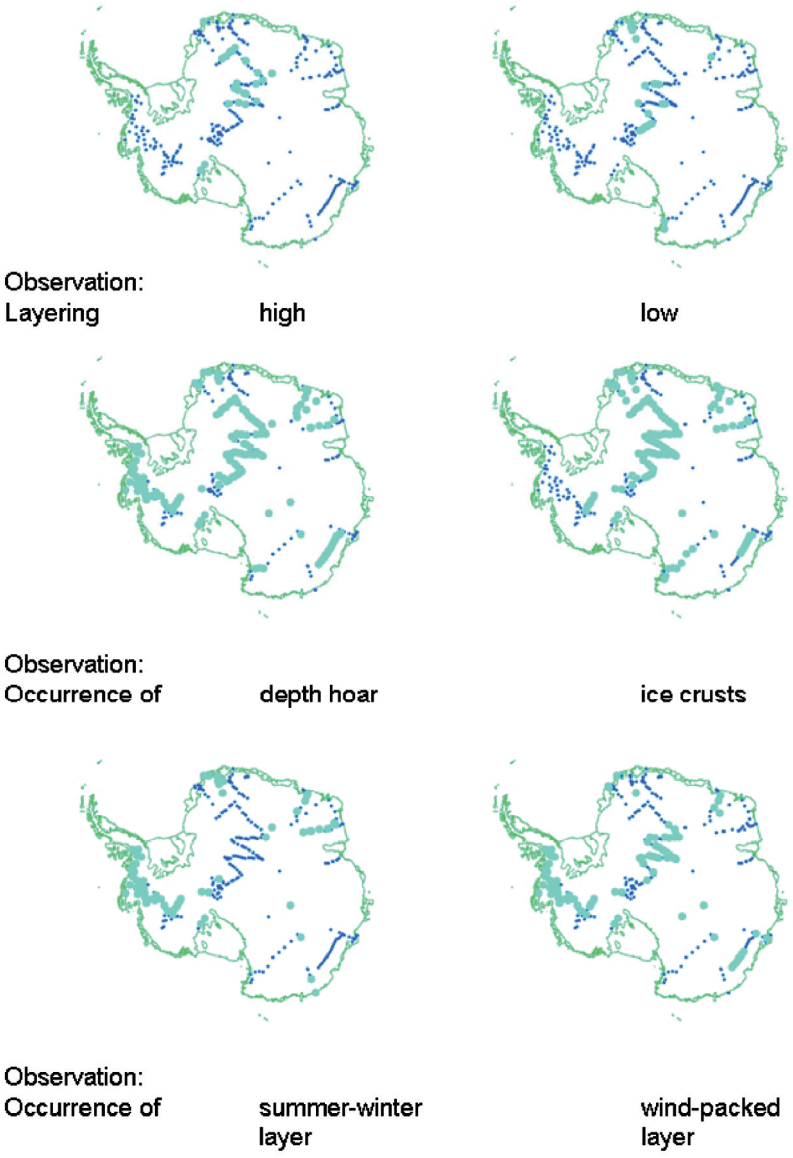

Figure 6.8: Example of the literature survey. Dark blue points represent sites described in literature in terms of stratigraphy, and sites, where the below stated observation was reported, are highlighted in light blue. Not that no regional differentiation is possible from these observations.

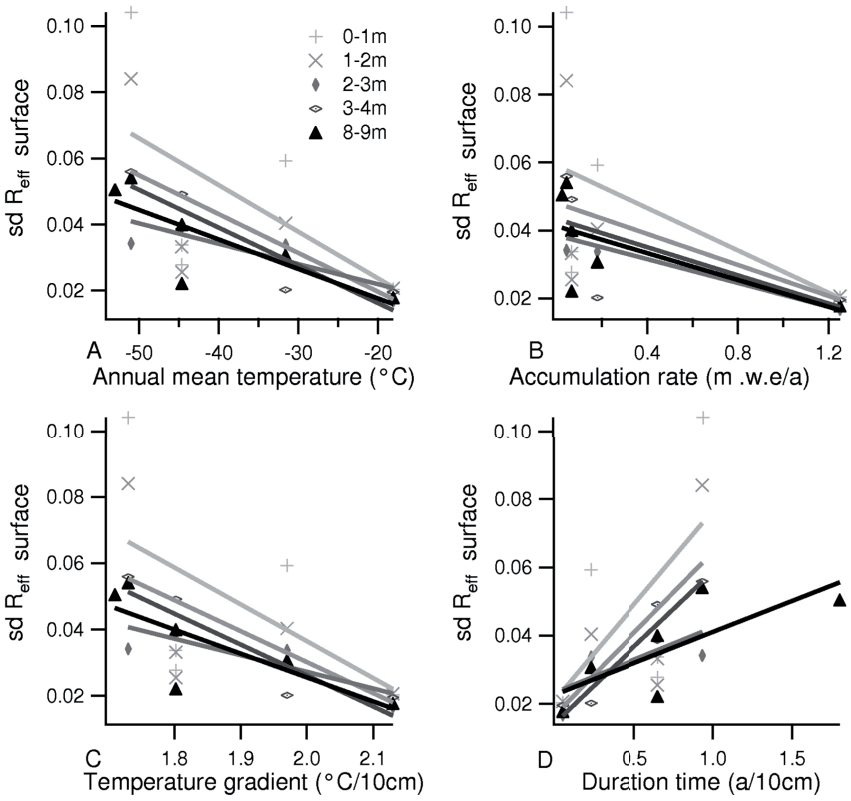

Figure 6.9: The standard deviation of R_{eff} of the upper depth-intervals with annual mean temperature (a), accumulation rate (b), temperature gradient at the surface in late summer (c) and duration time within 10 cm (d)

surface and which is correlated to density. Pore size, anisotropy and air permeability do not only vary because of the initial layering but change their variability as a result of coarsening and sintering.

The variability of the different microstructure properties can behave dynamically with depth at a single site. The degree in variability at the surface and the evolution with depth differ significantly for the different sites. This very different implementation and evolution of variability at the different sites can help to understand the observed difference in backscatter behavior of different firn types. Not only the degree in layering but also the variability in grain size within a certain depth-interval will alter the backscatter

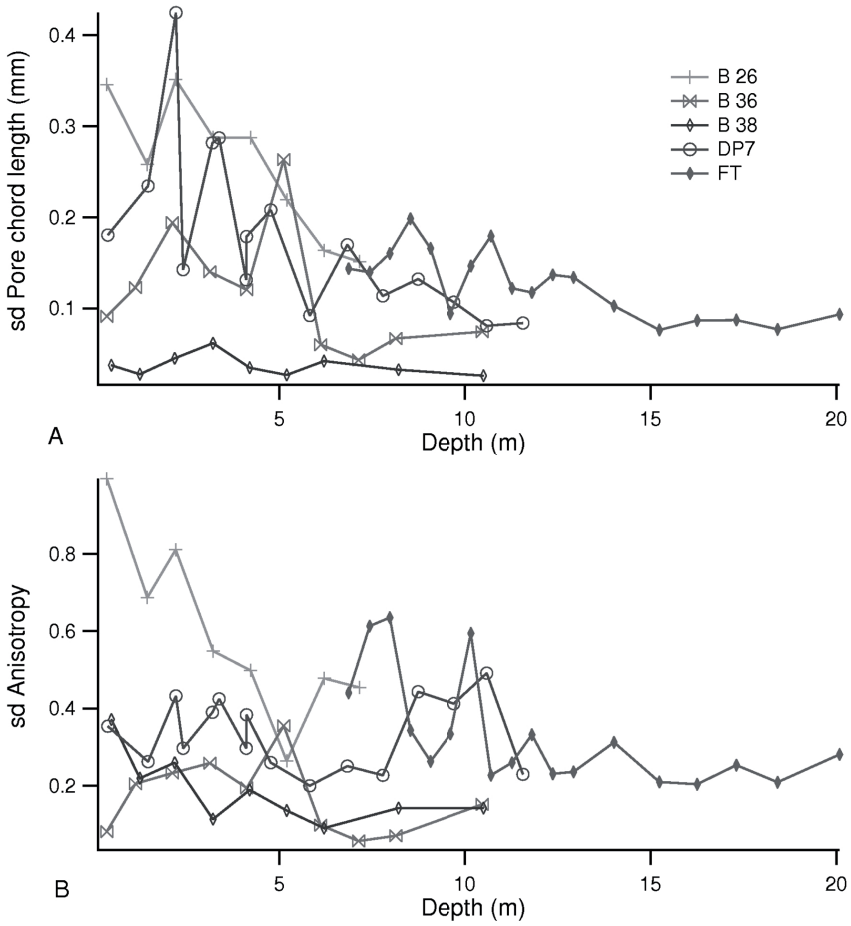

Figure 6.10: The standard deviation of pore chord length (a) and anisotropy (b) with depth for the different sites.

of microwaves. The quantification of variability obtained in this study can be used to identify the firn characteristics generating certain backscatter behavior in future investigations.

Contribution Topic E: The most common idea in literature is, that high accumulation rate sites show a higher degree in layering and thus a higher variability in density than low accumulation rate sites. The data presented here show, that the variability is higher at low accumulation and low temperature sites. This is well displayed in the microstruc-

ture variability (Publication 3) and density variability (Publication 1). High temperature and high accumulation sites show less variability in both density and microstructure. Grain size and density variability can be taken in the future to better understand the backscatter behavior of the firn in different regions of Antarctica.

7 Conclusions

With high resolution density data and microstructure information from X-ray-microfocus-computer-tomography the layering can be described and quantified by using the standard deviation as parameter. It is shown, that low accumulation and annual mean temperature sites are characterized by a larger degree of layering than high accumulation and annual mean temperature sites. But they also show an increased coarsening in the upper firn meters, inducing an increase in pore size and permeability down to 2-4 meter depths. Despite the increased layering and thus variability in density and microstructure, the air permeability can be larger and the convection zone more extended, than at sites with higher accumulation rate and less layering. Low accumulation sites show largest surface variability, whereas high accumulation sites show largest variability at the depth interval of the second density variability maximum and the firn-ice-transition. The results of this study point out, that the stratigraphy, i.e. the amplitude and the frequency of the density variability, is not a constant property of firn, which is continuously buried in the firn column with depth and time. The original surface density and its variability, the original surface grain size and its variability and incorporated impurities as well as the interaction of the frequencies of the density variability and impurity concentration variability configure the dynamic evolution of the layering of the firn with depth. The expression of layering in the microstructure properties is changing with depth and time. The initial microstructure variability, created at the surface by deposition is superposed by the interaction of sintering or densification and coarsening. This interplay is governed by the local climate conditions and induces differences in the correlation of density and microstructure, such as grain size or specific surface area. The findings

of this study imply, that the layering has no static memory. The layering is not kept constantly with depth and sequences of layers from the surface do not correspond to similar sequences of layers at the firn-ice-transition. The primary surface information such as starting density, microstructure and impurity content determine the subsequent evolution of the layering with depth. But there is no linear transformation of surface properties to greater depths. Any link of surface properties in terms of layering to local climate conditions cannot be directly extrapolated to the properties at the depth of the firn-ice transition and vice versa.

The layering of polar firn shows a random generation at the surface and a very dynamic evolution with depth, which is influenced not only by the microstructure and the local climate conditions but also by impurities incorporated into the firn at the surface.

8 Problems and Open Topics

8.1 Methodical limitations

The limitations of the measurements of high resolution density and microstructure from X-ray-microfocus-computer-tomography analysis are shortly discussed here.

Hoar layers, as often observed in the field to form below the surface or thin ice crusts are difficult or impossible to detect with the gamma absorption method. Hoar layers form loose and very fragile firn layers layers and get destroyed during the drilling, transport and measurement procedure. Ice crusts are very thin, often in a range of one mm and are therefore not detectable with the resolution and measurement set up used in this study. This gives a definite limitation of the method.

The problem of missing low density layers due to the drilling and measurement procedure could have an effect on the calculated variability value, i.e. decreased variabilities due to lacking extreme values in the lower range, or on the frequency analysis, since missing peaks could change the observed frequency. It can be assumed, that due to the very high number of firn cores included in this study, and the very broad range in local climate conditions, these firn cores represent, any irregularities can be neglected. However, only measurements of complete firn core sections in original condition can prove these findings. Therefore a drilling device, which is able to capture fragile low density layers, especially from low accumulation areas, is needed, in order to get more complete firn core pieces for density analysis.

The X-ray-microfocus-computer-tomography measurements allow a more careful han-

dling of fragile firn samples, but the limitation in sample resolution and discontinuity leads to a different calculation of standard deviation of the microstructure. In order to compare the variability of density and microstructure, high resolution continuous measurements of microstructure properties are necessary. The newly installed ice core X-ray-microfocus-computer-tomography-scanner at the Alfred-Wegener-Institute (J. Freitag) enables a continuous high resolution measurement of both, density and microstructure and therefor provide a much more detailed image of the link and evolution of these properties.

Next to density and grain size impurities seem to play an important role in the whole process of sintering and densification of polar firn. In order to understand the interaction of impurities, density and microstructure the data set of high resolution density and microstructure needs to be completed with high resolution ion measurements from Continuous Flow Analysis . From the result of this study, the merge of these three data sets seems to be the most challenging and most essential step in the near future.

8.2 "Global" microstructure

The microstructure data of the X-ray-microfocus-computer-tomography measurements allow an intense study of polar firn metamorphism, due to the large range in local climate conditions represented in this data set, and the large age distribution they cover. The basic idea is to find a global description of the metamorphism process, which enables a direct comparison of the microstructure of different sites. Therefore the degree or stage of metamorphism, i.e. a metamorphose factor, needs to be derived, including not only local climate conditions, but also the local temperature gradients at different depths, the time a certain firn layer spends within these different temperature gradients, and age. First tests were done, but no sufficient description for the metamorphose factor was obtained yet. This needs to be continued in future studies.

However, the data show a surprisingly definite behavior in terms of shape. In order to compare the shape of the ice grains or structure of the different firn samples, the

structure model index is calculated (Figure 8.1). With decreasing porosity the index decreases from values around 2 to values of approximately -3. The most striking feature is, that despite their very different grain sizes and local climate conditions, almost all samples of all firn core sites follow a defined line. Only at high porosities the DP7 samples scatter around 1. And at low porosities B 38 samples scatter at values above zero, even though all other samples show negative values at similar porosities (Figure 8.1). It seems that there is a clear link between porosity, which is an indicator for density and thus depth and time, and the structure of the ice phase of the firn.

For high porosity firn, the ice phase shows either single grains or bonded grains, with sintered necks and an overall convex structure. Very fresh surface snow with dendritic shapes or cup shaped hoar crystals would show even higher values such as the snow from DP7. As older the snow, the ice phase becomes smoother. Towards decreased porosity the ice phase becomes a solid matric with pores included. Thus the surface of the ice can be expected to turn to concave values for the index, since it is then enclosing the pores. The B 38 firn is buried so fast due to its outstanding high accumulation rate, that the structure has no time to evolve much even though porosity is decreasing rapidly. Accordingly the shape of single grained matrix is kept even at very low porosities.

Nevertheless, all other firn core sites show a remarkably unique pattern in this structure model index and porosity. Despite their extremely different local climate conditions, density profiles and microstructure evolution, a globally similar behavior in shape can be extracted from the data. This shape could be an indicator of the degree of sintering at a certain porosity of polar firn.

This finding is a first hint for a similar topological evolution of polar firn structure under snow metamorphism, even though the local conditions differ significantly. Future studies could concentrate on the determining factors, that control the structure evolution of the firn, especially under consideration of the metamorphose factor.

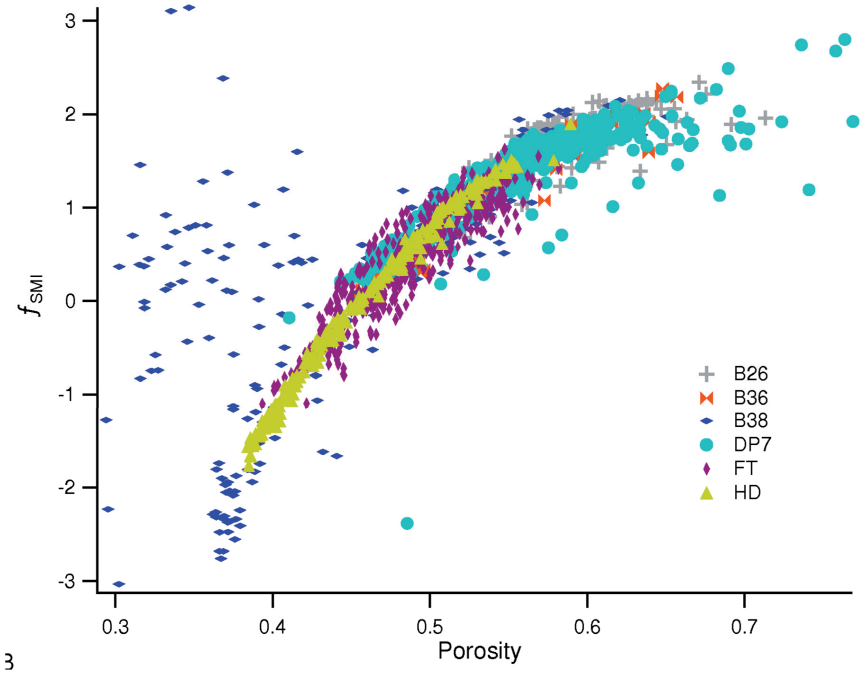

Figure 8.1: The structure model index with porosity of all sites and samples. Note the high values at low porosities of the B 38 firn core and the scattered values at high porosities of the DP7 site.

8.3 Convection of the upper firn

The ventilation of the upper snow and firn pack is difficult to access, since it includes a horizontal component, which can not be addressed with firn core studies. Horizontally permeable firn layers can lead to a intense ventilation of the firn, even when they are buried under less permeable layers. Often firn layers show a rather discontinuous extent and undulations, which enable the convection within the firn under horizontal pressure gradients. This problem is even more emphasized by the reported observation of nets of cracks in the upper snow and firn layers at extremely low accumulation rate sites. These cracks form deep vertical channels in the firn and introduce a much more complex and larger scale phenomenon of air ventilation than can be analyzed with single point firn core measurements. However, considering less extreme conditions, linking

measurements of microstructure and direct measurements of air permeability can deliver a coarse understanding of the magnitude of the ability to ventilate air in connection to snow metamorphism at the different sites. The direct measurement of air permeability of polar snow and firn is rather time-consuming and time extensive. Therefore former studies tried to link microstructure characteristics to air permeability, in order to parameterize air flow with easy-to-measure microstructure properties.

With 3-D X-ray-microfocus-computer-tomography information not only of the pore size but also of the tortuosity and connectivity of the pores can be obtained. First tests yield, that simple empirical relationships can fairly well predict low to medium permeability values and the variability of permeability due to the layering to a certain degree. But high permeable layers are always underestimated, since simple microstructure properties do not display the existence of large air pathways within the sample. With the available data set of two directly measured permeability profiles together with 3-D microstructure analysis, a comprehensive study can be conducted and even extended on more firn core sites, where only microstructure data are available. This is part of a future project together with Dr. Zoe Courville from Cold Region Research and Engineering Laboratory, USA. Pore size distributions in comparison to tortuosity measurements and direct permeability measurements can improve the understanding of the connection of air permeability and microstructure and the overall picture of firn convection.

The overall goal could be to deviate a rough estimation of the extent of the convection zone by knowing the depth, at which maxima in air permeability are obtained at the different sites. If it is possible to model the air permeability with the available microstructure data, than the set of firn cores investigated in this study allows a comparison of the snow metamorphism in connection to the coarsening, the development of the air permeability maximum with depth and the local climate conditions. This in turn would help to understand the formation and extension of a convection zone at the different locations with different climate conditions, even extended to glacial times.

9 Acknowledgement

This work is funded by the Deutsche Forschungsgemeinschaft (DFG) grant FR2527/1-1. I very much thank my supervisors Prof. Heinrich Miller and Prof. Katrin Huhn for their support and complaisant guidance in the last years.

I am very grateful to Prof. Mary Albert and Dr. Zoe Courville for a long-lasting and fruitful cooperation, an invitation to Greenland and many helpful comments and exchange of ideas. The project would have been much less colorful without you. Thank you so much. No expedition without lovely fancy people - thanks to the NEEM-Traverse team 2007 for a great time and much patience with us and our rolling coffee bar. And thanks to the unforgettable best "Snow-freaks" team ever (Zoe!), for the good time and the good job at Summit Station and a polar bear necklace.

A large thanks is due to Dr. Johannes Freitag and Dr. Sepp Kipfstuhl for the longsome support of and in daily life. Much of the progress of this thesis is due to your unbowed ability to challenge well-believed theories.

Dr. Sergio Faria has not only spend much time in understanding the problems and helping with this thesis. He also found the right words at the right time (more often, than he thinks). Thank you very much, Sergio.

I warmly thank Peter Sperlich for being the most relaxed office mate and the best expedition mate one can imagine - I have learned a lot from you. For her friendship and her much needed company in our office I thank Katrin Wolff. For their friendship, the offer to get help and answers all the time and the best "monday-motivation-cake" I thank Ilka Weikusat and Birthe Twarloh. My computer and me would have never become best friends without the unweary help of Christine Wesche, thanks for that and everything

else you helped with, no matter what time of the day. Days and nights in the cold lab can also turn out to feel like an expedition and I very much thank Andreas Frenzel for his companionship and never-ending support at good and at bad days. I cannot name all members of the AWI-glaciology group - I thank you all for a good time and the best coffee on earth and I wish you all the best for the future.

Last but not least I thank Prof. Dr. h.c. Sauerbrey and Frau Dr. Bohnet for their trust and support, which enabled me finishing the thesis.

Bibliography

Albert, M. R. & Perron, F. E. (2000), 'Ice layer and surface crust permeability in a seasonal snow pack', *Hydrological Processes* **14**, 3207–3214.

Albert, M. R., Shultz, E. F. & Perron, F. E. (2000), 'Snow and firn permeability and siple dome, antarctica', *Annals of Glaciology* **31**, 353–356.

Albert, M., Shumann, C., Courville, Z., Bauer, R., Fahnenstock, M. & Scambos, T. (2004), 'Extreme firn metamorphism: impact of decades of vapor transport on near-surface firn at a low-accumulation glazed site on the east antarctic plateau', *Annals of Glaciology* **39**, 73–78.

Alley, R. B. (1988), 'Concerning the deposition and diagenesis of strata in polar firn', *Journal of Glaciology* **34**, 283–290.

Arnaud, L., Barnola, J.-M. & Duval, P. (2000), 'Physical modelling of the densification of snow/firn and ice in the upper part of polar ice sheets', **26**, 285–305.

Benson, C. S. (1971), 'Stratigraphic studies in the snow at byrd station, antarctica, compared with similiar studies in greenland', *Antarctic snow and ice studies 2* **2**, 333–353.

Blunier, T. & Schwander, J. (2000), 'Gas enclosure in ice: age difference and fractionation', *Physics of Ice core records* pp. 307–326.

Courville, Z. R., Albert, M. R., Fahnenstock, M. A., Cathless, L. M. & Shumann, C. A.

(2007), ‘Impacts of an accumulation hiatus on the physical properties of firn at a low-accumulation polar site’, *Journal of Geophysical Research* **112**.

Cuffey, K. M. (2008), ‘A matter of firn’, *Science* **320**.

Davis, R., Arons, E. & Albert, M. (1996), ‘Metamorphism of polar firn: Significane of microstructure in engergy, mass and chemical species transfer’, *NATO ASI Series Chemical Exchange Between the Atmosphere and Polar Snow* **143**, 379–401.

Freitag, J., Wilhelms, F. & Kipfstuhl, S. (2004), ‘Microstructure-dependent densification of polar firn derived from x-ray microtomography’, *Journal of Glaciology* **30**, 243–250.

Fujita, S., Okuyama, J., Hori, A. & Hondoh, T. (2009), ‘Metamorphism of stratified firn at dome fuji, antarctica: A mechanism for local insolation modulation of gas transport conditions during bubble close-off’, *Journal of Geophysical Research* **114**.

Gerland, S., Oerter, H., Kipfstuhl, J., Wilhelms, F., Miller, H. & Miners, W. D. (1999), ‘Density log of a 181m long ice core from berkner island, antarctica’, *Annals of Glaciology* **29**, 215–219.

Goujon, C., Barnola, J.-M. & Ritz, C. (2003), ‘Modeling the densification of polar firn including heart diffusion: Application to close-off characteristics and gas isotopic fractionation for antarctica and greenland sites’, *Journal of Geophysical Research* **108**.

Gow, A. J. (1965), ‘On the accumulation and seasonal stratification of snow at the south pole’, *Journal of Glaciology* **5(40)**, 467–477.

Hawley, R. L. & Morris, E. (2006), ‘Borehole optical stratigraphy and neutron-scattering density measurements at summit, greenland’, *Journal of Glaciology* **52**, 491 – 496.

Herron, M. M. & Langway, C. C. (1980), ‘Firn densification: An empirical model’, *Journal of Glaciology* **25**, 373 – 385.

Jun, L. & Zwally, H. J. (2002), 'Modeled seasonal variations of firn density induced by steady-state surface air-temperature cycle', *Annals of Glaciology* **34**(147), 299–302.

Kaempfer, T. & Schneebeli, M. (2007), 'Observation of isothermal metamorphism of new snow and interpretation as a sintering process', *Journal of Geophysical Research* **112**, D24101.

Kang, S.-J. L. (2005), *Sintering - Densification, Grain Growth and Microstructure*, Butterworth-Heinemann, Elsevier Science Ltd. Linacre House, Jordan Hill, Oxford, POX2 8DP, England.

Kärkäs, E., Granberg, H., Kanto, K., Rasmus, K., Lavoie, C. & Leppäranta, M. (2002), 'Physical properties of the seasonal snow cover in dronning maud land, east antarctica', *Annals of Glaciology* **34**, 89–94.

Karlöf, L., Winebrenner, D. P. & Percival, D. B. (2006), 'How representative is a time series derived from a firn core? a study at a low accumulation site on the antarctic plateau', *Journal of Geophysical Research* **111**.

Kawamura, K., Severinghaus, J. P., Ishidoya, S., Sugawara, S., Hashida, G., Motoyama, H., Fujii, Y., Aoki, S. & Nakazawa, T. (2006), 'Convective mixing of air in firn at four polar sites', *Earth and Planetary Science Letters* **244**, 672–682.

Kreutz, K. J., Mayewski, P. A., Twickler, M. S., Whithlow, S. I., White, J. W. C., Shuman, C. A., Raymond, C. F., Conway, H. & McConnel, J. R. (1999), 'Seasonal variations of glaciochemical, isotopic and stratigraphic properties in siple dome (antarctica) surface snow', *Annals of Glaciology* **29**, 38–44.

Landais, A., Barnola, J. M., Kawamura, K., Caillon, N., Delmotte, M., Van ommen, T., Dreyfus, G., Jouzel, J., Masson-Delmotte, V., Minster, B., Freitag, J., Leuenberger, M., Schwander, J., Huber, C., Etheridge, D. & Morgan, V. (2006), 'Firn $\delta^{15}n$ in modern polar sites and glacial-interglacial ice: a model-data mismatch during glacial period in antarctica?', *Quaternary Science Reviews* **25**, 49–62.

Legresy, B. & Remy, F. (1998), 'Using the temporal variability of satellite radar altimetric observations to map surface properties of the antarctic ice sheet', *Journal of Glaciology* **44**(147), 197–206.

Li, J. & Zwally, H. J. (2004), 'Modeling the density variation in the shallow firn layer', *Annals of Glaciology* **38**, 309–313.

Maeno, N. & Ebinuma, T. (1983), 'Pressure sintering of ice and its implication to the densification of snow at polar glaciers and ice sheets', *The Journal of Physical Chemistry* **87**, 4103– 4110.

Marshall, H.-P., Schneebeli, M. & Koh, G. (2007), 'Snow stratigraphy measurements with high-frequency fmcw radar: Comparison with snow micro-penetromter', *Cold Regions Science and Technology* **47**, 108–117.

Martinerie, P., Raynaud, D., Etheridge, D. M., Barnola, J.-M. & Mazaudier, D. (1992), 'Physical and climatic parameters which influence the air content in polar ice', *Earth and Planetary Science Letters* **112**, 1–13.

Nakaya, U. & Kuroiwa, D. (1970), *Physical Properties and internal Structure of Greenland Snow*, ERDC/CRREL DA Task 1T061102B52A02, Hanover, NH, USA.

Ohser, J., Redenbach, C. & Schladitz, K. (2009), 'Mesh free estimation of the structure model index', *Image Analysis and Stereology* **28**, 179–185.

Palais J. M., Whillans I. M., B. C. (1982), 'Snow stratigraphy studies at dome c, east antarctica: an investigation of depositional and diagenetic processes', *Annals of Glaciology* **3**, 239–242.

Pielmeier, C. & Schneebeli, M. (2003), 'Develpments in the stratigraphy of snow', *Surveys in Geophysics* **24**, 389–416.

Rick, U. K. & Albert, M. R. (2004), 'Microstructure and permeability in the near-surface firn near a potential us deep-drilling site in west antarctica', *Annals of Glaciology* **39**, 62–65.

Rotschky, G., Rack, W., Dierking, W. & Oerter, H. (2006), 'Retrieving snowpack properties and accumulation estimates from a combination of sar and scatterometer measurements', *IEEE Transactions on Geoscience and Remote Sensing* **44**(4), 943–956.

Rott, H., Sturm, K. & Miller, H. (1993), 'Active and passive microwave signatures of antarctic firn by means of field measurements and satellite data', *Annals of Glaciology* **17**, 161–166.

Rundle, A. S. (1971), 'Snow accumulation and firn stratigraphy on the east antarctic plateau', *Antarctic Snow and Ice Studies 2* pp. 239–255.

Schneebeli, M. & Sokratov, S. (2004), 'Tomography of temperature gradient metamorphism of snow and associated changes in heat conductivity', *Hydrological Processes* **18**, 3655–3665.

Severinghaus, J. P. & Battle, M. O. (2006), 'Fractionation of gases in polar ice during bubble close-off: New constrains from firn air ne, kr and xe observations', *Earth and Planetary Science Letters* **244**, 474–500.

Shimizu, H. (1970), 'Air permeability of deposited snow', *Contributions from the Institute of Low Temperature Science, Series A* **22**, 1–32.

Stenberg, M., Hansson, M., Holmlund, P. & Karlöf, L. (1999), 'Variability in snow layering and snow chemistry in the vicinity of two drill sites in western dronning maud land, antarctica from dronning maud land, antarctica 2. seasonally resolved chemical records', *Annals of Glaciology* **29**.

Surdyk, S. & Fily, M. (1993), 'Comparison of passive microwave spectral signature of the antarctic ice sheet withground traverse data', *Annals of Glaciology* **17**, 161–166.

Tran, N., Remy, F., Feng, H. & Femenias, P. (2008), 'Snow facies over ice sheets derived from envisat active and passive observations', *IEEE Transactions on Geoscience and Remote Sensing* **46**, 3694–3708.

Wilhelms, F. (1996), 'Measuring the conductivity and density of ice cores', *Berichte zur Polarforschung, Alfred Wegener Insititut für Polar- und Meeresforschung* **191**.

Wilhelms, F. (2000), 'Measuring the dieelectric properties of ice cores', *Berichte zur Polarforschung, Alfred Wegener Insititut für Polar- und Meeresforschung* **367**.

Zwally, H. J. & Jun, L. (2002), 'Seasonal and interannual variations of firn densification and ice-sheet surface elevation at the greenland summit', *Journal of Glaciology* **48**, 199–207.

A Publication 1 - The densification of layered polar firn

Hörhold, M. W., Kipfstuhl, S., Wilhelms, F., Freitag, J., Frenzel, A.

Journal of Geophysical Research, Earth Surface, accepted.

The densification of layered polar firn

M. W. Hörhold,[1] S. Kipfstuhl,[1] F. Wilhelms,[1] J. Freitag[1] A. Frenzel[1]

M. W. Hörhold, Alfred Wegener Institute for Polar and Marine Research, Am Handelshafen 12 Building D, Bremerhaven, D 27568, Germany. (Maria.Hoerhold@awi.de)

S. Kipfstuhl, Alfred Wegener Institute for Polar and Marine Research, Am Handelshafen 12 Building D, Bremerhaven, D 27568, Germany. (Sepp.Kipfstuhl@awi.de)

F. Wilhelms, Alfred Wegener Institute for Polar and Marine Research, Am Handelshafen 12 Building D, Bremerhaven, D 27568, Germany. (Frank.Wilhelms@awi.de)

J. Freitag, Alfred Wegener Institute for Polar and Marine Research, Am Handelshafen 12 Building D, Bremerhaven, D 27568, Germany. (Johannes.Freitag@awi.de)

A. Frenzel, Alfred Wegener Institute for Polar and Marine Research, Am Handelshafen 12 Building D, Bremerhaven, D 27568, Germany. (Andreas.Frenzel@awi.de)

[1]Alfred Wegener Institute for Polar and
Marine Research, Bremerhaven, Germany

Abstract. High-resolution density profiles of 16 firn cores from Greenland and Antarctica are investigated in order to improve our understanding of the densification of layered polar firn. A vertical resolution of 1 to 5 mm enables us to study the detailed densification processes, and the evolution of the layering and the resulting variability in density with increasing depth. The densification of layered firn is important for the process of air enclosure in ice and is connected with the observed formation of a non-diffusive zone. We find that (1) mean density profiles, obtained from high-resolution measurements, only partly show clear transitions in densification rate at densities of 550, 730 or 820-840 kg/m^3, as they are commonly used in literature. (2) The density variability, induced by the layering, shows a similar pattern at all sites: high variabilities at the surface, a rapid drop to a relative minimum in variability at mean density of 600 - 650 kg/m^3, followed by a second relative maximum. (3) This leads to increased variability at densities of the firn-ice transition for most of the sites. (4) The variability at the surface decreases with increasing mean annual temperature and accumulation rate, whereas the variability at the firn-ice transition increases. We can exclude a change in local climate conditions as an explanation for the density variability since the firn cores in this study cover a broad range in mean annual temperature, accumulation rate and age. Overall, high-resolution density profiles deliver a more complex picture of compaction of polar firn as a layered granular medium than has been obtained from mean density profiles in the past.

1. Introduction

Density, as a physical property of polar firn, is important not only as a material characteristic, but for many topics of polar research. This includes the monitoring and modeling of ice sheet mass balance, by means of ground-penetrating radar or satellite laser altimetry [*Li and Zwally*, 2002, 2004; *Rott et al.*, 1993; *Rotschky et al.*, 2006], and the enclosure of air bubbles in the ice during the transformation from snow to ice [*Martinerie et al.*, 1992; *Schwander et al.*, 1997].

Different densification processes, acting at certain depth intervals of the firn column, have been investigated and discussed by others [*Anderson and Benson*, 1962; *Alley et al.*, 1982; *Maeno and Ebinuma*, 1983; *Alley*, 1987; *Ebinuma and Maeno*, 1987; *Paterson*, 1994; *Arnaud et al.*, 1998; *Salamantin et al.*, 2009]. Mean "critical" density values of 550, 730 and 820 - 840 kg/m^3 are often denoted for changes in the predominance of micro-scale processes. Examples are particle rearrangement [*Gow*, 1974; *Herron and Langway*, 1980; *Ebinuma and Maeno*, 1987; *Paterson*, 1994; *Salamantin et al.*, 2009], grain boundary sliding, recrystallization, creep [*Maeno and Ebinuma*, 1983; *Ebinuma and Maeno*, 1987] and air bubble shrinking [*Gow*, 1974; *Martinerie et al.*, 1992]. Yet there are hints that these critical densities vary considerably for different snow and firn types [*Alley et al.*, 1982; *Johnson*, 1998; *Freitag et al.*, 2004]. Deformation and grain boundary sliding seem to occur concurrently from the very beginning of compaction [*Arnaud et al.*, 2000], and grain boundaries in microstructure images show signatures of dynamic recrystallization in shape, orientation and number rather than structures resulting from normal grain growth [*Kipfstuhl et al.*, 2009]. Models of firn densification usually consider a mean density profile

[*Herron and Langway*, 1980; *Barnola et al.*, 1991; *Arnaud et al.*, 1998, 2000; *Goujon et al.*, 2003]. The evolution of density with depth is often linked to mean annual air temperature, accumulation rate and surface density [*Herron and Langway*, 1980; *Maeno and Ebinuma*, 1983; *Martinerie et al.*, 1992], overburden pressure [*Kameda et al.*, 1994] or surface winds [*Craven and Allison*, 1998].

Polar firn is a highly layered medium and thus exhibits heterogenous material properties [*Gow*, 1974; *Hansen and Brown*, 1986]. Stratigraphy is created by seasonal changes of the local climatic conditions. At high accumulation sites the stratigraphy is made by layers from single snow fall or drift events, while at low accumulation sites most likely only summer and winter precipitation create stratigraphy. Layers can be distinguished not only by their bulk density but also by grain size and shape, hardness, viscosity and coordination number. Accordingly, variability in such different properties will lead to different response to pressure loads [*Palais et al.*, 1982; *Hansen and Brown*, 1986; *Johnson*, 1998; *Alley et al.*, 1982].

Furthermore, the increase in density seems to vary not only within the firn layers but also with time. Zwally and Li (2002) observe seasonal variations in ice-sheet elevation and link these to variable densification rates through the year. The variability in densification is caused by seasonally changing temperatures and accumulation rates. Their models show that the amplitude of density variability increases with the accumulation rate, whereas the frequency decreases with increasing accumulation rate. This variability vanishes with depth [*Li and Zwally*, 2004].

The layering and the related variability in density is an important factor when discussing the age difference between air enclosed in bubbles and the surrounding ice. As long as

the pores are connected with the surface, an exchange with the atmosphere by diffusion is possible. The depth, and thus age, when pore close-off is expected, is often derived using mean density critical values [*Martinerie et al.*, 1992; *Schwander et al.*, 1997]. However, considering layering, and thus density variability, consequently leads to depth intervals where some layers have already reached the pore close-off density. Other layers still show connected pores. This depth interval is often referred to a non-diffusive zone, where air can escape upwards but no downward air exchange is possible. It is common to interpret the high-density layers, which approach the pore close-off density first, as the initially high-density layers originating at the surface (often referred to winter precipitation) [*Martinerie et al.*, 1992; *Severinghaus and Battle*, 2006].

Recently, the degree of layering has been considered as a parameter influencing the extent of the non-diffusive zone. Landais et al. (2006) suggest that strong layering, as is expected for high accumulation sites, results in the existence of a non-diffusive zone. At low accumulation sites, the layering vanishes at the surface and a non-diffusive zone is not expected. Also Kawamura et al. (2006) suggest that the thickness of the non-diffusive zone generally depends on the amplitude of density variability due to the layering at the surface and the horizontal extent of single layers, typically generated by seasonal variations of deposited snow density.

Density variability generated by layering can be investigated by using high-resolution density measurements. We use the term high-resolution to refer to a vertical resolution of 1 to 5 mm with depth, which is much higher than the typical 1 m averages. This resolution is small compared to the thickness of single layers, which is usually found to be in the range of several cm. High-resolution density measurements of polar firn were

published by Gerland et al. (1999) for the B25 core from Berkner Island, Antarctica, and by Freitag et al. (2004) from site B26, Greenland. Both observed that the variability decreases rapidly in the upper 20 - 30 m. Below, the variability increases again, yielding a second relative maximum. Gerland et al (1999) also found a negative correlation between density and electrical conductivity measurements (ECM) in the upper firn column, which changed at 30 m depth to a positive correlation. Hawley and Morris (2006) published high resolution profiles of borehole density logging techniques and optical stratigraphy at Summit, Greenland. They find a positive correlation between optical brightness reflections and density, which decreases with depth and turns to a negative correlation between 20 and 25 m depth.

Gerland et al. (1999) and Freitag et al. (2004) explained the second relative maximum in density variability by the more efficient densification of coarse grained, initially low-density firn, compared to fine grained, initially high-density firn. This would lead to a crossover in the density profiles. The depth at which the densities of coarse and fine grained firn are approximately equal is associated with the minimum in density variability. This observation indicates that below the variability minimum, the initially low density firn layers show higher densities than the initially high density firn layers, which would explain the switch in the ECM - density correlation. Other authors considered this second maximum in density variability as a singular abnormal finding, possibly due to interannual changes in weather conditions [*Li and Zwally*, 2002]. Hawley and Morris (2006) explain the change from positive to negative correlation between density and brightness by the transition from grain boundary sliding to pressure sintering as the dominant firn densification mechanism. Recently, discontinuous high-resolution profiles of density and

crystal orientation of a firn core from Dome Fuji were published [*Fujita et al.*, 2009] showing a switch from positive to negative correlation between density maxima and structural anisotropy at 30 m depth, supporting the ideas of Gerland et al.(1999) and Freitag et al.(2004).

These publications presented the results of firn cores from single sites. In this study we extend the work by Gerland et al.(1999) and Freitag et al.(2004) with 14 more firn cores from Greenland and Antarctica, covering a broad range of local climate conditions. High-resolution density measurements are obtained with the gamma-attenuation method. We shortly discuss the possible impact of microstructure and impurities on the density and densification. At this point we can not prove the role of microstructure (on a grain-scale) in this study since no microstructure data are available with this resolution. However, the available data allow a profound examination of macro-structural properties of the firn and the densification. Our high-resolution density measurements reveal the following results:

1. Mean density profiles obtained from high-resolution measurements do only partly display a transition in densification rate at 550, 730 and 820-840 kg/m^3.

2. All firn cores presented here show a second maximum of density variability, as first reported by Gerland et al. (1999). Accordingly an effect of changes in local climate or weather, as suggested by Li and Zwally (2002), can be excluded. The minimum in variability is reached at mean densities around 600 - 650 kg/m^3, while the mean density and amplitude of the second maximum in variability varies from site to site.

3. A more efficient compaction of initially less dense layers leading to a crossover, as suggested by Gerland et al. (1999) and Freitag et al.(2004), can explain the observed density variability and the switch in correlation of density to ECM and brightness. This

process of differential compaction also means that the initially dense layers from the surface exhibit lower densities at the firn-ice-transition. The high-density layers which create a sealing effect at the firn-ice transition might originate as low-density layers at the surface.

4. The variability at the firn-ice transition increases with increasing mean annual temperature and accumulation rate, whereas the variability at the surface decreases. Low accumulation sites also show relatively high near-surface density variability. This observation gives reason to question a direct link between the degree of surface layering and the extent of a non-diffusive zone.

2. Methods

2.1. Material and Instrument

The high-resolution density profiles of 16 different sites from Greenland and Antarctica are investigated. The firn cores were drilled and measured in a time interval over almost 20 years. The firn cores are from areas which cover a broad range in mean annual surface temperature, accumulation rate and elevation and origin from Greenland and Antarctic Plateau regions but also from Antarctic coastal regions. For further details see Table 1 and Table 2.

The density was measured using a non-destructive logging system including a Löffel densimeter [*Wilhelms*, 1996]. The measured intensity I of the attenuated gamma-ray beam through the ice core is converted into a density signal. Using Beer's law, the intensity of the beam in air I_0, the mass absorption coefficient μ_{ice} =0.085645 m^2kg^{-1} $\pm$ 0.1 % [*Wilhelms*, 1996, 2000] and the diameter d of the ice core, the density ρ can be calculated by:

$$\rho = \frac{-1}{d \cdot \mu} \cdot ln(\frac{I}{I_0}) \quad (1)$$

Details and background of the method are given in Wilhelms (1996; 2000). Gerland et al. (1999) and Freitag et al.(2004) discussed density data obtained by this method and compared it to density profiles obtained with computer-tomography [*Freitag et al.*, 2004]. Usually two one meter long core pieces are put in a cradle for a measurement run. The diameter is measured every 10 cm manually with a calliper and then interpolated over the length of the core piece. Scratches from core catchers and breaks are documented. All measurements were conducted between temperatures of -10 °C and - 35 °C either in the cold laboratory of the Alfred Wegener Institute (AWI), Bremerhaven, Germany or in the field, using a comparable measurement set up.

2.2. Data Processing

After the measured diameter is interpolated and used to calculate the density according to equation (1), the raw data are corrected for core breaks and scratches, by manually removing single outliers and linearly interpolating over the resulting data gaps.

Two different processing strategies are used. First, the density versus depth profile is investigated and average values are compared to field data and to the Herron-Langway model [*Herron and Langway*, 1980]. The measured raw high resolution density is shown in Figure 1A (light grey). A running mean using a sliding window of one meter length is calculated (Figure 1A, dark grey line). Comparison with field data of one meter long ice core sections yields good agreement (Figure 1A, brown line). The mean density deter-

mined from high-resolution measurements, noted as mean density in sections 3.1 and 4.1, is compared to density values calculated from the Herron-Langway model.

Secondly, the density profile is converted to water equivalent depth (m w.e.). Again average values are calculated as well as a standard deviation as a measure of density variability. The conversion leads to unequal distances between data points (i.e. low density snow at the surface corresponds to smaller increments in m w.e. depth than high-density firn at greater depths). Therefore each density profile is re-sampled to equidistant points as noted in Table 2 (column point-distance), depending on the sampling rate of the measurements (Figure 1B, light grey line).

The conversion from actual depth to water equivalent depth enables a comparison of the layers from the near-surface area with layers from greater depths, since the effect of the thinning of layers due to compaction is taken into account. Furthermore the water equivalent depth scale provides a measure of the overburden pressure and enables a comparison of the cores at similar overburden pressures. In order to remove fluctuations or noise on smaller length scales than the layering, the data are smoothed using a moving average window (Figure 1B, dark grey line covering the raw data; window size in Table 2 (last column)). To study the density variability the data are detrended, using an exponential fit (Figure 1B, blue line):

$$\rho = y_0 + A_1 \cdot exp(-\tau_1 z) + A_2 \cdot exp(-\tau_2 z) \tag{2}$$

After detrending, the standard deviation σ_ρ, with a sliding window of size $N = 1000$ and a step size of 500 data points (Figure 1B, brown line) is:

$$\sigma_\rho = \sqrt{\frac{\sum_i^N (\rho_i - \bar{\rho})^2}{N}} \tag{3}$$

where ρ_i is the density at point i and $\bar{\rho}$ the mean density of window N. In order to compare the different cores and their standard deviation we have several possibilities to define N: we either calculate the standard deviation over a fixed water equivalent depth interval or over a fixed time interval. The former results in the comparison of different time-intervals, the latter in the comparison of different depth-intervals. We calculated the standard deviation by taking a fixed number of data points ($N = 1000$), over which the standard deviation is calculated. For a sufficiently large N, the calculated standard deviation is independent of the window size.

For the same window size, a mean density of the depth-density profile in water equivalent depth is calculated (Figure 1B, yellow line). This value is the mean density at a certain depth (m w.e.) corresponding to the standard deviation at this depth (m w.e.). In the following we refer to this value as mean density of the density-depth profile in water equivalent depths in sections 3.2, 4.2, 4.3 and 4.4..

Martinerie et al. (1992) introduced an empirical linear relationship of measured air volume in ice cores to annual mean surface temperature and the critical density ρ_{crit} at which the air isolation occurs. We use this relation to calculate the mean close-off density ρ_{crit} at our firn sites:

$$\rho_{crit} = (\frac{1}{\rho_{ice}} + 7.6 \times 10^{-4} \times T - 0.057)^{-1} \tag{4}$$

214 with $\rho_{ice} = 917\,\mathrm{kg/m^3}$ the density of pure ice and T the annual mean surface temperature
215 in Kelvin. Knowing the close-off density, the measured variability σ_ρ at that density is
216 then determined from the measurements.

217 To test the assumption of a relationship between the layering at the surface and the
218 extent of the non-diffusive zone, we compare the density variability at the surface with
219 the density variability at the firn-ice transition. The latter is defined by the mean density
220 obtained from equation (4) and the related standard deviation. To determine surface
221 variability we first define intervals for which the standard deviation is calculated. We
222 chose to show more than one interval to illustrate the extremely different accumulation
223 rates at the sites. Therefore from each site, one-meter depth intervals starting from the
224 surface (interval 1, figure 9) to 6 m depth (interval 6, figure 9) are converted to water
225 equivalent depth and the standard deviation is calculated following equation (3). This
226 time, N is the number of points within each of the one meter long intervals.

227 To estimate the relative error of the density measurements, the errors in each term of
228 equation (1) have to be considered. The relative error in density has been estimated as
229 4.24% at the top 2 m and 1.47% at 100 m depth for the cores B16, B18, B31, B32, B33
230 [*Wilhelms*, 2000]. The resulting absolute errors are 10 - 15 $\mathrm{kg/m^3}$ in the upper meters
231 and 8 - 12 $\mathrm{kg/m^3}$ in greater depths. For cores B17, B19 and B21, B38, B39, DML95,
232 DML97, B36/B37 and EDC2 the relative error is reduced to 1.65% in the upper 2 m,
233 decreasing to 0.66% at 100 m depth [*Wilhelms*, 1996, 2000]. The error reduces because
234 of the use of either a stronger gamma-ray source or a higher resolution measurement
235 [*Wilhelms*, 1996, 2000]. This leads to absolute values around 5 - 6 $\mathrm{kg/m^3}$ for all depths.
236 The standard deviation is calculated over 1000 data points and thus averages over the

237 random error associated with each single measurement point. We therefore assume that
238 the standard deviation obtained by the processing described above gives a good measure
239 of the variability in density due to the different strata in the firn. The standard deviation
240 as a term of density variability has been used by Gerland et al. 1999, Freitag et al. 2004
241 and Fujita et al. 2009. For more detailed discussion of error estimation of the gamma-
242 attenuation method see [*Wilhelms*, 1996, 2000] and [*Breton et al.*, 2009].

3. Results

3.1. Mean Density

243 The mean density profiles obtained from high-resolution data are shown and discussed
244 with respect to changes in densification rate at different critical densities and with respect
245 to predicted profiles using the Herron-Langway model.

246 First, the measured high-resolution density profiles of the B25 core [*Gerland et al.*, 1999]
247 and the B26 core [*Freitag et al.*, 2004] are displayed, together with the 1 m averages (Fig-
248 ure 2). The previously published data were included in this study to show that applying
249 the above described procedures yields similar results as shown in earlier publications. All
250 mean density profiles are shown and the commonly assumed mean critical densities, at
251 which a change in densification rate is expected, are indicated with dashed lines (Fig-
252 ure 3). For some sites the Herron-Langway model was used to predict density and the
253 results are compared to the mean density profiles obtained from high-resolution density
254 measurements (Figure 4).

255 Assuming a change in densification rate at the critical densities of 550, 730 or 820-840
256 kg/m^3, the slope of the density-depth profiles should show a distinct change at these
257 densities. This is expressed in the Herron-Langway model, where the density increases

with different rates as a function of depth below and above a density of 550 kg/m^3 [*Herron and Langway*, 1980]. Hence, even though we do not consider the increase in density as a function of time, we can study the density-depth profiles in terms of an abrupt change in the slope, when a critical density is reached (Figures 3 and 4). We observe a weak transition in the slope of the density-depth profiles at densities between 550 and 580 kg/m^3 for high accumulation sites such as DML95 (Figure 3), whereas the cores B26 and B29 show this transition at much lower densities below 500 kg/m^3; the same holds for B36/B37 (Figure 4). The B25 core shows a distinct change in the slope at approximately 550 kg/m^3 but the EDC2 core shows no abrupt change at all (Figure 4). A change of densification rate at 730 kg/m^3 is not observed in any of our density-depth profiles. Also a distinct change at 820-840 kg/m^3 is not apparent, however a slow-down in density-increase is present for densities higher than 840 kg/m^3.

Some examples of the mean density profile and the predicted profiles using the Herron-Langway model are plotted in Figure 4. The profiles of B25, B29 and B26 with moderate temperatures of -27 °C and approximately -30 °C and accumulation rates of 0.14-0.18 m w.e. per year are predicted fairly well (B25, B26, and B29), but for the EDC2 site, the Herron-Langway model overestimates the measured density. This leads to a 5-6 meter offset in the depth at which the density of 840 kg/m^3 is reached. The firn is older when reaching this density than the model predicts. On the other hand, the Herron-Langway model underestimates the densification at B38. The model run ends at a mean density of approximately 794 kg/m^3 at 83 m depth. This density is obtained in the mean measured profile at a depth of approximately 59 m. The firn approaching a certain density is much younger than predicted by the model (Figure 4).

3.2. Density Variability

The layering of polar firn induces a variability observed in high-resolution density profiles. The variability changes with increasing depth and mean density (Figure 5). The standard deviation, σ_ρ, as a measure of this layering is shown as water equivalent depth (Figure 6A) and with mean density of the density-depth profile in m w.e. (Figure 6B). The behavior of σ_ρ at different local climate conditions is displayed in Figure 7.

The evolution of a typical high-resolution density profile, here B26, is shown in detail (Figure 5). B26 represents a typical firn-core site from the Greenland plateau, with a moderate mean annual temperature of - 30.6 °C and accumulation rate of 0.18 m w.e. per year. Visually, the density variability changes its shape, amplitude and frequency with increasing density and depth. Large fluctuations are observed at lower mean densities (Figure 5, 5 and 8 m depth interval). At higher mean densities around 600 kg/m^3 (20 m) the amplitude decreases, but for even higher densities around 700 kg/m^3 the amplitudes increase again (25 and 40 m depth). The variability vanishes at densities above 800 kg/m^3 (Figure 5, 75 m depth).

The variability, σ_ρ, with depth and increasing mean density (of the density-depth profile in water equivalent depth) is displayed for all firn cores (Figure 6). The amplitude reaches a minimum at a depth of approximately 10 m w.e. and then increases again. This yields a second relative maximum before it finally falls towards zero (Figure 6A). The minimum in density variability occurs at mean densities between 600 - 650 kg/m^3 (Figure 6B), whereas the mean density of the following second maximum in variability seems to vary slightly. At mean densities of the firn-ice transition some cores show high amplitudes in σ_ρ (B38, B39 for example) while for other cores the amplitude is decreasing (EDC2 and B36/B37).

In order to get a better overview of the influence of local climate conditions, the profiles have been sorted into five groups, A - E, of similar annual mean temperature and accumulation rate (Figure 7). In all five groups the structure of rapid decrease of σ_ρ to a minimum at 600 - 650 kg/m^3 and a second maximum below is found. B25 is plotted in two groups. The density variability decrease of B25 in the upper core is similar to the Antarctic cores, while the second maximum is more consistent with the Greenland cores, as are the climate conditions. Finally we calculated the average for each group to determine typical behavior (Figure 7f). For comparison the averages of each group A - E can be seen in Figure 7F. Except for group C, the drop to the minimum is similar, but the patterns clearly diverge in extent and amplitude of the second maximum. Whereas groups A, B, C, and D differ in amplitude of the second maxima, but not that much in position, group E shows the second maximum at distinctively larger mean densities.

In summary, all firn cores, covering a broad range of climate conditions, show a similar rapid decrease followed by a second maximum of density variability. The cores show a similar structure of σ_ρ above the minimum. The mean density of the minimum variability seems to be always at approximately 600-650 kg/m^3, whereas the magnitude and the position of the second maximum seem to vary according to the environmental climatic conditions of a site.

4. Discussion

4.1. Mean Density

According to the literature, depth-density profiles should show changes in the slope at densities of 550, 730 and 820 - 840 kg/m^3. We expected the mean density-depth profiles from high resolution density measurements to clearly show these transitions. The first

transition in densification rate is suggested at a mean density of 550 kg/m^3 [*Herron and Langway*, 1980] as a result of particle rearrangement gaining maximum packing density [*Arnaud et al.*, 2000]. In our results the density at which this change occurs varies from densities below 500 kg/m^3 at B36/B37 or B29 up to densities close to 600 kg/m^3 at B38 (Figure 4). It seems that the critical density, at which the densification rate changes, varies at the different sites. Different snow and firn types may exhibit a different density at which the compaction mechanism changes. At a single site with strong layering each layer will react differently to the applied load [*Freitag et al.*, 2004; *Alley et al.*, 1982]. Transitions at the other densities of 730 and 820 - 840 kg/m^3 are not clearly detectable. It is reasonable to assume that different microstructural processes and deformation patterns take place at all depths and the dominance of each of these processes will shift rather smoothly from one to another within the firn column [*Kipfstuhl et al.*, 2009]. Different processes can also occur concurrently [*Arnaud et al.*, 1998; *Salamantin et al.*, 2009] and critical densities, marking a transition of the dominance of microstructural processes, can vary over a large density range [*Johnson*, 1998].

The firn cores representing climate conditions considered in the set-up of the Herron-Langway model are very well reproduced by the model (Figure 4). For a density-depth relationship at medium climate conditions this rather simple, phenomenological model is still applicable, even if a sharp transition at a mean density of 550 kg/m^3 is not apparent in most of the profiles presented here. Arnaud et al. (2000) showed that the maximum packing density (theoretically 550 kg/m^3) is temperature dependent. It decreases with decreasing annual mean temperature of a site. This would explain the range of densities at which a change in the slope in the density-depth profile can be observed in our data.

Decreasing or increasing this critical density would probably reveal a better fit of the Herron-Langway model with the EDC2 or B38 firn core data. Salamatin et al. (2008; 2009) find the critical density at generally higher densities, corresponding to the cessation of particle rearrangement at the closest packing density. They explain the lower critical density of 550 kg/m^3 to be only an intermediate stage in which particle rearrangement and plasticity work together, as has been proposed by Ebinuma and Maeno (1987). No such sharp transitions at densities between 640 and 680 kg/m^3, as were found with the model by Ebinuma and Maeno (1987), are identified in our measured profiles.

The Herron-Langway model included firn cores from a broad range of local climate conditions, including South Pole and Vostok at the lower end of accumulation rate and surface temperature range [*Herron and Langway*, 1980]. Nevertheless, the model is not applicable to the conditions at Dome C and to those at the PreIPICS core sites (i.e. B38). One possible explanation for the distinct deviation of the Dome C firn core is the different deposition and local climate pattern. So called diamond dust accompplishes much of the accumulation at Vostok or Dome Fuji, whereas the mass input at Dome C is dominated by precipitation from synoptic-scale weather systems. The problem of extending empirical models to a broader range of climate conditions has been discussed earlier [*Arnaud et al.*, 2000; *Martinerie et al.*, 1992]. Our data emphasize the need for a physical model [*Arnaud et al.*, 2000; *Salamatin and Lipenkov*, 2008; *Salamantin et al.*, 2009], but the high-resolution measurements need to be considered in the overall concept of critical densities.

4.2. Density Variability

Whenever a granular medium compacts, the mean density increases. What happens to the density variability is not known. To our knowledge no work is published that investigates the densification of a granular medium until pore closure. If we assume homogenous compaction with similar densification rates for different layers in a granular stratified medium, we would expect a steady decrease in variability. The densities of low-density and high-density layers originating at the surface increase steadily. Thus, their density values converge with a corresponding reduction in variability and obtain a common value at the density of ice (Figure 8A, dashed line).

We applied two densification models to look at the model behavior in terms of density variability. The Herron-Langway model [*Herron and Langway*, 1980] is parameterized with mean annual temperature and accumulation rate. We can use different surface densities to simulate variability. By starting with two layers of different density at the surface, we obtain three stages in the evolution of σ_ρ (Figure 8A, diamonds). In the first stage, the linear increase in density of the two layers is similar, giving no change in σ_ρ, in the second stage, the layer with the initially higher density has already passed the density of 550 kg/m^3 and continues to densify at an exponential rate, while the other layer still experiences linear growth. This leads to a rapid drop in σ_ρ in the second stage. At the third stage, the second layer has entered the exponential growth regime, and σ_ρ decreases almost linearly with depth.

The model introduced by Barnola and Pimienta [*Barnola et al.*, 1991] includes an empirical function that considers structural variations during densification [*Arnaud et al.*, 2000]. It starts at a density of 550 kg/m^3. We used measured values for σ_ρ at mean

density of 550 kg/m^3 to start the model. The model produces an exponential drop of σ_ρ (Figure 8A, circles). Neither of the two employed models can reproduce or explain the measured evolution of density variability (Figure 8A, crosses).

The driving force for the densification in the upper part of the firn column is the overburden pressure due to ongoing accumulation of new snow on top of each layer. The overload pressure is determined by the density and thickness of the layers on top. Thus the water equivalent depth gives a measure of the overburden pressure and enables a comparison of the driving force at the different sites. Until the minimum variability at approximately 600 - 650 kg/m^3 or approximately 10 m w.e. depth is reached, the variability profiles for all sites are similar (Figure 6A), but below, this depth, density variability diverges.

If we assume that the overburden pressure determines the densification rate down to the variability minimum, the explanation for the observed densification behavior is the manner in which fine and coarse firn structures respond to load [*Alley et al.*, 1982]. Whereas coarse crystals are joined by relatively wide necks to few neighbors, crystals in fine firn tend to be more spherical and are joined by narrow necks to many neighbors. Thus the former structure is far from closest packing and will undergo significant particle rearrangement under an applied load, whereas the latter is more stable [*Alley et al.*, 1982]. Gow (1974) observed firn layers with low density, corresponding to coarse-grained layers, to show less strength to overload pressure than high-density firn, corresponding to fine grains. The surface layers with different densities compact at different rates, the low-density layers faster than the high-density layers, leading to a fast decrease of σ_ρ until a minimum in density variability is reached. At this minimum in variability the layers have the same

density. Continuous densification with different rates leads to equal densities of the layers at a certain depth (crossover), after which the initially low-density layers become denser at a faster rate and exhibit higher densities than the original high-density layers.

By applying a simple exponential fit to the minimum and maximum densities of the high-resolution profile with a crossover at a mean density of approximately 600-650 kg/m^3, we can highlight the different compaction rates and the resulting variability (Figure 8B). We do not consider to what extent the low and high-density layers contribute to the mean density. A better approach could be obtained by using equation (2), where the depth - density relation is represented by two coefficients and amplitudes, which would have the physical meaning of the different densification rates.

Currently, few detailed microstructural data are available. Freitag et al. (2004) showed that the negative grain-size - density correlation observed in the near-surface firn switches to a positive correlation below the minimum at the B26 core. Below the crossover, high-density layers contain large grains [*Freitag et al.*, 2004], whereas in the near-surface layers, low-density layers are usually characterized by large grain sizes. This implies that high-density layers at the firn-ice transition do not necessarily result from high-density layers at the surface and vice versa. Fujita et al. (2009) also find a switch in density and structural anisotropy obtained from microstructure analysis. The switch in the correlation of density and backscattered light, as observed by Hawley and Morris (2006) at depths of approximately 20 meters could also be explained by such a crossover of coarse-grained and fine-grained firn layers in their densities. Of course firn consists of more than these two example layers and not all will show such a relationship in grain size and density-increase.

Nevertheless, it can be hypothesized that the two examples (lowest and highest density) determine the boundary values in which the density variability is created.

Below the minimum, the profiles of σ_ρ diverge considerably. It is apparent that the overload pressure is no longer the determining factor below this depth. The amplitudes in variability clearly increase again, but not as a function of overload pressure. Other factors, independent from the load, seem to modulate the density variability at this point. The firn cores cover different time intervals - from less than 60 years (B38) to more than 2900 years (EDC2). Accordingly, the behavior of the density variability is not a local climate signal, because we study different time series intervals, but a structural property of layered firn compaction.

A crossover in density of initially coarse-grained, low-density layers and fine-grained, high-density layers, as discussed above, could be one possible explanation. High-resolution grain size data are needed to examine the impact of grain size on the densification of the different layers. Another possibility could be the inclusion of impurities or chemistry into the firn. The interaction of impurities with the firn is rarely investigated. From ice core data the coherence of high dust concentrations with very small grains in the ice matrix is known, which indicates an impact of impurities on physical properties of the ice [*Svensson et al.*, 2005]. Also microstructural parameters apparent in single layers, such as grain shape or textural anisotropy might come to play a role, after a certain density or grain-geometry is obtained. Salamatin et al. (2009) showed the importance of grain size and coordination number in the densification process and thus in the determination of the close-off density and depth. Both impurities and microstructure can alter the densification

457 rate of the firn. The analysis of this impact is beyond the scope of this paper, but a topic
458 of future research.

4.3. Variability at the firn ice transition

459 In order to test the assumption of a direct link of surface layering to the variability at the
460 firn-ice transition, related to an extension of a non-diffusive zone [*Landais et al.*, 2006], we
461 compare the density variability at the firn-ice transition with the density variability at the
462 surface and link it to the mean annual temperature and accumulation rate. We calculate
463 the mean densities for air enclosure, using equation (4) and determine the corresponding
464 value in σ_ρ (Table 3). We find an increase in variability at the firn-ice transition with
465 increasing mean annual temperature (correlation coefficient of the fit r = 0.822) and
466 increasing accumulation rate (Figure 9A, r = 0.634 and 9B, r = 0.73, orange line). This
467 observation supports the assumption of a dependency of density variability at the firn-
468 ice transition on mean annual temperature and on accumulation rate, as suggested by
469 Landais et al.(2006) and Kawamura et al. (2006).

470 For the surface variability we find a clear negative trend with temperature (r = -0.35
471 in the uppermost layers and r = -0.92 at 6 m depth) and accumulation rate (r = -0.617 /
472 -0.44 in the uppermost layers and -0.73 / -0.86 at 6 m depth). The higher the temperature
473 or accumulation rate at a site, the lower the density variability, which is the opposite of the
474 trend of the variability at the firn-ice transition. We first calculate the trend for the whole
475 range of accumulation rates (Figure 9A1). In order to make sure that the extremely high
476 accumulation rates of the PreIPICS cores do not influence the trend, we then exclude the
477 PreIPICS data and re-calculate the trend over the residual range of accumulation rates
478 (Figure 9A2). The result is the same in both cases - the density variability at the surface

479 decreases with mean annual temperature and accumulation rate. This decrease indicates
480 a decrease in the number of layers apparent at a certain depth interval with increasing
481 mean annual temperature and accumulation rate. Accordingly low-accumulation sites
482 seem to have more pronounced layering than high-accumulation sites. This finding is in
483 contradiction to the common assumption that low-accumulation sites show only weak or a
484 lack of layering compared to high-accumulation sites [*Landais et al.*, 2006] because of the
485 long exposure to temperature gradients and insulation. Because of the opposite trends
486 of density variability at the surface and at the firn-ice transition with increasing mean
487 annual temperature and accumulation rate (Figure 9) we can not confirm a direct link of
488 layering at the surface to the extent of a non-diffusive zone near the firn-ice transition. It
489 seems that the surface stratigraphy of polar firn does not directly imply the variability at
490 the firn-ice transition or the thickness of a non-diffusive zone.

491 Equation (4) estimates the mean density of close-off [*Martinerie et al.*, 1992]. It is
492 assumed that high-density layers approaching close-off density at shallower depths seal
493 off low-density layers from the free atmosphere and thus increase the air volume enclosed
494 in low-density firn. The depth at which this density is approached is crucial for the
495 estimation of the age difference of ice and air. However, the problem of density variability
496 makes the definition of this close-off depth very varied and it is used very differently in
497 the literature [*Arnaud et al.*, 1998, 2000; *Landais et al.*, 2006; *Kawamura et al.*, 2006;
498 *Loulergue et al.*, 2007]. In Table 3 we list the mean density and mean depth at which the
499 air isolation is obtained from equation (4), together with some data from literature. Even
500 though no physical meaning can be extracted from these values, we also show the depth
501 values at which these densities occur for the first and the last time in the high-resolution

density profile. Examination of these depths highlights the variability and randomness of the occurrence of critical densities and depth intervals with respect to mean annual temperature, accumulation rate, location or measured density variability.

The question is whether the degree of vertical density variability is the key parameter for the air close-off depth. The horizontal extent of high-density layers at the firn-ice transition (initially low-density layers at the surface) and thus the horizontal variability or the roughness of layers [*Martinerie et al.*, 1992], might play an important role in defining the depth at which firn air is finally sealed off from the pore space above [*Freitag et al.*, 2001]. In that case the parameters to examine more carefully are the conditions at which layers are formed and how layers are extended horizontally in plane. This includes not only the precipitation itself, but the wind and redistribution by wind, which shape the surface, create surface roughness and generate single snow layers with a certain thickness and horizontal continuity. It might be necessary to consider the wind duration, speed and redistribution of snow particles. It might also be important to link the surface variability with the amplitude of temperature variation at a site: a broader temperature range occurring over the year generates a larger difference in the density between single layers. With increasing accumulation rate this impact will cease, thus the degree of variability will decrease, as is suggested by Li and Zwally (2004).

4.4. Conclusion

We investigated mean density profiles and density variability obtained from high resolution firn core measurements. Our results emphasize the need for a physical model for predicting mean density profiles, in order to be able to apply it to a broad range of climate conditions. Furthermore the study of high-resolution density gives detailed insight into

the physical process of compaction of stratified firn. In the density profiles investigated we find few or no distinct transitions in the density-increase with depth at mean densities of 550, 730 and 820-840 kg/m^3, as found elsewhere in the literature.

Density variability as a measure of the layering of polar firn shows a distinct pattern at all sites, excluding local climate conditions as an explanation, and questioning the common idea of homogenous polar firn densification. The more efficient and fast densification of initially low-density layers, overcoming the density of initially high-density layers (crossover), explains the observations of the variability pattern and a switch in correlation of density and electrical conductivity [*Gerland et al.*, 1999] and density and intensity of back-scattered light [*Hawley and Morris*, 2006]. It also implies, that the high-density layers at the firn-ice transition do not originate from high-density layers at the surface. In order to understand the evolution of the density variability and to verify the crossover in density profile of different layers or the impact of impurities and microstructure, the densification process needs to be investigated on a micro-scale. Therefore a firn core study including high resolution profiles of chemistry, microstructure and density is strongly needed. Traditional methods to obtain such profiles are very time consuming. But new methods are progressing, enabling a fast and accurate analysis of microstructure [*Kipfstuhl et al.*, 2009]. These techniques will provide more detailed information in the future. In order to link firn layers in their extent, thickness and initial density to the air enclosure process, the lateral extension and continuity of theses layers needs to be considered as well. Therefore knowledge about wind intensity, duration of wind deposition events and the subsequent creation of wind-packed layers on one hand, the extent and distribution of low density layers at the surface, on the other hand, is crucial.

547 **Acknowledgments.** We thank the field team of the North-Greenland traverse 1993
548 - 1995; Daniel Steinhage and the team of the PreIPICS traverse 2006/2007 and Hans
549 Oerter and the team of the DML-pre-site survey 1997/1998. We are very grateful to
550 Dr. Zoe Courville for careful reading of the manuscript. We also thank the two anony-
551 mous reviewers for their helpful comments. This work is partly funded by the Deutsche
552 Forschungsgemeinschaft (DFG) grant FR2527/1-1.

References

553 Alley, R. B., Firn densification by grain-boundary sliding: a first model, in *VIIth Sympo-*
554 *sium on the Physics and Chemistry of Ice, Journal de Physique*, vol. 48, pp. 249–254,
555 1987.

556 Alley, R. B., J. F. Bolzan, and I. M. Whillans, Polar firn densification and grain growth,
557 *Annals of Glaciology*, *3*, 7–11, 1982.

558 Anderson, D. L., and C. S. Benson, The densification and diagenesis of snow, in *Ice and*
559 *Snow - properties, processes and applciations*, 1962.

560 Arnaud, L., V. Lipenkov, J.-M. Barnola, M. Gay, and P. Duval, Modelling of the densifi-
561 cation of polar firn: characterization of the snow-firn transition, *Annals of Glaciology*,
562 *26*, 39–44, 1998.

563 Arnaud, L., J.-M. Barnola, and P. Duval, Physical modelling of the densification of
564 snow/firn and ice in the upper part of polar ice sheets, *Physics of Ice Core Records*,
565 285–305, 2000.

566 Barnola, J.-M., P. Pimienta, D. Raynaud, and Y. S. Korotkevich, Co_2-climate relationship
567 as deduced from the Vostok ice core: a re-examination based on new measurements and

on re-evaluation of the air dating, *Tellus*, *43B*, 83–90, 1991.

Breton, D. J., G. S. Hamilton, and C. T. Hess, Design, optimazation and calibration of an automated density gauge for firn and ice cores, *Journal of Glaciology*, *55*, 1092–1100, 2009.

Craven, M., and I. Allison, Firnification and the effect of wind-packing on Antarctic snow, *Annals of Glaciology*, *27*, 239–245, 1998.

Ebinuma, T., and N. Maeno, Particle rearrangement and dislocation creep in a snow-densification process, *VIIth Symposium on the Physics and Chemistry of Ice, Journal de Physique 48*, 263–268, 1987.

EPICA, c. m., Eight glacial cycles from an Antarctic ice core, *Nature*, *429*, 623–628, 2004.

EPICA, c. m., One-to-one coupling of glacial climate variabiltiy in Greenland and antarctica, *Nature*, *444*, 195–198, 2006.

Freitag, J., U. Dobrindt, and S. Kipfstuhl, A new method for predicting transport properties of polar firn with respect to gases on the pore space scale, *Annals of Glaciology*, *35*, 538–544, 2001.

Freitag, J., F. Wilhelms, and S. Kipfstuhl, Microstructure-dependent densification of polar firn derived from X-ray microtomography, *Journal of Glaciology*, *30*, 243–250, 2004.

Fujita, S., J. Okuyama, A. Hori, and T. Hondoh, Metamorphism of stratified firn at dome fuji, antarctica: A mechanism for local insolation modulation of gas transport conditions during bubble close off, *Journal of Geophysical Research*, *114*, 2009.

Gerland, S., H. Oerter, J. Kipfstuhl, F. Wilhelms, H. Miller, and W. D. Miners, Density log of a 181m long ice core from Berkner Island, Antarctica, *Annals of Glaciology*, *29*, 215–219, 1999.

591 Goujon, C., J.-M. Barnola, and C. Ritz, Modeling the densification of polar firn including
592 heat diffusion: Application to close-off characteristics and gas isotopic fractionation for
593 Antarctica and Greenland sites, *Journal of Geophysical Research*, *108*, 2003.
594 Gow, A. J., Time-temperature dependence of sintering in perennial isothermal snowpacks,
595 *Snow Mechanichs Symposium, IAHS-AISH Publication*, *114*, 25–41, 1974.
596 Hansen, A. C., and R. L. Brown, The granular structure of snow: an internal-state variable
597 approach, *Journal of Glaciology*, *32*, 434–438, 1986.
598 Hawley, R. L., and E. Morris, Borehole optical stratigraphy and neutron-scattering density
599 measurements at Summit, Greenland, *Journal of Glaciology*, *52*, 491 – 496, 2006.
600 Herron, M. M., and C. C. Langway, Firn densification: An empirical model, *Journal of*
601 *Glaciology*, *25*, 373 – 385, 1980.
602 Johnson, J. B., A preliminary numerical investiagtion of the micromechanics of snow
603 compaction, *Annals of Glaciology*, *26*, 51– 54, 1998.
604 Kameda, T., H. Shoji, K. Kawada, O. Watanabe, and H. B. Clausen, An empricial relation
605 between overburden pressure and firn density, *Annals of Glaciology*, *20*, 87–94, 1994.
606 Kaspers, K. A., R. S. W. van de Wal, M. R. van den Broeke, J. Schwander, N. P. M. van
607 Lipzig, and C. A. M. Brenninkmeijer, Model calculations of the age of firn air across
608 the Antarctic continent, *Atmospheric Chemostry and Physics*, *4*, 1365–1380, 2004.
609 Kawamura, K., J. P. Severinghaus, S. Ishidoya, S. Sugawara, G. Hashida, H. Motoyama,
610 Y. Fujii, S. Aoki, and T. Nakazawa, Convective mixing of air in firn at four polar sites,
611 *Earth and Planetary Science Letters*, *244*, 672–682, 2006.
612 Kipfstuhl, S., S. H. Faria, N. Azuma, J. Freitag, I. Hamann, P. Kaufmann, H. Miller,
613 K. Weiler, and F. Wilhelms, Evidence of dynamic recrystallization in polar firn, *Journal*

of Geophysical Research, *114*, 2009.

Landais, A., et al., Firn δ^{15}n in modern polar sites and glacial-interglacial ice: a model-data mismatch during glacial period in Antarctica?, *Quaternary Science Reviews*, *25*, 49–62, 2006.

Li, J., and H. J. Zwally, Modeled seasonal variations of firn density induced by steady-state surface air-temperature cycle, *Annals of Glaciology*, *34*, 299–302, 2002.

Li, J., and H. J. Zwally, Modeling the density variation in the shallow firn layer, *Annals of Glaciology*, *38*, 309–313, 2004.

Loulergue, L., F. Parrenin, T. Blunier, J.-M. Barnola, R. Spahni, A. Schilt, G. Raisbeck, and J. Chappellaz, New constrains on the gas age-ice age difference along the epica ice cores, 0-50 kyr, *Climate of the Past*, *3*, 527–540, 2007.

Maeno, N., and T. Ebinuma, Pressure sintering of ice and its implication to the densification of snow at polar glaciers and ice sheets, *The Journal of Physical Chemistry*, *87*, 4103– 4110, 1983.

Martinerie, P., D. Raynaud, D. M. Etheridge, J.-M. Barnola, and D. Mazaudier, Physical and climatic parameters which influence the air content in polar ice, *Earth and Planetary Science Letters*, *112*, 1–13, 1992.

Oerter, H., F. Wilhelms, F. Jung-Rothenhäusler, F. Göktas, H. Miller, W. Graf, and S. Sommer, Accumulation rates in dronning maud land, Antarctica, as revealed by dielectrical-profiling measurements of shallow firn cores, *Annals of Glaciology*, *30*, 27–34, 2000.

Palais, J., I. Whillans, and C. Bull, Snow stratigraphy studies at dome c, East Antarctica: an investigation of depositional and diagenetic processes, *Annals of Glaciology*, *3*, 239–

242, 1982.

Paterson, W. S. B., *The Physics of Glaciers, third edition*, Butterworth-Heinemann, Elsevier Science Ltd. Linacre House, Jordan Hill, Oxford, POX2 8DP, England, 1994.

Rotschky, G., W. Rack, W. Dierking, and H. Oerter, Retrieving snowpack properties and accumulation estimates from a combination of SAR and Scatterometer measurements, *IEEE Transactions on Geoscience and Remote Sensing*, *44*, 943–956, 2006.

Rott, H., K. Sturm, and H. Miller, Active and passive microwave signatures of antarcitc firn by means of field measurements and satellite data, *Annals of Glaciology*, *17*, 337–343, 1993.

Salamantin, A. N., V. Y. Lipenkow, J. M. Barnola, A. Hori, P. Duvan, and T. Hondoh, Snow/firn densification in polar ice sheets, *Physics of Ice Core Records II, Supplement Issue*, *68*, 195–222, 2009.

Salamatin, A. N., and V. Y. Lipenkov, Simple relations for the close-off depth and age in dry-snow densification, *Annals of Glaciology*, *49*, 71–76, 2008.

Schwager, M., Ice core analysis on the spatial and temporal variability of temperature and precipitation during the Late Holocene in North Greenland, *Berichte zur Polarforschung*, *362*, 2000.

Schwander, J., T. Sowers, J.-M. Barnola, T. Blunier, A. Fuchs, and B. Malaize, Age scale of the air in the Summit ice: Implication for glacial-interglacialtemperature change, *Journal of Geophysical Research*, *102*, 45–47, 1997.

Severinghaus, J. P., and M. O. Battle, Fractionation of gases in polar ice during bubble close-off: New constrains from firn air Ne, Kr and Xe observations, *Earth and Planetary Science Letters*, *244*, 474–500, 2006.

660 Sommer, S., D. Wagenbach, R. Mulvaney, and H. Fischer, Glacio-chemical study covering
661 the past 2kyr on three ice cores from Dronning Maud Land, Antarctica 2, seasonally
662 resolved chemical records, *Journal of Geophysical Research*, *15*, 29,423–29,433, 2000.
663 Svensson, A., S. W. Nielsen, S. Kipfstuhl, S. J. Johnson, S. J. P., M. Bigler, U. Ruth,
664 and R. Rthlisberger, Visual stratigraphy of the Northern Greenland Ice Core Project
665 (Northgrip) ice core during the last glacial period, *Journal of Geophysical Research*,
666 *110*, doi:10.1029/2004JD005134, 2005.
667 Wilhelms, F., Measuring the conductivity and density of ice cores, *Berichte zur Polar-*
668 *forschung, Alfred Wegener Insititut für Polar- und Meeresforschung*, *191*, 1996.
669 Wilhelms, F., Measuring the dieelectric properties of ice cores, *Berichte zur Polar-*
670 *forschung, Alfred Wegener Insititut für Polar- und Meeresforschung*, *367*, 2000.
671 Zwally, H. J., and J. Li, Seasonal and interannual variations of firn densification and ice-
672 sheet surface elevation at the Greenland Summit, *Journal of Glaciology*, *48*, 199–207,
673 2002.

Table 1. The 16 firn core sites with position, mean annual temperature, T, and accumulation rate, b. References for the data are: (1) *Schwager* [2000], (2) *Wilhelms* [1996, 2000], (3) *Freitag et al.* [2004], (4) *Gerland et al.* [1999], (5) *Sommer et al.* [2000], (6) *Oerter et al.* [2000], (7) *EPICA* [2006], (8) Schwander, Oerter, pers. comm, (9) *EPICA* [2004].

Campaign/ region	Name	lat °	lon °	h a. s.l. m	T °C	b. m w.e.	Year of drilling	Reference
Greenland								
NGT	B 16	75.9402	-37.6299	3040	-27	0.142	1993-1995	(1), (2)
NGT	B 17	75.2504	-37.6248	2820			1993-1995	(1), (2)
NGT	B 18	76.6170	-36.4033	2508	-30	0.104	1993-1995	(1), (2)
NGT	B 21	80.000	-41.1374	2185	-30	0.108	1993-1995	(1), (2)
NGT	B 26	77.2533	-49.2167	2598	-30.6	0.18	1993-1995	(1), (3)
NGT	B 29	76.0039	-43.4920	2874	-31.6	0.153	1993-1995	(1), (2)
Antarctica								
Berkner Is.	B25	-79.6142	-45.7243	886	-27	0.14	1995	(4)
DML	B 31	-75.5815	-3.4303	2669	-42	0.063	1997	(5), (6)
DML	B 32	-75.0023	0.0070	2882	-42	0.061	1997	(5), (6)
DML	B 33	-75.1670	6.4985	3160		0.044	1998	(5), (6)
DML	B 36/37	-75.0025	0.0684	2891	-44.6	0.067	2005/2006	(7)
PreIPICS	B 38	-71.1621	-6.6989	690	-18.1	1.25	2006/2007	(8)
PreIPICS	B 39	-71.4083	-9.9167	654	-17.9	0.77	2006/2007	(8)
PreIPICS	DML 95	-71.5680	-6.6670	540	-19.2	0.55	2006/2007	(8)
PreIPICS	DML 97	-72.0640	-9.5583	760	-20.4	0.49	2006/2007	(8)
Dome C	EDC2	-75.1000	123.35000	3233	-53	0.025	1999	(9)

Table 2. The measurement setups and the data processing parameters for the 16 firn cores.

More details are given in [*Wilhelms*, 1996, 2000].

Campaign/ region	Name	Year of measurement	Activity source (1990) G Bq	Sampling rate mm	Point distance mm w.e.	Averaging window points
Greenland						
NGT	B 16	1995/1996	25.96	3	3	5
NGT	B 17	1995/1996	111	1	0.9	16
NGT	B 18	1995/1996	111	3	3	5
NGT	B 21	1995/1996	111	3	3	5
NGT	B 26	1995/1996	25.96	1	0.9	16
NGT	B 29	1995/1996	25.96	1	0.9	16
Antarctica						
Berkner Is.	B 25	1995	25.96	3	3	5
DML	B 31	1997/1998	25.96	5	4.4	3
DML	B 32	199/1998	25.96	5	4.4	3
DML	B 33	1998	25.96	5	4.4	3
DML	B 36/37	2007/ 2006	111	1	0.9	11
PreIPICS	B 38	2007	111	1	0.9	16
PreIPICS	B 39	2007	111	1	0.9	16
PreIPICS	DML 95	2007	111	1	0.9	16
PreIPICS	DML 97	2007	111	1	0.9	16
Dome C	EDC2	2008	111	1	0.9	11

Table 3. The air isolation density ρ_{crit}, calculated using equation (4) [*Martinerie et al.*, 1992], the corresponding density variability σ_ρ, close-off depth (mean depth) and the depth at which the air isolation density is reached the first (top depth) and the last time (bottom depth) within the high resolution density profile. In the last column measured/ modeled mean close-off depths are added from the following references: (1) [*Schwander et al.*, 1997] for NGRIP and GISP2 as closest points to B 16 , (2) [*Kaspers et al.*, 2004], (3) [*Landais et al.*, 2006] after Models by Arnaud et al. (2000) and Pimienta et al. (1991); with NGRIP as the closest point to B29.

Campaign/ region	Name	ρ_{crit} kg/m^3	$\sigma_\rho(\rho_{crit})$ kg/m^3	mean depth (ρ_{crit}) m	top depth (ρ_{crit}) m	bottom depth (ρ_{crit}) m	Literature depth m
Greenland							
NGT	B 16	819.273	12.2627	63	56	69	71 /72 (1)
NGT	B 17						
NGT	B 18	820.806	12.8078	59	54	66	
NGT	B 21	820.806	12.9072	62	51	72	
NGT	B 26	820.848	13.225	69	59	78	
NGT	B 29	821.319	10.5	68	53	77	66 /67 (3)
Antarctica							
Berkner Is.	B 25	819.156	14.5719	56	50	67	60 /59 (3)
DML	B 31	826.997	10.2713	82	75	86	
DML	B 32	826.997	11.2794	86	77	93	
DML	B 33						
DML	B 36/ 37	827.495	8.1154	88	77	98	74 (2)
PreIPICS	B 38	815.003	16.586	68	56	83	
PreIPICS	B 39	814.91	17.108	58	48	77	
PreIPICS	DML95	815.514	13.4153				
PreIPICS	DML97	816.072	10.0261				
Dome C	EDC2	832.019	4.5932	99	93	104	98.6 (2)/ 100 (3)

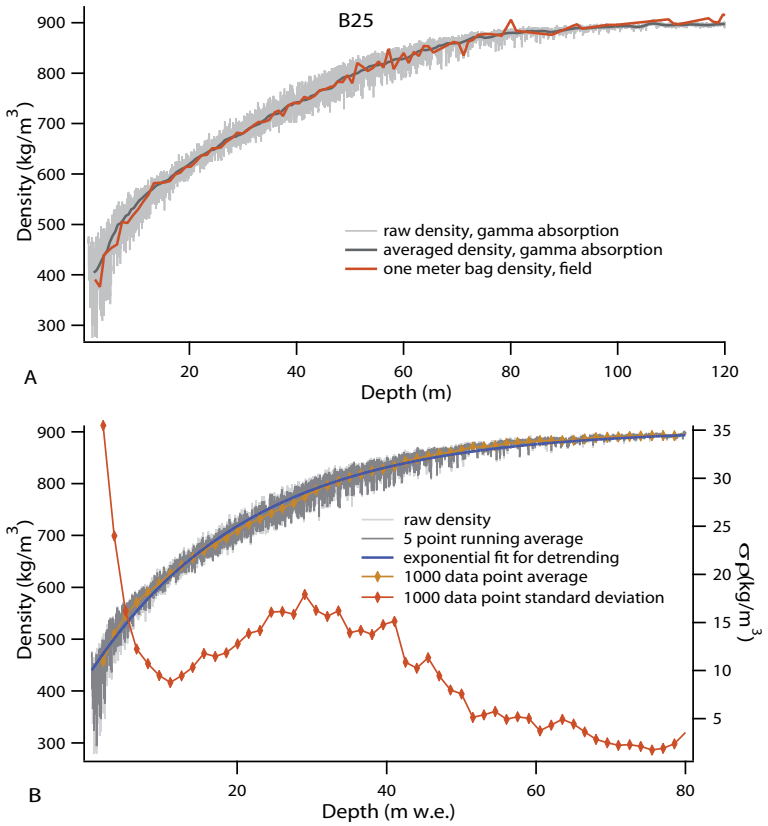

Figure 1. The measured high-resolution (grey line) density raw data with depth (A) together with the one meter average (running mean) from high-resolution density measurements (dark line) and the one meter bag values measured in the field (brown line) for comparison. The high-resolution density raw data with depth in meter water equivalent (B) after re-sampling to equidistant points (light grey line), together with the smoothed data after applying a running mean average window of size as denoted in Table 2 (dark grey line). The exponential fit for detrending is displayed (blue line) as well as the mean values of a sliding window of 1000 data points (yellow), corresponding to the standard deviation of the sliding window of 1000 data points after detrending (brown).

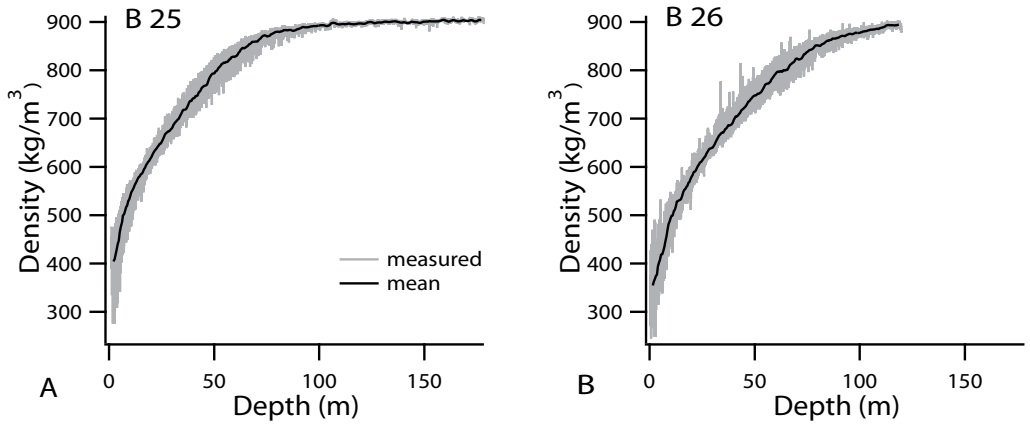

Figure 2. High-resolution density profiles (grey line) of B25 (after Gerland et al. 1999) and B26 (after Freitag et al. 2004), together with the 1 meter average (black line). The large variability in the density becomes visible, even at greater depths.

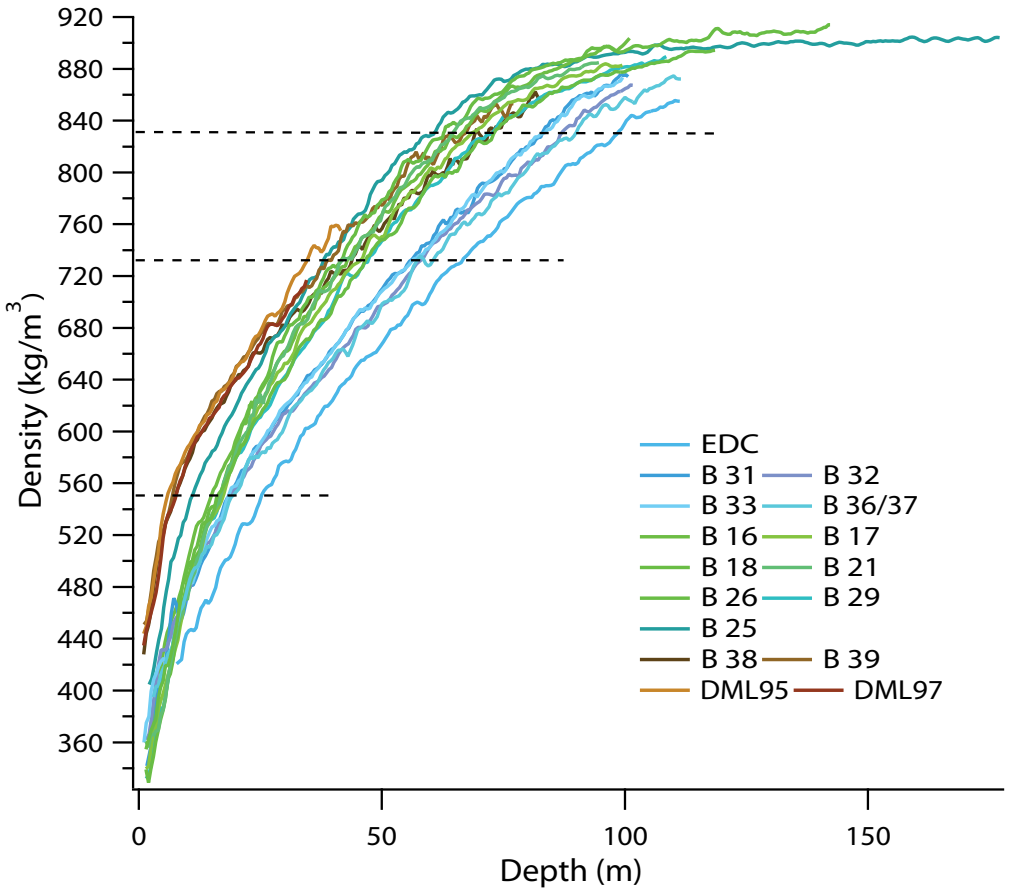

Figure 3. Mean density profiles (1 m running mean average). Low accumulation sites are plotted in blue, medium accumulation sites in green and high accumulation sites in brown. Commonly considered "critical density" values of 550 kg/m^3, 730 kg/m^3 and 820 - 840 kg/m^3 are indicated by dashed lines. For most of the cores a transition at 550 kg/m^3 is not obviously detectable. A transition at density around 730 kg/m^3 is not visible in any profile. For most of the cores a change in densification rate occurs at densities above 840 kg/m^3, but a distinct transition is not apparent.

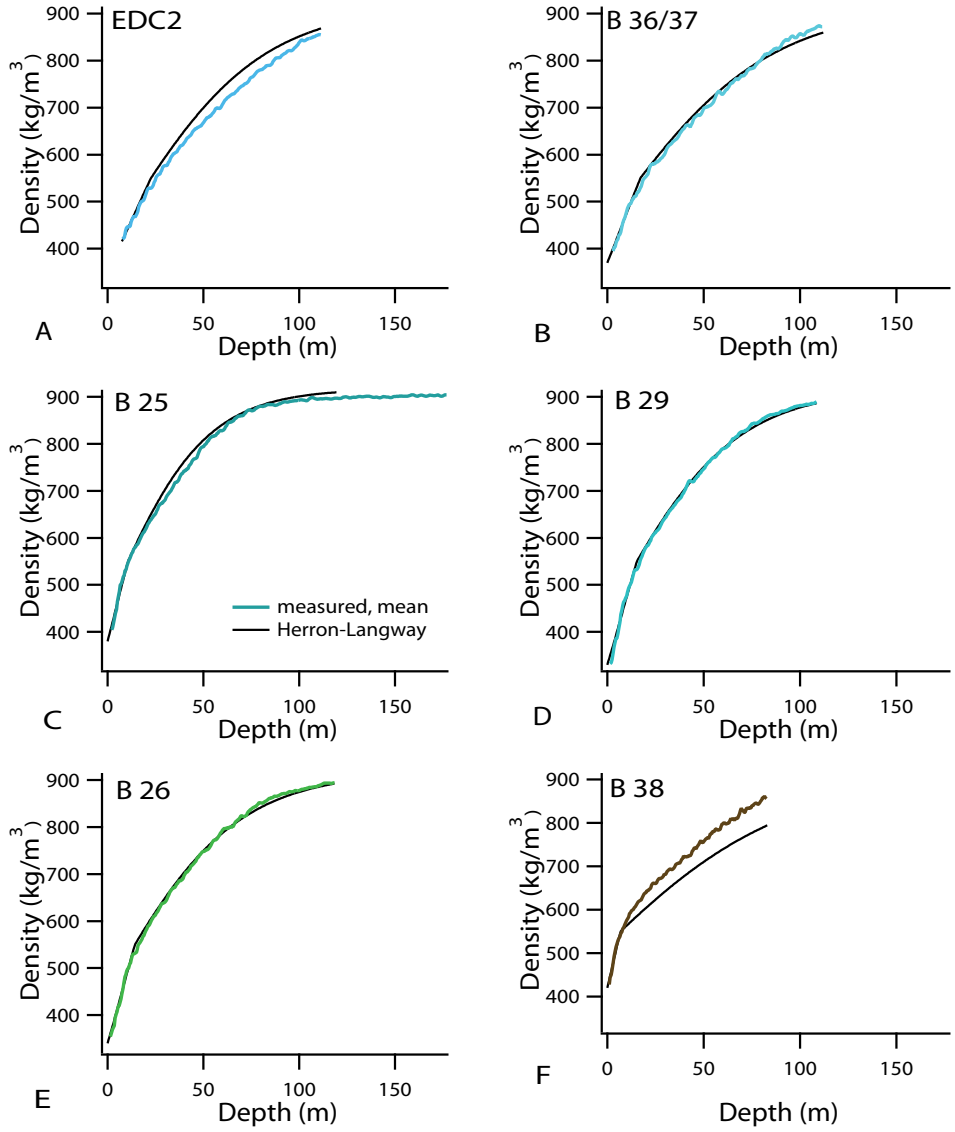

Figure 4. Selected mean density profiles in comparison to modeled density profiles using the Herron-Langway model (black line). The Herron-Langway model reproduces the profiles of the B25, B26 and B29 cores - with moderate mean annual temperatures and accumulation rates (C - E)well. But the model fails for the EDC2 core with low accumulation rate and temperature and the B38 core with high accumulation rate and temperature (A and F).

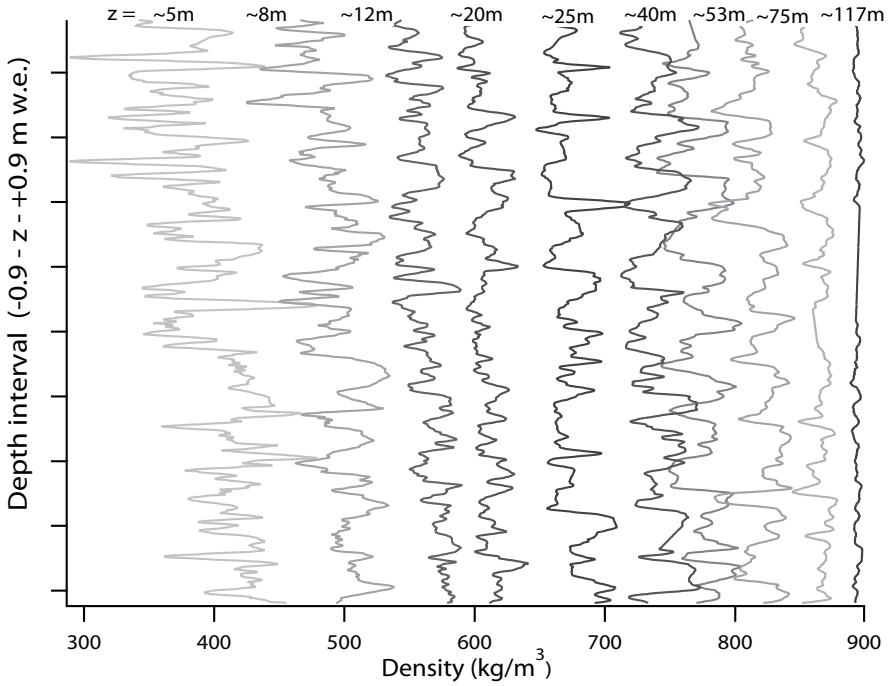

Figure 5. Details of the high-resolution density of B26 core. This core represents a typical firn core from the Greenland plateau, with moderate mean annual temperature and accumulation rate. From left to right the mean density and depth increase. Each profile covers 1.8 m depth w.e., which equals approximately 10 years at this site. In the upper part (5 and 8 m depth) the density variations are characterized by large amplitudes and random frequencies. Towards greater depths (20 m depth) the amplitudes decrease. Below the amplitudes increase again and more regular frequencies seem to appear (25 - 53 m depth). Below 53 m depth the variability decreases until it vanishes at depths of 75 m.

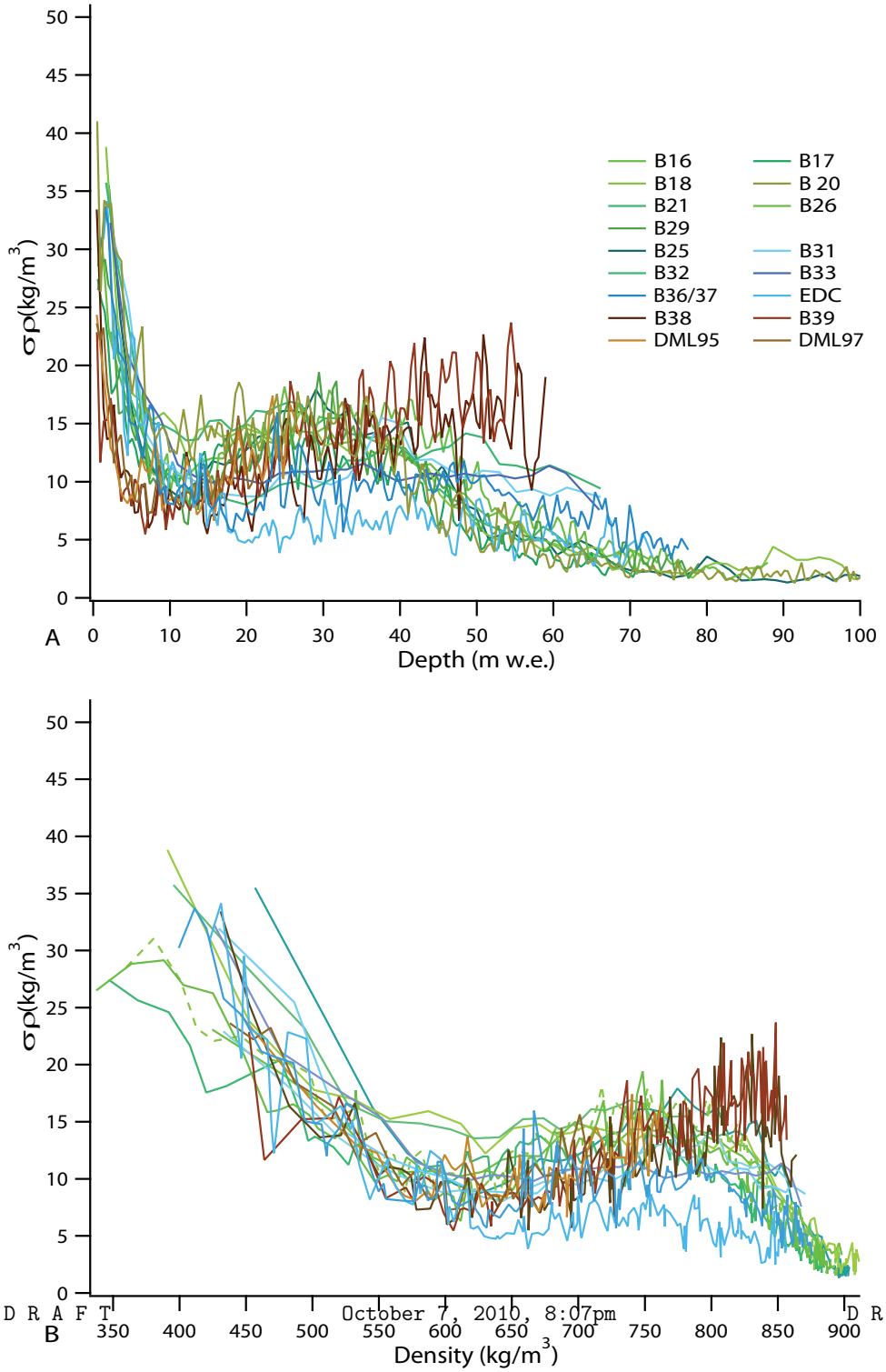

Figure 6. Measured density variability σ_ρ of all cores as a function of depth in m w.e. (A) and mean density (B). All profiles show a rapid drop in σ_ρ with a minimum at approximately 10 m

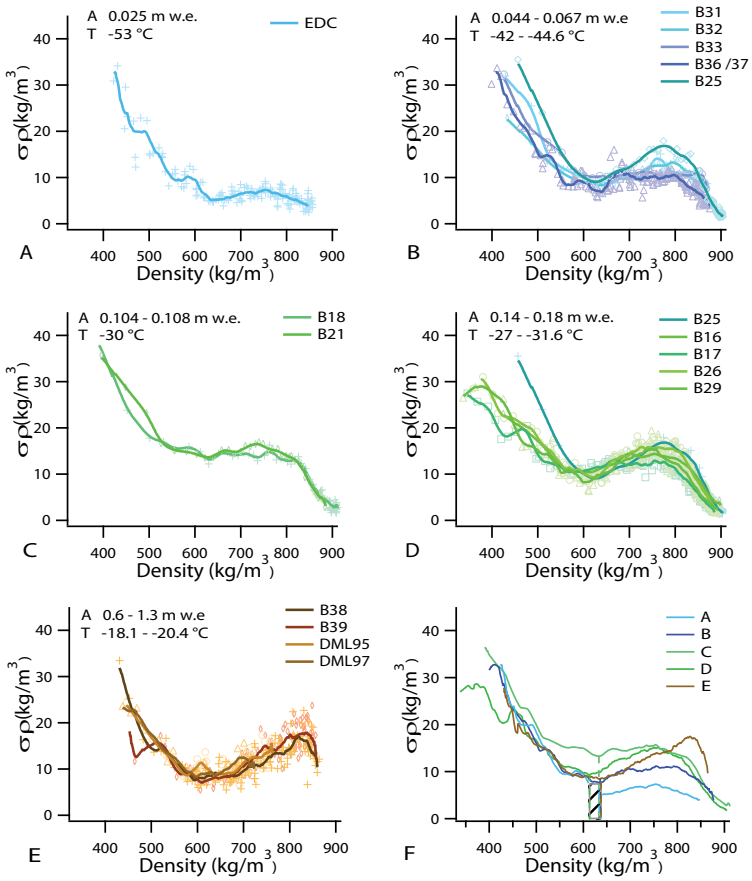

Figure 7. Measured σ_ρ of the firn cores grouped by temperature and accumulation rate intervals. The lowest temperature and accumulation rate in A (EDC2), second lowest in B (DML). The low accumulation sites from Greenland are shown in C, note that the minimum is not well developed, the moderate Greenland cores are shown in D. The B25 core is plotted with B and D, since the drop seems to better fit with the DML cores, whereas the second maximum fairly well fits to the Greenland cores. Finally E shows the PreIPICS cores with highest temperatures and accumulation rates. In F the averaged profiles of each of the groups are plotted. The mean density of the minimum is restricted to 660 - 650 kg/m^3 (grey shaded area).

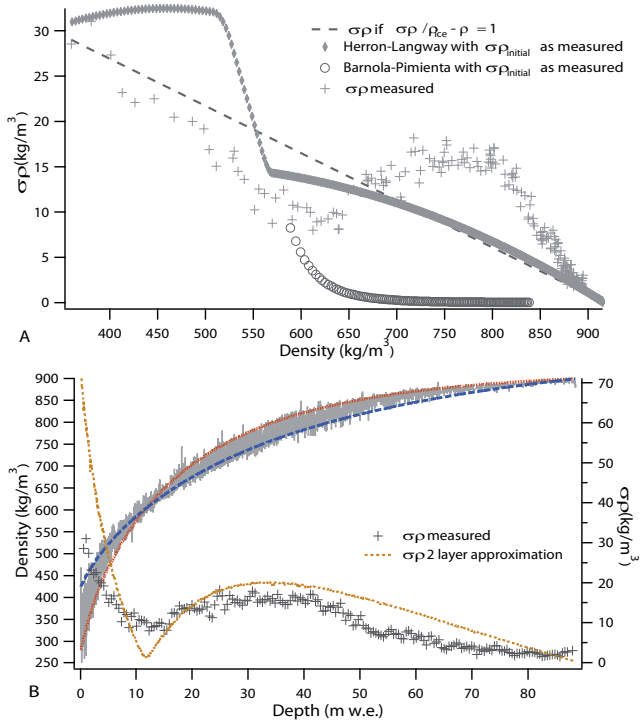

Figure 8. Measured (crosses) and modeled σ_ρ of B26. Assuming a linear drop of σ_ρ with increasing ρ (dashed line), modeled σ_ρ using the Herron-Langway model with two different starting densities (diamonds) and $\sigma\rho$ when applying the Pimienta model, starting at a density of 550 kg/m^3 (circles). Three different stages of the latter occur due to the set up of the Herron-Langway model (see text). In B the high-resolution density profile of B26 is shown with the resulting σ_ρ (grey). In addition, two exponential fits are indicated - one starting at lower densities (orange line) and the other starting at higher densities (blue line). Due to different rates in densification, the modeled density profiles cross each other and deviate from each other once more below the crossover depth. Towards the density of ice both fits converge. The resulting σ_ρ is plotted with brown dots.

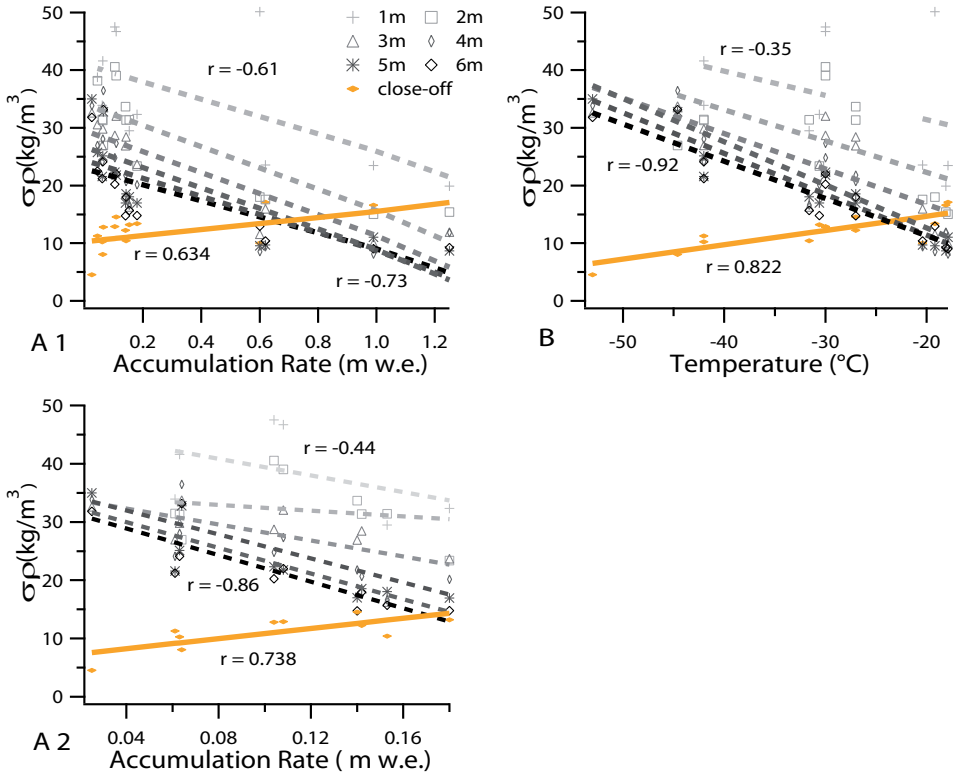

Figure 9. Relationship between σ_ρ at the surface and at close-off densities. Density variability σ_ρ at pore close-off densities (brown line), calculated after equation (4) and σ_ρ at the surface (dashed lines) for depth intervals from 0 (bright grey) to 6 m (dark grey) depth are shown against increasing accumulation rate (A1 and A2) and temperature B. In A1 the whole accumulation rate range of all firn cores is plotted. In A2 the extremely high accumulation rates of the PreIPICS cores are excluded and the new fits are calculated. For increasing accumulation rate and mean annual temperature σ_ρ at the surface is decreasing, whereas $\sigma\rho$ at the pore close-off is increasing.

B Publication 2 - From random deposition to a firn core record - on the impact of impurities on the densification of polar firn -a first approach

In preparation. Hörhold, M. W., Laepple, T., Freitag, J., Kipfstuhl S., Bigler, M. and Fischer, H.

Manuscript prepared for J. Name
with version 3.2 of the LaTeX class copernicus.cls.
Date: 16 December 2010

On the impact of impurities on firn density

M. W. Hörhold, T. Laepple, J. Freitag, S. Kipfstuhl, M. Bigler, and H. Fischer

Alfred Wegener Institute for Polar and Marine Research, Bremerhaven, Germany

Climate and Environmental Physics, Physics Institute, University of Bern and Oeschger Centre for Climate Change Research, University of Bern, Switzerland

Correspondence to: M. W. Hörhold (Maria.Hoerhold@awi.de)

1 Introduction

Ice cores provide highly resolved records of atmospheric parameters for the last 1,000,000 years (EPICA, 2004). Aerosols and dust particles are deposited and incorporated into the ice and allow together with isotopes climate and temperature reconstruction of the past. Together with the enclosure of air into bubbles within the ice during the densification, which provide a direct measurement of former atmospheric composition, these proxies make ice cores a unique climate archive.

At adequate accumulation rates the chemical components, ion concentrations or dust impurities are detected within firn and ice cores with seasonal variability (Fischer et al., 1998; Göktas et al., 2002; Kreutz et al., 1999; Sommer et al., 2000). These seasonal variations are often used to date the cores (Rasmussen et al., 2006).

An improved understanding of the fundamental factors that control the chemistry of a snow or ice sample, the transfer from a surface signal to an ice core record and the densification process with the related air enclosure will allow an even more detailed and accurate interpretation of records, reconstructing past climate conditions. The densification and the evolution of density variability of polar firn is a crucial process which is still not fully understood. Just recently the importance of the exact knowledge of firn densification for analyzing elevation maps over time for mass balance estimates (Li and Zwally, 2002) via remote sensing has been emphasized (Cuffey, 2008; Helsen et al., 2008). To improve the analysis of both, data obtained by remote sensing methods as well as the records measured in ice cores, it is necessary to determine the processes and interactions of chemistry, impurities and physical properties of the firn.

In many applications the density profile is described by continuously increasing 1 meter bulk

densities or approximated by empirical density-depth relationships (Alley et al., 1982; Arnaud et al., 1998, 2000; Arthern and Wingham, 1998; Freitag et al., 2004; Herron and Langway, 1980; Li and Zwally, 2004; Wilhelms, 2000; Zwally and Li, 2002; Salamantin et al., 2009). But the firn column is composed of alternating layers distinguishable in microstructure and density. Snow pit studies deliver detailed observations of the different snow layers, presumably created by seasonal variations in local climate conditions (Alley, 1988; Benson, 1971; Cameron, 1971; Gow, 1965; Koerner, 1971; Kreutz et al., 1999; Palais et al., 1982; Rundle, 1971; Shiraiwa et al., 1996). The density profile in snow pits is supposed to be the most reliable indicator of seasonal variations in the firn (Taylor, 1971; Hori et al., 1999). Accordingly, these seasonal cycles of snow and firn layer density are considered in many applications such as the modeling of firn densification for the validation of air borne mass balance studies (Li and Zwally, 2002; Zwally and Li, 2002; Helsen et al., 2008). In these models it is common to assume an asymptotically decrease of density variability with depth (2002).

However, detailed knowledge about the transfer of surface density variability down the firn column is lacking. It is a common idea that the seasonal variability in polar firn density created at the surface is preserved in the firn and ice column (Kawamura et al., 2006; Landais et al., 2006; Li and Zwally, 2002; Martinerie et al., 1992; Severinghaus and Battle, 2006; Zwally and Li, 2002). The implicit assumption is that the density variation at the surface survives the densification process over the entire firn column and causes measured density variability also at the close-off depth. In return these density fluctuations could impact the bubble enclosure process during close-off (Martinerie et al., 1992; Kawamura et al., 2006; Landais et al., 2006; Severinghaus and Battle, 2006).

The snow deposition is determined by combined effects of the annual cycle in atmospheric processes, irregular surface deposition and erosion and re-distribution disrupting the interpretation of annual layering and diagenetic processes occurring after burial (Palais et al., 1982; Jones, 1983; Fisher et al., 1985). Therefore the interpretation of stratigraphic observations is not straight forward. Because of strongly varying or even missing accumulation, erosion and re-deposition, layers are created, which can obliterate or combine several years of accumulation (Rundle, 1971; Petit et al., 1982). The seasonal variation in the atmosphere is not necessarily displayed in the snow (Wolff et al., 1998; Udisti et al., 2004) and a clear correlation between density variability and isotope signature could not be found yet (Stenberg et al., 1999).

The link between any signal incorporated into the snow and the actual signal that remains in ice cores is unclear (Fisher et al., 1985; Karlöf et al., 2006; Birnbaum et al., 2010). The assumption of a persistent density seasonality throughout the firn column does not necessarily hold. With this study we aim to improve the understanding of densification and the role of impurities in the densification process.

We analyze the evolution of density variability with depth of firn cores from Greenland and Antarctica, obtained from of high-resolution density measurements. We find no seasonal variability in density at the surface but a distinct seasonality in greater depths in high accumulation rate sites.

We hypothesize, that impurities in the snow and firn of polar ice sheets alter the densification and thus the variability of firn density, introducing a seasonal signature with depth. Unfortunately multi-specific ion records do not exist for most of the firn cores in high resolution. Accordingly we concentrate here on seasonal resolution Ca records measured by continuous flow analysis (Röthlisberger et al., 2000; Kaufmann et al., 2008), which are available for an extended set of firn cores. For these cores we study the co-evolution of density and Ca concentration.

2 Method

High resolution density measurements are conducted at 17 firn cores from Greenland and Antarctica (Wilhelms, 1996, 2000; Freitag et al., 2004; Hörhold et al., accepted). The vertical resolution varies between 1-5 mm. The firn cores cover a broad range in annual mean temperature and accumulation rate. Position of the cores can be found in table one. The density is measured using a non-destructive logging system including a Löffel densimeter. Details are given in Wilhelms (1996; 2000).

We further more use high resolution ion measurements from continuous flow analysis (CFA) (Röthlisberger et al., 2000; Sommer et al., 2000; Kaufmann et al., 2008). The measurements of the firn cores B31, B32, and B33 from Dronning Maud Land, Antarctica were carried out at Neumeyer Station (Sommer et al., 2000; Göktas et al., 2002). Further more two unpublished data sets from firn cores from Greenland are analyzed. The CFA measurements were conducted at the cold laboratory at the Alfred-Wegener-Institute, Bremerhaven, Germany and at the University of Bern, Switzerland. For analysis we restrict ourself to the Ca ion which is usually deposited with a seasonal amplitude (Ruth et al., 2004).

Core breaks and core cuts are manually removed from the density datasets. A small number of outliers (<1%) are removed from the Ca datasets by visually investigating the histogram. Ca concentrations are analyzed on a logarithmic scale, as the concentration values follow a log-normal distribution. The density and chemistry data are transferred to the water equivalent (w.e.) depth scale and averaged to 5 mm w.e. mean values. Low frequency variations in the density records are removed using a finite response highpass filter (cutoff frequency for B38 and B39 0.2 m w.e., 0.5 m w.e. for all other cores). The depth dependence of the density variability and that of the Ca-density relationship are analyzed on a 5 m w.e. sliding window. For this analysis, the statistics standard deviation as a measure of variability and Pearson correlation as a measure for the Ca-density relationship are used. As the density and Ca analysis were performed on different measurement devices, a slight depth uncertainty between both measurements cannot be excluded. This is accounted for by calculating the maximum cross correlation in a 50mm w.e. window instead of a single correlation estimate. The statistical significance of the running correlation, including the depth uncertainty, is determined by a Monte Carlo experiment. Therefore, the chemistry data was replaced by surrogate data with the same autocovariance structure, and the correlation analysis is repeated 10000 times.

To analyze the depth dependent behavior of density and chemistry in the frequency domain, we estimate the wavelet sample spectrum using the Morley wavelet (*sowas* package (Maraun and Kurths, 2004; Maraun et al., 2007)). Wavelet analysis is a common tool for analyzing localized variations of power within a data series (Torrence and Compo, 1998), even if the dominant modes of variability are non-stationary. It is therefore perfectly suited for our application in which we seek to identify annual cycles and their dependence on firn depth. Pointwise significant areas against a white noise background spectrum are estimated using Monte Carlo experiments (Maraun et al., 2007). However, one must note that pointwise significance testing will result in a large of spurious significant patches, as a wavelet transform contains multiple testing, and adjacent areas in the wavelet sample spectrum are not independent (Maraun et al., 2007), (also see Supplement Figure 1). The results are not sensitive on the choice of the interpolation resolution (1-10 mm), the lowpass filtering method (Finite response filter, or spline fit) and the cutoff frequency. To investigate potential artifacts caused by the calculation process (transfer to water equivalent scale, interpolation, filtering and statistical analysis on a moving window), we additionally perform the complete calculation process on a surrogate dataset. This consists of the B19 ice core data with density values replaced by a random timeseries with the same autocovariance structure as the B19 density. The results (Supplement Figure 1) show that our statistical procedure does not produce any artifacts.

3 Results

3.1 Density Variability

To investigate the densification process we analyze the evolution of the density variations with depth. The variability is first analyzed on the firn core B29 from Central Greenland, that exhibits a 0.15 m w.e./a accumulation rate (Figure 1).

The strength of the density variability, calculated as standard deviation in a 5 m w.e. sliding window, is decreasing with depth to roughly 40 $\%$ of its initial standard deviation (Figure 1, top panel). This variability minimum is found at a mean density of 600-650 kg/m^3 corresponding to 12 m w.e. depth. Below this depth the variability increases again, obtaining a second peak around 30 m w.e. depth. At depths and densities of the firn-ice transition (820-840 kg/m^3) the variability is still high, until it vanishes at the mean density of ice.

This rapid drop of variability from the top of the core down to a variability minimum and the following increase to second maximum presumably results from the fast densification of initially low density layers (Gerland et al., 1999; Freitag et al., 2004; Fujita et al., 2009; Hörhold et al., accepted). This behavior was found for all firn cores investigated in this study (Hörhold et al., accepted).

To analyze the evolution of the density in the frequency domain and to investigate if the annual cycle can be detected, a wavelet analysis is applied to the B29 core (Figure 1, lower panel). At the surface, the signal covers a broad range in the frequency domain. With increasing depth the vari-

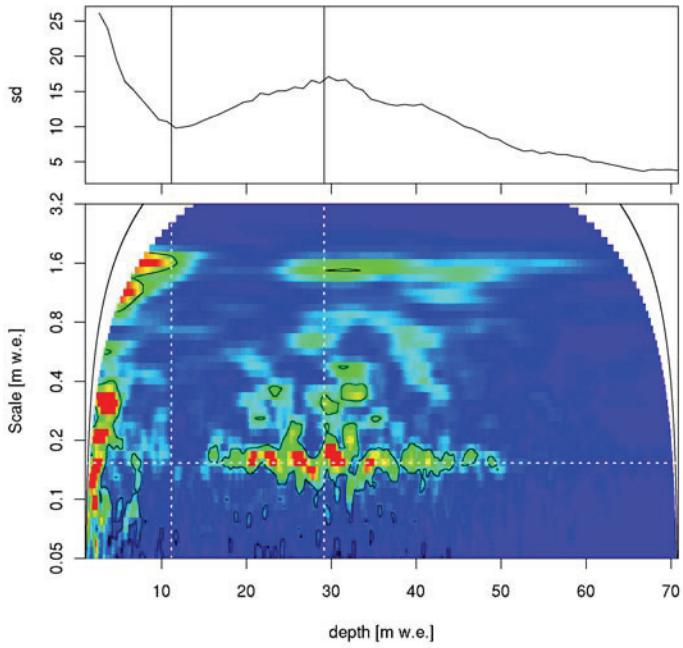

Fig. 1. Depth dependence of the density variability (upper panel) and wavelet spectrum of the density (lower panel) of the B29 firn core from Greenland. The minimum and secondary maximum of the density variability are marked with vertical lines. In the wavelet spectrum, the scale corresponding to the accumulation rate (horizontal line) and pointwise significant areas (black contours) are marked. At the surface, the density exhibits strong variability spread over a large range of frequencies. Below a density minimum at around 12m w.e. a secondary variability maximum is detected at around 30 m w.e. depth. At this depth, the main density variations are concentrated at the frequency of the accumulation rate.

ability decreases at all frequencies. The area of minimum variability and therefore low amplitudes in the frequency spectrum, represents the depth interval, where the difference in density between the different layers is minimal. Below, at approximately 15 m w.e. depth, a distinct signal at the frequency of the accumulation rate of the firn core is found. This signal shows the maximum amplitude at around 30 m w.e. depth which is simultaneous with the overall second maximum in density variability (Figure 1, top panel).

This maximum in seasonal density variations at 30 m w.e. depth is particulary remarkable, as no seasonal density signal was detected at the surface. Thus, the development of the seasonality in the firn density takes place below the column that is influenced by the seasonal cycle of temperature and related climate variables.

The behavior of the firn density variability is not limited to the firn core B29 but is found in most

of the cores investigated in this study. Therefore the same wavelet analysis is applied to all 17 firn cores (Figure 3, 4 and Supplement Figure 2). In the following wavelet spectra, the depths, at which the minimum and the second maximum in density variability occur, are indicated with a vertical dashed line, the variability itself is not shown.

In almost all cores, the density variability at the surface is distributed over a broad range of frequencies. Only at firn core B26 a distinct peak in intensity at the accumulation rate is observed at the surface. The B20, B25 and B29 firn cores show a broad frequency signal at the surface, including the frequency of the accumulation rate.

In all cores, the surface signal is followed by a zone with a minimum in density variability. In many cases this zone is followed by an interval, where a distinct signal in the frequency of the accumulation rate appears (B16, B17, B26, B29, B38 and B39 towards the end of the record, Figure 3, 4 and Supplement Figure 2). Other cores show patches and islands with pointwise significantly increased intensities around the frequency of the accumulation rate (B18, B20, B21, B25, B32 and B36). The EDC2, B31 and B33 firn cores do not show a significant intensity at any frequency, apart from the surface signal (Supplement Figure 2). The maximum in intensity occurs at the depth of the second maximum density variability.

It appears that the occurrence of significant intensity of the frequency of the accumulation rate at the depth of the second maximum in density variability is linked with the amount of accumulation. Firn cores with a relatively high accumulation rate, such as the B38 and B39 firn cores from Antarctica and the B16, B17, B26, B29 firn cores from Greenland (all with accumulation rates larger than 0.142 m w.e./a) show a significant intensity of the frequency of the accumulation rate at the second maximum in density variability. Firn cores with relatively low accumulation rates such as the EDC, B31-B33 and B36 cores from Antarctica (all with accumulation rates smaller than 0.067 m w.e./a) do not show any increased intensity at the depth of second maximum variability in density. The Greenland cores with relatively moderate accumulation rates around 0.1 m w.e./a as well as the B25 core from Antarctica with a relatively high accumulation rates of 0.14 m w.e./a show no clear peak in intensity of the frequency of accumulation rate but patches with increased intensities at several frequencies at the depth of the second maximum in density variability.

Our finding, that in many cores seasonal variations in density develop with depth, question the the origin of the annual cycle in density. Since it can be excluded, that a new property is introduced into the firn at the depth where the seasonality is developing, we must consider a parameter, which is deposited at the surface, preserved in the firn column and altering the densification of the firn. Impurities could be a candidate as they are often deposited with the snow and exhibit a seasonal varying concentration. To test this hypothesis we analyze the high-resolution Ca concentration profiles of 5 firn cores. Our choice of Ca is simply due to the fact that Ca is the impurity parameter for which the largest amount of measurements were available.

3.2 Link between density- and Ca concentration variability

To visualize the Ca concentration and density profiles in detail, short intervals from three stages of the core B29 are shown (Figure 2). The correlation coefficient between density and Ca concentration is displayed for comparison. The first interval from the surface is characterized by high variability in density and no relationship between density and chemistry variability is observed (Figure 2, upper panel). The density shows chaotic fluctuations and no correlation to the Ca concentration record can be detected (panel A). The second interval from the approximately 12 m w.e. depth is characterized by minimum density variability (Figure 2, upper panel) and a significant correlation with Ca concentration variability is visible (Figure 2, panel B). At the third interval from approximately 30 m w.e. depth, both, the variability as well as the Ca concentration-density relationship reach a maximum (Figure 2, upper panel and panel C). At the B29 firn core the correlation between density and Ca concentration increases with depth and reaches a maximum at the second maximum of density variability.

We further analyze the Ca concentration-density relationship for the firn cores B20, B31, B32 and B33 and (Figure 3 and 4). All five firn cores show an increase in density-Ca concentration correlation with depth, and a significant correlation at the depth of the second maximum in density variability (Figure 3 and 4, upper panel).

For the Greenland cores, with relatively high (B29 with 0.15 m w.e./a) and medium accumulation rate (B20 with 0.1 m w.e./a) the correlation between density and Ca concentration is distinct (Figure 3, upper panel). In firn core B29 the accumulation rate frequency is clearly detected in the chemistry profile for all depths (Figure 3, lowermost panel). In the density profile the accumulation rate frequency develops with depth and appears at the variability maximum (Figure 3, mid panel). B20 does not show the accumulation rate frequency in the chemistry or density variability profile (Figure 3, lowermost panel), but nevertheless a significant Ca concentration-density correlation is developed (Figure 3, upper panel).

For the Antarctic firn cores B31 - B33 with accumulation rates of 0.044 - 0.063 m w.e./a the Ca concentration-density relationship is not as high but still significant (Figure 4, upper panel). A significant signature of accumulation rate frequency can not be detected in the density variability wavelet (Figure 4, mid panels). The Ca concentration variability wavelet does show significant intensity close to the frequency of the accumulation rate, but not clear (Figure 4, lowermost panels).

4 Discussion

The wavelet analysis can help to study the evolution of the density variability with depth and to detect an annual cycle in the variations. The presented results questions the seasonality of snow layers at the surface as they are often reported from snow pit studies. Most of the firn cores do not show a distinct signal of accumulation rate frequency in the density variability at the surface. This

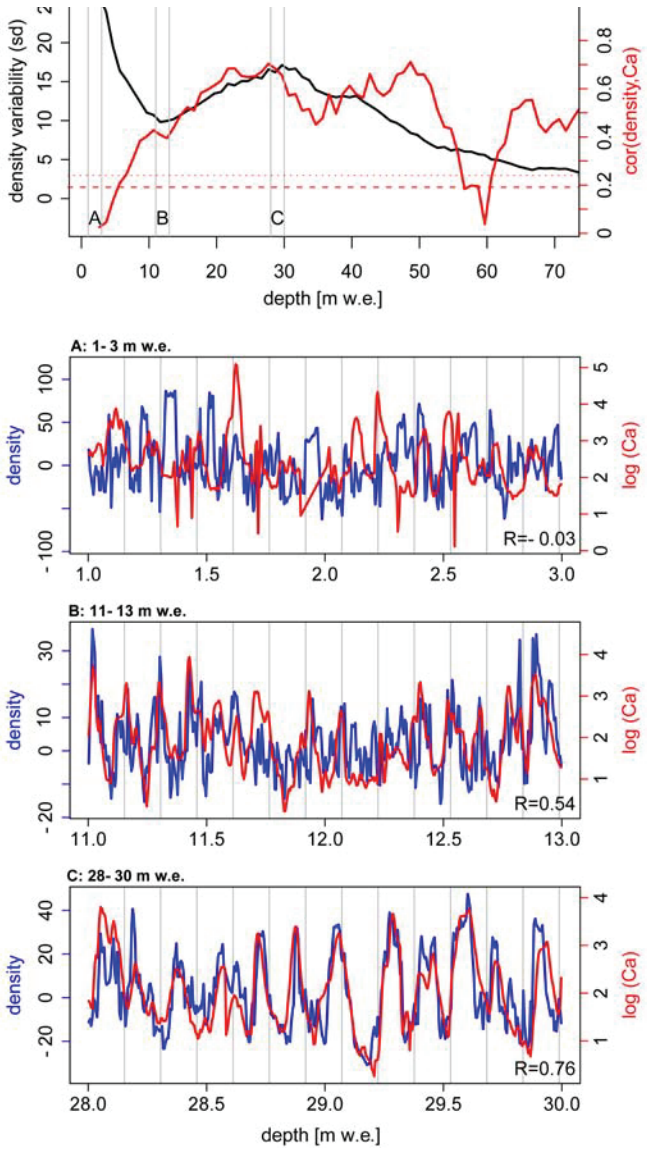

Fig. 2. Density-Ca relationship of the B29 firn core. The density variability (black line) and the correlation between density and Ca concentration (red line) are shown in the upper panel. Horizontal lines mark the 95% (dashed) and 99% (dotted) confidence intervals of the correlation. The lower panels A-C show detailed profiles of the density and Ca evolution in the depth intervals marked in the upper panel (vertical grey lines). The correlation values of the shown depth intervals are given in the panels. At the surface (A), high density variability and no correlation are detected. At the minimum of density variability (B) a positive correlation between density and Ca concentration is found that increases at the secondary maximum of density variability (C).

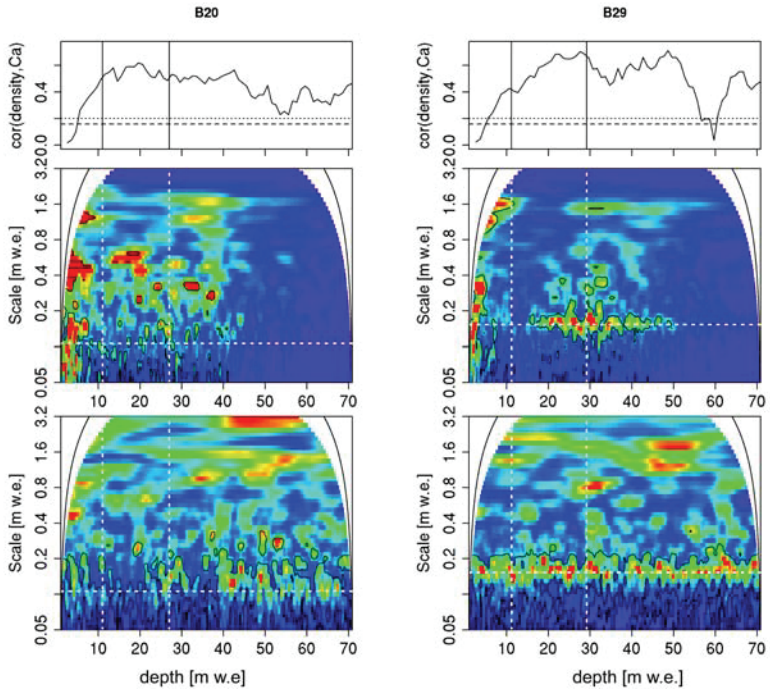

Fig. 3. Density-Ca relationship (upper panel) and wavelets spectra of density (middle panel) and Ca concentration (lower panel) of the B20 and B29 firn cores. The minimum and secondary maximum of the density variability are marked with vertical lines. In the wavelet spectra, the scale corresponding to the accumulation rate (horizontal line) and pointwise significant areas (black contours) are marked. In both cores, the density variability evolves from random variations at the top, to a variance minimum at around 12 m w.e. and to a secondary maximum in density variations concentrated around the accumulation rate in greater depths. The spectrum of the Calcium concentration is less depth dependent and shows variability at the accumulation rate in all depths. The correlation between density and Ca changes from no correlation at the surface to strong correlation values between 10-50 m w.e.depth.

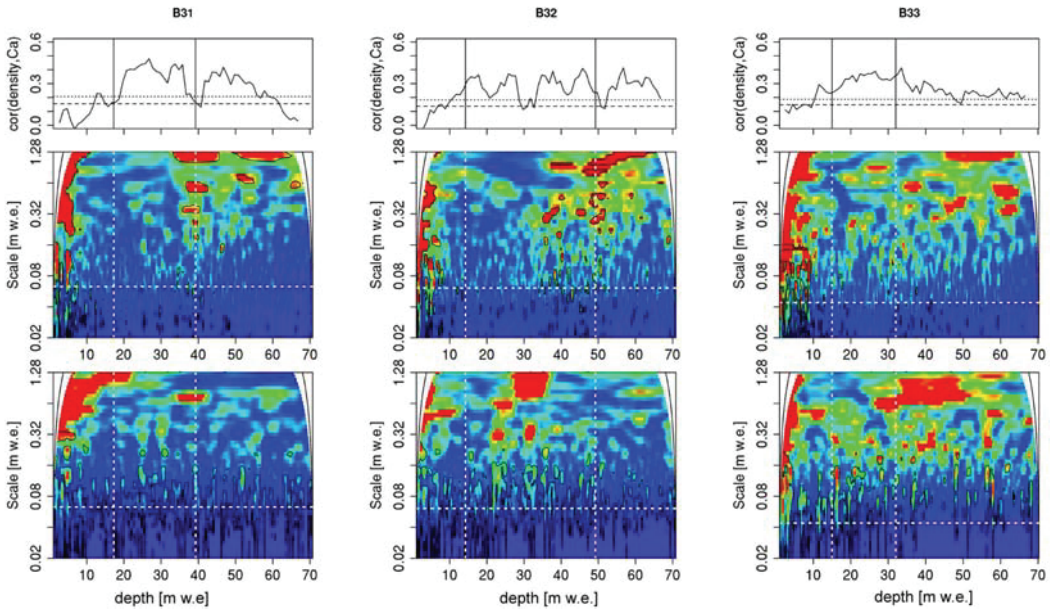

Fig. 4. As Fig.3 but for Antarctic cores B31, B32 and B33. In all cores, a significant correlation between density and Calcium is detected in depths deeper than the density variability minimum, although the density-Ca relationships are weaker than in the Greenland cores (Fig 3). The density and Ca variability are not confined to the frequency of the accumulation rate. This might be caused by a strong interannual variability in accumulation.

indicates, that in the near surface snow no seasonal variability in the density is apparent. This is in line with the observation by Stenberg et al (1999), who did not find a relation between seasonally varying isotope measurements and density profiles in snow pit analysis. Also at Dome Fuji the density variability did not reflect seasonal variations (Hori et al., 1999). This might be the result of discontinuous precipitation through the year as well as redistribution and erosion of deposited surface snow by wind. The interaction between wind and unbounded particles at the snow surface controls the initial density of the snow. The meteorological data show no clear seasonal signal in wind speed at almost all locations (Birnbaum et al., 2010). Furthermore the rough surface introduces a high spatial variability of patches with different density. Therefore it can be assumed that at most sites the initial density has no annual cycle. The post depositional snow metamorphism is driven by temperature and temperature gradients with an inherent clear annual cycle. However, this seasonality seems to be not imposed on the density variations because of their strong dependence on initial density.

The wavelet analysis also delivers surprising results about the evolution of the variability with depth. For all firn cores we find rapid drop in density variability until a minimum, displayed by the blank zone within the power spectra at approximate 10 - 12 m depth w.e. (Figure 1 and Supplement

Figure 2). Below, the amplitude in variability increases again, but with different frequencies. We observe, that at some firn cores, the increased density variability in greater depths, shows the frequency of the accumulation rate, and thus a seasonal variability. This is in contrast to Li and Zwally (2002, 2004), who state that the seasonal variability in density, created at the surface is kept all the way down, while the amplitude is reduced with depth. Our results imply, that the seasonality is developing with depth at these sites, even though no seasonal frequency is apparent at the surface. This could be a hint, that the density records partly loose their memory of density fluctuations from the surface. With our results the assumption of a seasonal varying density which is preserved in the firn and ice column, cannot be confirmed.

We also observe, that mainly sites with moderate to high accumulation rates show this development of a seasonal frequency with depth (Supplement Figure 2). This indicates, that the appearance of the accumulation rate frequency in greater depths is related to the magnitude and variability of the accumulation rate. At sites with high and stable accumulation rates, the seasonal variability develops with depth, whereas sites with low or varying accumulation rates do not show this pattern.

4.1 Why is a seasonal frequency created with depth?

The presented data do not allow a sufficient analysis of the reason for the observed development of seasonality with depth. We can only compare the high-resolution density data in terms of local climate conditions, the appearance and intensity of the seasonality with depth and a few Ca concentration profiles. Nevertheless we start here a preliminary discussion on possible mechanism, since the question is important for the analysis and interpretation of density-related properties such as the air content in bubbly ice.

The Ca concentration exhibits a strong increasing correlation with density with increasing depth. This correlation does not necessarily reflect the causal reason of the increase of seasonality in density with depth. Any parameter present with seasonal variability in the firn could cause the observed change in the density variability frequency. Possible candidates, which could alter the firn densification, are impurities or the microstructure of the snow layers itself, i. e. grain size. In the following we discuss the likelihood of grain size, and impurities altering firn density. We consider the Ca concentration as a proxy, representing an unknown parameter, which is deposited with a similar frequency as the Ca concentration.

Microstructural properties such as the grain size and coordination number are considered as parameters influencing the densification (Alley et al., 1982; Alley, 1987; Salamatin and Lipenkov, 2008; Salamantin et al., 2009). Coarse firn is characterized by low density and few large connections to neighbors and densifies faster than fine firn, characterized by high density and high connectivity (Alley et al., 1982). If grain size shows seasonal variations it could be a possible reason for the observed development of seasonality in density with depth. There are observations from snow pits, linking microstructure properties to distinct seasons. For example, depth hoar layers formed in fall

or spring could carry another chemical composition and concentration then fine grained snow from either winter deposition (Jones, 1983) or summer deposition (Koerner, 1971; Gow, 1965; Birnbaum et al., 2010). However, microstructure seems to be closely linked to density. The starting density and a related coordination number of the grains leads to a different extent of the interval at which grain boundary sliding acts as mean densification regime (Alley, 1987; Salamantin et al., 2009). Further more a strong linear relationship between density and coordination number in polar firn has been found by Freitag et al. (2008), indicating that single layers are characterized by specific grain size, coordination number and density. These findings question the independence of grain size and density as physical properties of the upper polar firn layers. Additionally recent findings on irregular grain boundaries and changing grain size distributions with depth in polar firn indicate dynamic recrystallization to happen at all depth intervals in the firn column (Kipfstuhl et al., 2009). This implies that the firn microstructure is not stationary but changes continually with depth and thus does probably not carry a seasonal signal in greater depths. If grain size and density are related to each other in the surface firn, and if the grains undergo dynamic recrystallization, grain size must be questioned as the parameter introducing seasonality in the density variability at greater depth.

Polar firn impurities on the other hand consists of soluble contents and micro-particles and both can be thought to alter the density of the firn. The impact of micro-particles, i.e dust concentration, on the physical firn properties has been observed earlier (Svensson et al., 2005). The impact of soluble chemistry on the snow and firn properties has been investigated only for surface snow.

For deeper firn and ice the impact of impurities on the grain growth (grain boundary migration) has been shown in theory (Alley et al., 1986a,b). Impurities and inclusions such as micro particles or air bubbles can hinder the migration of grain boundaries and therefore reduce the rate of grain growth. This altered grain growth might have an impact on the density of single firn layers. From deep ice core observations of grain size and dust concentrations it seems, that depth intervals with high dust concentration, correlated with high Ca concentrations, show smaller grain sizes and a higher degree of deformation than depth intervals with lower dust concentration (Svensson et al., 2005). On the other hand the theory and ice core observations hold for matrices of ice crystals, with contact areas all around each grain. So it is questionable if these processes are relevant for the highly porous snow and firn at the surface, where much more mobility and degrees of freedom of the snow grains and ice cluster is possible.

From Snow-Air Interaction studies it is known, that due to its high porosity much of the snow pack volume consists of air that can be readily exchanged. Numerous physical and chemical processes can affect trace gases in the snow pack (Domine and Shepson, 2002). There is a lack of knowledge of the physical and chemical nature of natural ice surfaces. A disordered layer, often called the quasi-liquid layer, exists on ice surfaces and its thickness increases with temperature and ion solute concentration (Domine and Shepson, 2002).

In principle there are two ways how an increased solute concentration may influence the interme-

diate densification below 12 m w.e. depth and the bubble close-off. Doping the individual (mono-crystalline) snow grains with ionic impurities generally increases the ductility of ice, i.e. its creep (Kang, 2005). Thus, layers with higher impurity content can in principle densify faster.

Alternatively, a higher impurity content at the grain boundaries and triple junctions should increase the thickness of the quasi-liquid layer coating individual grains. The migration of this quasi-liquid by capillary forces has been hypothesized to contribute to the sintering process during firn densification (Dash, 1989; Dash et al., 2006). Again a high impurity content at the grain boundaries would lead to an acceleration of the densification process. A detailed theoretical assessment of these phenomena is beyond the scope of this paper, however, recent studies of the location of impurities in poly-crystalline ice point to larger impurity concentrations at the grain boundaries and smaller ones in the bulk of the snow grains. Obviously this is dependent on the ionic species considered but overall could support the quasi-liquid layer effect to be a possible explanation for the observed faster densification of high impurity layers in polar firn.

Both, increased micro-particle or soluble component concentration could change the properties of the firn in terms of density. It seems possible, that firn layers carrying more impurities densify faster, than firn with layers with less impurities. Such a trend can be detected in the presented data: Layers with a high Ca concentration are correlated with high density values and vice versa (Figure 2, lowermost panel). But the mechanism for the impact of impurities on the density of the firn ca not be detected within this study.

On the base of the presented results we hypothesize that seasonally deposited chemical impurities lead to the observed signal of the accumulation rate frequency in the Ca concentration wavelet (for example B29). This Ca concentration variability with its specific frequency will be superposed on the density variability, leading to the observed intensity peak in accumulation rate frequency at greater depths. All of the five firn cores, where Ca concentration measurements are available show a significant increasing Ca concentration-density correlation with increasing depth.

But since the three Antarctic cores do not show a distinct peak in the frequency of the accumulation rate in their density variability wavelet, we assume, that the temporal variability of accumulation rate determines, whether a seasonal signal in chemical impurity concentration is influencing the density profile. Sites with high accumulation rates and with relatively small inter-annual variability in accumulation rate show a seasonal deposition of chemical components, which will be superposed on the density variability. If accumulation rate is small or shows a large variability, even a seasonal chemistry deposition would not lead to a accumulation rate frequency in the depth domain. Nevertheless a coherent density and chemistry variability relationship is found below the minimum in density variability, indicating the impact of impurities on the density of polar firn.

5 Summary and Conclusion

We observe 1. that a seasonal signal in density develops with depth, 2. the correlation between density and Ca concentration develops with depth and conclude 3. that impurities or a yet unknown parameter incorporated into the snow with the same frequency as the Ca concentration, alters the firn densification. The snow density variability at the surface is rather random and only for some sites inhabits a seasonal signal. The density variability at the firn-ice-transition shows a seasonal signal at some sites, but this seasonality has developed with depth and does not originate from the surface. Either impurities or any parameter with likewise frequency in deposition does alter the firn densification.

At densities and depths of the firn-ice transition we find increased variability in density. This density varies with a seasonal frequency (Supplement Figure 2, B16, B17, B26, Figure 1,B29). So one could indeed identify layers, which show a summer or winter signal, as is commonly assumed (Landais et al., 2006; Severinghaus and Battle, 2006; Kawamura et al., 2006). However, the variability and thus the distribution in high and low density layers is not a result of density distribution at the surface. The density variability at the firn-ice-transition seems to be the result of unknown process altering the density during burial and accordingly a link to original surface characteristics in terms of density is not possible. The assumption of a direct link to surface conditions, governing the layering and density variability at the firn-ice transition is not confirmed.

Our findings have also important ramifications on the cause of precessional O_2/N_2 variations found in records derived from air bubbles in polar ice (Bender, 2002; Kawamura et al., 2007). Those variations are caused by a size dependent fractionation during the bubble close-off (Severinghaus and Battle, 2006). Since the density signal looses its initial stratigraphic information completely in the top 10 - 15 m of the firn column, a direct line of influence of the local radiation balance on the surface snow density cannot be the ultimate reason for the observed O_2/N_2 fractionation at close-off depth.

Acknowledgement.

References

Alley, R. B.: Firn densification by grain-boundary sliding: a first model, in: VIIth Symposium on the Physics and Chemistry of Ice, Journal de Physique, vol. 48, pp. 249–254, 1987.

Alley, R. B.: Concerning the deposition and diagenesis of strata in polar firn, Journal of Glaciology, 34, 1988.

Alley, R. B., Bolzan, J. F., and Whillans, I. M.: Polar firn densification and grain growth, Annals of Glaciology, 3, 7–11, 1982.

Alley, R. B., Perepezko, J. H., and Bentley, C. R.: Grain Growth in Polar Ice: 1. Theory, Journal of Glaciology, 32, 415–424, 1986a.

Alley, R. B., Perepezko, J. H., and Bentley, C. R.: Grain Growth in Polar Ice: 2. Application, Journal of Glaciology, 32, 425–433, 1986b.

Arnaud, L., Lipenkov, V., Barnola, J.-M., Gay, M., and Duval, P.: Modelling of the densification of polar firn: characterization of the snow-firn transition, Annals of Glaciology, 1998.

Arnaud, L., Barnola, J.-M., and Duval, P.: Physical modelling of the densification of snow/firn and ice in the upper part of polar ice sheets, 26, 285–305, 2000.

Arthern, R. J. and Wingham, D. J.: ....Geodetic Determination of Ice Sheet Mass Balance, Climatic Change, 40, 605–624, 1998.

Bender, M. L.: Orbital tuning chronology for the Vostok climate record supported by trapped gas composition, Earth and Planetary Science Letters, 204, 275–289, 2002.

Benson, C. S.: Stratigraphic studies in the snow at Byrd station, Antarcitca, compared with similar studies in Greenland, Antarctic Research Series, Antartic snow and ice studies 2, 2, 333–353, 1971.

Birnbaum, G., Freitag, J., Brauner, R., König-Langlo, G., Fischer, E., Kipfstuhl, S., Oerter, H., Reijmer, C., Schlosser, E., Faria, S. H., Ries, H., Loose, B., Herber, A., Duda, M. G., Powers, J. G., W., M. K., and van den Broeke, M.: Strong-wind events and their influence on the formation of snow dunes: Observations from Kohnen Station, Dronning Maud Land, Journal of Glaciology, 2010.

Cameron, R. L.: Glaciological studies at Byrd Station, Antarctica, 1963-1965, Antarctic Research Series, Antarctic Snow and Ice Studies 2, 2, 317–332, 1971.

Cuffey, K. M.: A Matter of Firn, Science, 320, 1596–1597, 2008.

Dash, J., Rempel, A. W., and Wettlaufer, J. S.: The physics of premelted ice and its geophysical concequences, Reviews of modern physics, 78, 695–741, 2006.

Dash, J. G.: Surface melting, Contemporary Physics, 30, 89–100, 1989.

Domine, F. and Shepson, P. B.: Air-Snow Interactions and Atmospheric Chemistry, Science, 297, 1506–1510, 2002.

EPICA, c. m.: Eight glacial cycles from an Antarctic ice core, Nature, 429, 623–628, 2004.

Fischer, H., Wagenbach, D., and Kipfstuhl, J.: Sulfate and nitrate firn concentrations on the Greenland ice sheet 1. Large-scale geographical deposition changes, Journal of Geophyscial Research, 103, 21 927–21 934, 1998.

Fisher, D., Reeh, N., and Clausen, H. B.: Stratigraphic noise in time series derived from ice cores, Annals of Glaciology, 7, 76–83, 1985.

Freitag, J., Wilhelms, F., and Kipfstuhl, S.: Microstructure-dependent densification of polar firn derived from X-ray microtomography, Journal of Glaciology, 30, 243–250, 2004.

Freitag, J., Kipfstuhl, S., and Faria, S. H.: The connectivity of crystallite agglomerates in low-density firn at

Kohnen station, Dronning Maud Land, Antarctica, Annals of Glaciology, 49, 114–120, 2008.

Fujita, S., Okuyama, J., Hori, A., and Hondoh, T.: Metamorphism of stratified firn at Dome Fuji, Antarctica: A mechanism for local insolation modulation of gas transport conditions during bubble close off, Journal of Geophysical Research, 114, 2009.

Gerland, S., Oerter, H., Kipfstuhl, J., Wilhelms, F., Miller, H., and Miners, W. D.: Density log of a 181m long ice core from Berkner Island, Antarctica, Annals of Glaciology, 29, 215–219, 1999.

Göktas, F., Fischer, H., Oerter, H., Weller, R., Sommer, S., and Miller, H.: A glacio-chemical characterization of the new EPICA deep-drilling site on Amundsenisen, Dronning Maud Land, Antarctica, Annals of Glaciology, 35, 347–354, 2002.

Gow, A. J.: On the accumulation and seasonal stratification of snow at Sout Pole, Journal of Glaciology, 5 (40), 467–477, 1965.

Helsen, M. M., van den Broeke, M. R., van den Wal, R. S. W., van de Berg W. J., van Meijgaard E., Davis, C. H., Li, Y., and Goodwin, I.: Elevation Changes in Antarctica Mainly Determined by Accumulation Variability, Science, 320, 1626–1629, 2008.

Herron, M. M. and Langway, C. C.: Firn Densification: An Empirical Model, Journal of Glaciology, 25, 373 – 385, 1980.

Hörhold, M. W., Kipftuhl, S., Wilhelms, F., Freitag, J., and Frenzel, A.: The densification of layered polar firn, Journal of Geophysical Research, accepted.

Hori, A., Tayuki, K., Narita, H., Hondoh, T., Fujita, S., Kameda, T., Shoji, H., Azuma, N., Kamiyama, K., Fujii, Y., Motoyama, H., and Watanabe, O.: A detailed density profile of the Dome Fuji (Antarctica) shallow ice core by X-ray transmission method, Annals of Glaciology, 29, 211–214, 1999.

Jones, D.: Snow stratigraphy observations in the katabatic wind region of eastern Wilkes Land, Antarctica, ANARE Research Notes, 17, 1983.

Kang, S.-J. L.: Sintering - Densification, Grain Growth and Microstructure, Butterworth-Heinemann, Elsevier Science Ltd. Linacre House, Jordan Hill, Oxford, POX2 8DP, England, 2005.

Karlöf, L., Winebrenner, D. P., and Percival, D. B.: How representative is a time series derived from a firn core? A study at a low accumulation site on the Antarctic plateau, Journal of Geophysical Research, 111, 2006.

Kaufmann, P., Federer, U., Hutterli, M. A., Bigler, M., Schpbach, S., Ruth, U., Schmitt, J., and Stocker, T. F.: An improved Continuous Flow Analysis (CFA) system for high-resolution field measurements on ice cores, Environmental Science and Technology, 42, 8044–8050, 2008.

Kawamura, K., Severinghaus, J. P., Ishidoya, S., Sugawara, S., Hashida, G., Motoyama, H., Fujii, Y., Aoki, S., and Nakazawa, T.: Convective mixing of air in firn at four polar sites, Earth and Planetary Science Letters, 244, 672–682, 2006.

Kawamura, K., Parrenin, F., Uemura, R., Vimeux, F., Severinghaus, J. P., Hutterli, M. A., Nakazawa, T., Aoki, S., Jouzel, J, a. R. M. E., Matsumoto, K., Nakata, H., Motoyama, H., Fujita, S., Goto-Azuma, K., Fujii, Y., and Watanabe, O.: Northern Hemispheric forcing of climatic cycles in Antarctica over the past 360,000 years, Nature, 448, 912–917, 2007.

Kipfstuhl, S., Faria, S. H., Azuma, N., Freitag, J., Hamann, I., Kaufmann, P., Miller, H., Weiler, K., and Wilhelms, F.: Evidence of dynamic recrystallization in polar firn, Journal of Geophysical Research, 114, 2009.

Koerner, R. M.: A stratigraphic method of determining the snow accumulation rate at Plateau Station, Antarctica and application to South Pole - Queen Maud Land Traverse 2, 1965-66, Antarctic Research Series, Antarctic Snow and Ice Studies 2, 16, 225–238, 1971.

Kreutz, K. J., A., M. P., Twickler, M. S., Whitlow, S. I., White, J. W. C., Shuman, C. A., Raymond, C. F., Conway, H., and McConnell, J. R.: Seasonal variations of glaciochemical, isotopic and stratigraphic properties in Siple Dome (Antarctica) surface snow, Annals of Glaciology, 29, 38–44, 1999.

Landais, A., Barnola, J. M., Kawamura, K., Caillon, N., Delmotte, M., Van ommen, T., Dreyfus, G., Jouzel, J., Masson-Delmotte, V., Minster, B., Freitag, J., Leuenberger, M., Schwander, J., Huber, C., Etheridge, D., and Morgan, V.: Firn $\delta^{15}N$ in modern polar sites and glacial-interglacial ice: a model-data mismatch during glacial period in Antarctica?, Quaternary Science Reviews, 25, 49–62, 2006.

Li, J. and Zwally, H. J.: Modeled seasonal variations of firn density induced by steady-state surface air-temperature cycle, Annals of Glaciology, 34, 299–302, 2002.

Li, J. and Zwally, H. J.: Modeling the density variation in the shallow firn layer, Annals of Glaciology, 38, 309–313, 2004.

Maraun, D. and Kurths, J.: Cross Wavelet Analysis: Significance Testing and Pitfalls, Nonlinear Processes in Geophysics, 11(4), 505–514, 2004.

Maraun, D., Kurths, J., , and Holschneider, M.: Nonstationary Gaussian Processes in Wavelet Domain: Synthesis, Estimation and Significance Testing, Physical Review, E 75, 016 707, 2007.

Martinerie, P., Raynaud, D., Etheridge, D. M., Barnola, J.-M., and Mazaudier, D.: Physical and climatic parameters which influence the air content in polar ice, Earth and Planetary Science Letters, 112, 1–13, 1992.

Palais, J. M., Whillans, I. M., and C., B.: Snow stratigraphy studies at Dome C, East Antarctica: an investigation of depositional and diagenetic processes, Annals of Glaciology, 3, 239–242, 1982.

Petit, J. R., Jouzel, J., Pourchet, M., and Merlivat, L.: A detailed study of snow accumulation and stable isotope content in Dome C (Antarctica), Journal of Geophysical Research, 87 NO. C6, 4301–4308, 1982.

Rasmussen, S. O., Andersen, K. K., Svenson, A., Steffensen, J. P., Vinther, B., Clasuen, H. B., Siggaard-Andersen, M.-L., Johnson, S. J., Larsen, L. B., Bigler, M., Röthlisberger, R., Fischer, H., Goto-Azuma, K., Hansson, M. E., and Ruth, U.: A new Greenland ice core chronology for the last glacial termination, Journal of Geophysical Research, 111, 2006.

Röthlisberger, R., Bigler, M., Hutterli, M., Sommer, S., Stauffer, B., Junghans, H. G., and Wagenbach, D.: Technique for continous high resolution flow analysis of trace substances in firn and ice cores, Environmental science and Technology, 111, 338–342, 2000.

Rundle, A. S.: Snow accumulation and firn stratigraphy on the East Antarctic Plateau, Antarctic Research Series, Antarctic Snow and Ice Studies 2, 16, 239–255, 1971.

Ruth, U., Wagenbach, D., Mulvaney, R., Oerter, H., Graf, W., Pulz, H., and Littot, G.: Comprehensive 1000 year climatic history from an intermediate depth ice core from the south dome Berkner Island, Antarctica: methods, dating, and first results, Annals of Glaciology, 39, 146–154, 2004.

Salamantin, A. N., Lipenkow, V. Y., Barnola, J. M., Hori, A., Duvan, P., and Hondoh, T.: Snow/Firn Densification in Polar Ice Sheets, Physics of Ice Core Records II, Supplement Issue, 68, 195–222, 2009.

Salamatin, A. N. and Lipenkov, V. Y.: Simple relations for the close-off depth and age in dry-snow densification, Annals of Glaciology, 49, 71–76, 2008.

Severinghaus, J. P. and Battle, M. O.: Fractionation of gases in polar ice during bubble close-off: New constrains from firn air Ne, Kr and Xe observations, Earth and Planetary Science Letters, 244, 474–500, 2006.

Shiraiwa, T., Shoji, H., Saito, T., Yokoyama, K., and Watanabe, O.: Structure and dieelectrical properties of surface snow along the traverse route from coast to Dome Fuji Station, Queen Maud Land, Antarctica, Proc. NIPR Symp. Polar Meteorol. Glaciol., 10, 1–12, 1996.

Sommer, S., Wagenbach, D., Mulvaney, R., and Fischer, H.: Glacio-chemical study spanning the past 2 kyr on three ice cores from Dronning Maud Land, Antarctica 2. Seasonally resolved chemical records, Journal of Geophysical Research, 105, 29 423–29 434, 2000.

Stenberg, M., Hansson, M., Holmlund, P., and Karlf, L.: Variability in snow layering and snow chemistry in the vicinity of two drill sites in western Dronning Maud Land, Antarctica from Dronning Maud Land, Antarctica 2. Seasonally resolved chemical records, Annals of Glaciology, 29, 1999.

Svensson, A., Nielsen, S. W., Kipfstuhl, S., Johnson, S. J., P., S. J., Bigler, M., Ruth, U., and Rthlisberger, R.: Visual stratigraphy of the Northern Greenland Ice Core Project (NorthGRIP) ice core during the last glacial period, Journal of Geophysical Research, 110, 2005.

Taylor, L. D.: Glaciological Studies on the South Pole Traverse, 1962-1963, Antarctic Research Series, Antarctic Snow and Ice Studies 2, 16, 209–224, 1971.

Torrence, C. and Compo, G.: A practical guide to wavelet analysis, Bulletin of the American Meteorolical Society, 79(1), 61–78, 1998.

Udisti, R., Becagli, S., Benassie, S., Castellano, E., Fattori, I., Innocenti, M., Migliori, A., and Traversi, R.: Atmosphere-snow interaction by a comparison between aerosol and uppermsot snow-layers composition at Dome C, East Antarctica, Annals of Glaciology, 39, 2004.

Wilhelms, F.: Measuring the Conductivity and Density of Ice Cores, Berichte zur Polarforschung, Alfred Wegener Insititut für Polar- und Meeresforschung, 191, 1996.

Wilhelms, F.: Measuring the Dieelectric Properties of Ice Cores, Berichte zur Polarforschung, Alfred Wegener Insititut für Polar- und Meeresforschung, 367, 2000.

Wolff, E., Hall, J. S., Mulvaney, R., Pasteur, E. C., Wagenbach, D., and Legrand, M.: Relationship between chemsitry of air, fresh snow and firn cores for aerosol species in coastal Antarctica, Journal of Geophysical Research, 103, 11,057 – 11,070, 1998.

Zwally, H. J. and Li, J.: Seasonal and interannual variations of firn densification and ice-sheet surface elevation at the Greenland summit, Journal of Glaciology, 48, 199–207, 2002.

Table 1. The firn core sites with annual mean temperature, accumulation rate and references:

	Name	Lat	Lon	Elevation	Annual mean Temperature	Accumulation Rate	References
		deg	deg	m a. s.l.	deg C	m w.e.	
Greenland							
NGT	B 16	75.9402	-37.6299	3040	-27	0.142	(1), (2)
NGT	B 17	75.2504	-37.6248	2820			(1), (2)
NGT	B 18	76.6170	-36.4033	2508	-30	0.104	(1), (2)
NGT	B 20	78.49	-36.30	21476			(1), (2)
NGT	B 21	80.000	-41.1374	2185	-30	0.108	(1), (2)
NGT	B 26	77.2533	-49.2167	2598	-31.6	0.18	(1), (3)
NGT	B 29	76.0039	-43.4920	2874	-31.6	0.153	(1), (2)
Antarctica							
Berkner Is	B 25	-79.6142	-45.7243	886	-27	0.14	(4)
DML	B 31	-75.5815	-3.4303	2669	-42	0.063	(5)
DML	B 32	-75.0023	0.0070	2882	-42	0.061	(5)
DML	B 33	-75.1670	6.4985	3160		0.044	(5)
DML	B 36/37	-75.0025	0.0684	2891	-44.6	0.067	(6)
PreIPICS	B 38	-71.1621	-6.6989	690	-18.1	1.25	(7)
PreIPICS	B 39	-71.5680	-9.9167	654	-17.9	0.77	(7)
PreIPICS	DML95	-71.5680	-6.6670	540	-19.2	0.55	(7)
PreIPICS	DML97	-72.0640	-9.5583	760	-20.4	0.49	(7)
Dome C	EDC2	-75.1000	123.3500	3233	-53	0.025	(8)

510 Appendix 1 Supplement Figure 5

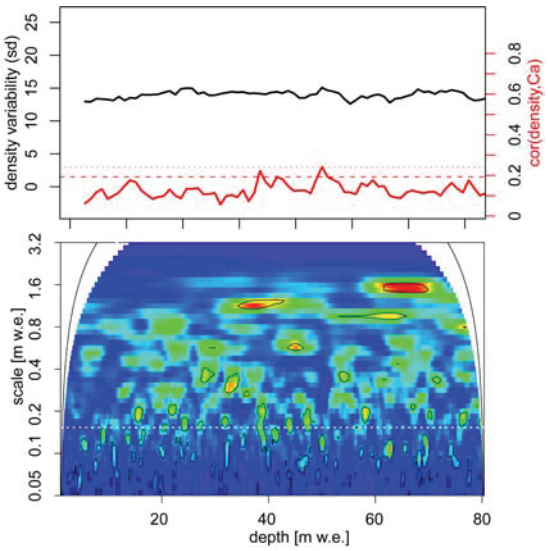

Fig. 5. Depth dependence of the density variability, density-Ca relationship (upper panel) and wavelet spectrum of the density (lower panel) of an artificial random density dataset. The results show constant density variability and very small correlation values as expected for a random data series. The small number of spurious significant correlation values, as well as some spurious significant patches in the wavelet spectra are expected, as both significance tests are local / pointwise, and multiple testings are performed

Appendix 2 Supplement Figure 6

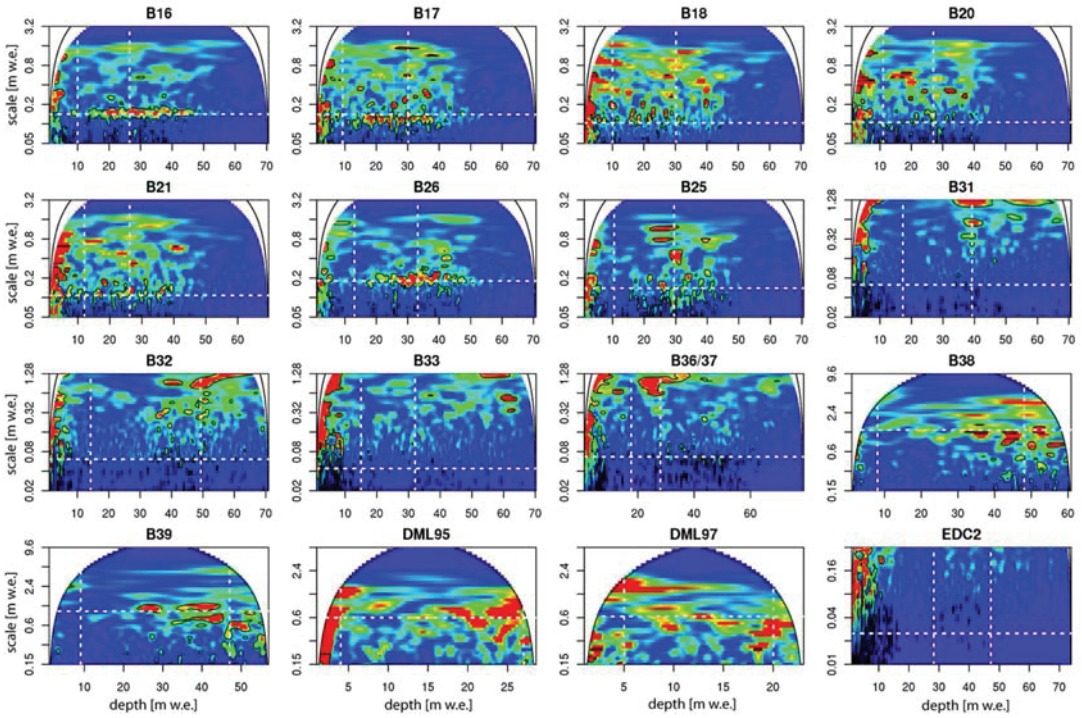

Fig. 6. Density wavelet spectra for the remaining 12 firn cores from Greenland and Antarctica. The minimum and secondary maximum of the density variability are marked with vertical lines and the scale of the accumulation rate as horizontal line. Pointwise significant areas are marked with black contours. All cores show a density variability at the surface, which is spread over a large range of frequencies. In greater depths, most cores exhibit density variability around the frequency of the accumulation rate.

C Publication 3 - Grain size of layered polar firn - evolution, variability and a new grain growth model

Hörhold, M. W., Linow, S., Dierking, W. and Freitag, J.

In preparation.

Grain size of layered polar firn - evolution, variability and a new grain growth model obtained by micro-Computer-Tomography

Maria W. Hörhold,[1] Stefanie Linow,[1] Wolfgang Dierking,[1] Johannes Freitag,[1]

[1]*Alfred-Wegener-Institute for Polar and Marine Research, Bremerhaven, Germany*

E-mail: maria.hoerhold@awi.de

ABSTRACT. Firn microstructure from six different sites in Greenland and Antarctica was investigated by means of X-ray-micro-Computer-Tomography. The effective radius was calculated from specific surface area (SSA) and used as a measure of grain size that avoids the ambiguities of alternative methods of grain size quantification. The evolution of grain size with depth, density and time was investigated at the different locations, covering a broad range in local climate conditions. The grain size shows large variations within single depth intervals at each site. Both density variability and grain size variability are strong indicators of layering of the firn. The variability in grain size seems to amplifiy with decreasing annual mean temperature and accumulation rate. A simple model of grain growth is developed which enables a prediction of the rapid grain growth at the uppermost meter driven by temperature gradients. This model can be used to simulate grain size profiles as an input for micro-wave backscatter models in a more realistic fashion.

INTRODUCTION

In-situ data of microstructure of the upper firn column are difficult and time consuming to obtain. Field data lack spatial representativity and upscaling field data can in principle be accomplished using remote sensing methods (Domine and others, 2008). Changes in mass balance of the polar ice sheets can be inferred from remote sensing signatures (Flach and others, 2005; Lacroix and others, 2008). For many cryospheric microwave remote sensing applications, it is necessary to consider microwave-firn interactions in the upper layers of the snow pack, with wavelength-dependent penetration depths ranging from centimeters to approximately 100 m (Legresy and Remy, 1998). In many studies the signal-snow microstructure interaction has been investigated (Flach and others, 2005; Rotschky and others, 2006; Srivastav and Singh, 1991; Tran and others, 2008). Regions with a certain pattern of backscatter signatures were

identified and assigned to have specific firn properties (Rotschky and others, 2006; Tran and others, 2008). However, distinct field data to parameterize these snow classes are still lacking.

Grain size data are available for single points of measurement in Antarctica and Greenland (Alley and others, 1982; Courville and others, 2007; Freitag and others, 2004; Gay and others, 2002; Gow, 1969; Gow and others, 2004; Shiraiwa and others, 1996). The problem of comparing the published data lies in the the application of very different measurement methods and the different definitions of grain size. Furthermore observations differ in their time of the year and in resolution. Seldom a single study considers very different sites, so that a relative comparison of grain size and grain size evolution with depth obtained by similar methods are available. Examples are Nishimura and Maeno (1985), Shiraiwa (1996), Gay et al. (2002) or Taylor (1971). Main characteristic difference in grain size and grain size variability in terms of layering were found between firn columns from near coastal areas, katabatic wind regions and the high Antarctic Plateau (Shiraiwa and others, 1996; Gay and others, 2002).

There is a lack of a comparable grain size definition. Recently, the effective radius determined from the specific surface area (SSA) as a grain size measure was introduced as a suitable parameter considering the interaction of the air-ice-interface in chemical or physical processes (Domine and others, 2008). Several alpine snow measurements and experiments were conducted using the effective radius, the SSA and other physical properties as comparable parameters for different snow types and their change with time (Flin and others, 2004; Schneebeli and Sokratov, 2004; Kaempfer and Schneebeli, 2007). Most comprehensive overview of available snow properties is given by Domine et al. (2008) for alpine snow and by Gay et al. (2002) for Antarctic snow. A comparable and systematic study of polar snow and firn, investigating the grain size in terms of layering and evolution with depth and time under different local climate conditions is missing. For remote sensing applications the knowledge on firn grain size is substantial. The signal return at the sensor is sensitive to grain size [e.g. Lacroix and others (2008); Shi and Dozier (2000)] or strong gradients in microstructure properties at the interface of different layers within the firn (Flach and others, 2005; Lacroix and others, 2008; Rott and others, 1993; Shiraiwa and others, 1996). Accordingly, the strongly non-linear particle growth in the upper firn layers influenced by the seasonal and diurnal thermal gradient needs to be considered to approximate a realistic grain size profile.

Various methods for modeling grain growth processes have been described in the literature. Jordan (1991), Colbeck (1983), Baunach and others (2001) model temperature gradient (TG) growth as a process driven by the saturation vapor pressure gradient. In this case, grains grow only when there is a temperature gradient present within the snowpack. Flanner and Zender (2006), among others, have created complex 3D models of firn metamorphism that consider physical processes of grain growth in great detail, but require substantial amounts of computation time. For a number of applications, it is desirable to use a simple, fast, empirical 1D approach to model firn properties. Maeno and Ebinuma (1983) found that snow grain growth can be described as a pressure sintering process, and there are many examples in literature where the Arrhenius equation is used to model equi-temperature (ET) grain growth as a function of depth e.g. by Alley and others (1982), Gow and others (2004), Flach and others (2005).

Due to a lack of inter-comparable grain size data, it has been difficult to asses the accuracy of grain size profiles simulated using above methods. Within this study we aim to fill the gap of missing comparable grain size data and present a set of grain size measurements from climatologically heterogeneous sites that can be used to verify and improve grain size modeling for remote sensing application. We use the effective radius obtained from specific surface area to investigate the grain size evolution with density, depth and time at 6 different polar sites in Greenland and Antarctica. We find variability due to the layering not only in density but also in grain size. We find that grain size and density are linked witch each other in specified depth intervals. Large grain size corresponds to low density and vice versa, whereas the overall trend with increasing depth and time shows an increase of grain size with increasing density. We find distinct differences in absolute grain size and grain growth at the different sites. But also the relation between density and grain size varies from site to site. We finally introduce a new simple grain growth model, which is able to capture the rapid grain growth in the uppermost depth intervals for a wide range of polar climate conditions.

METHODS

Firn Core Locations

Six surface firn cores, one from Greenland and five from Antarctica are analyzed. They cover a broad range in annual mean temperature, accumulation rate, elevation and distance to the coast (Figure 1, Table 1).

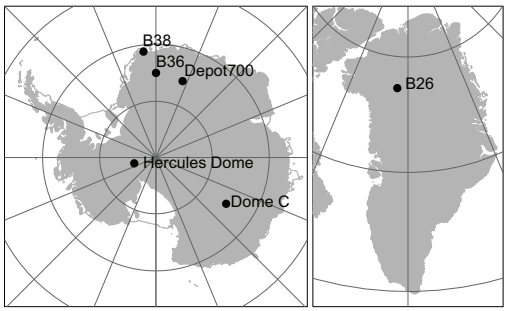

(a) Core location – Antarctica (b) Core location – Greenland

Fig. 1: The location of the firn cores in Antarctica (a) and Greenland (b).

The B 26 firn core represents medium accumulation rate and annual mean temperature of the Greenland Plateau. The firn core from Dome C represents lowest temperatures and accumulation rate in Antarctica but only material starting from 6.6 meter depth is available. The DP7 firn core site shows almost similar annual mean temperature (estimated from Moderate-resolution Imaging Spectroradiometer (MODIS) surface temperature data) and a slightly higher accumulation rate (estimated from from interpolation of

Table 1: Firn core locations and environmental conditions

Campaign/ Location	Name	Latitude deg	Longitude deg	Temperature degC	Accumulation [m w.e. · a^{-1}]	Elevation m a.s. l.
Greenland						
NGT	B 26	77.2533	-49.2167	-31.6	0.18	2598
Antarctica						
DML	B 35/36	-75.0025	0.0684	-44.6	0.067	2415.5
PreIPICS	B 38	-71.1621	-6.6989	-18.1	1.250	690
Norw.-amer. Traverse	DP7	-75.65343	19.24484	-51.0 *	0.045*	3530
Dome C	FT	-75.10	123.35	-53.0	0.025	3233
IPICS	HD	-86.00	-105.00	-37.0 **	0.180	2610

accumulation rates of nearby sites (Isaksson and others, 1999). From Kohnen station (EDML drilling site) 2 firn cores B 35 and B 36 are available. Furthermore 12 single surface measurements have been conducted in austral summer 2005/2006 at EDML. While the Hercules Dome firn core (HD) represents medium to low temperatures and medium accumulation rates, the B 38 firn core from the coastal area shows remarkable high accumulation rate and temperature. In a former study Antarctic surface snow has been classified into 10 classes, according to backscatter behavior of microwaves at two different frequencies (Rotschky and others, 2006). The firn core sites of this study cover 4 of these snow classes: B 38 falls into class 8, B 36 (B35) and DP7 into class 4, FT at the Dome C site into class 3 and Hercules Dome into class 10 (Table 2). The classification has been roughly described by known features of wind pattern, temperature and accumulation rate. But so far, no ground truth data were considered, in describing and parameterizing these snow classes.

Density

Densities are measured with a vertical resolution of 1 mm using a non-destructive logging system including a Löffel densimeter. As a radiation source ^{137}Cs was used. Using the measured gamma-ray signal intensity I in relation to the signal's intensity in air I_0, the mass absorption coefficient $\mu_{ice} = 0.085645 m^2 kg^{-1} \pm 0.01$ (Wilhelms, 1996, 2000) and the diameter d of the medium, the density ρ can be calculated. Details are given in Wilhelms (1996; 2000). All measurements were conducted at temperatures of -20 deg C in the cold laboratory of the Alfred Wegener Institute (AWI), Bremerhaven, Germany. High resolution density measurements were conducted at all but the Hercules Dome firn core.

Table 2: Firn core properties

Name	depth interval m	time interval a	number of samples
Greenland			
B 26	0.012-7.3	0.025-16.18	154
Antarctica			
B 35/36	0.29-10.94	1.79-71.26	114 / 121 /12
B 38	0.0325-10.96	0.157-4.4	180
DP7	0.05-11.978	0.37-112.27	369
FT	6.6125-20.36	110.825-367.912	374
HD	0.076-15.1	/	228

Computer Tomography and Image Analysis

Microstructure imaging was conducted by Micro-Computer-Tomography. Cylindric snow samples of 2.5 cm length and 2 cm in diameter (1 cm for B38) were placed on a table in front of a X-ray source. The table was rotated with steps of 0.9 deg and each time a shadow image is taken. With a back projection procedure these shadow images were converted to a stack of horizontal grey value images. The resolution of the imaging was 40 μm for the firn cores B26, B36, DP7, FT and HD. For the firn core B 38 a resolution of 15.73 μm was used. Microstructure data of snow and firn obtained from Computer-Tomography are shown to fairly well reproduce the snow parameter such as density (Freitag and others, 2004) and are used for many applications (Kaempfer and Schneebeli, 2007; Schneebeli and Sokratov, 2004).

CT measurements were conducted at all firn cores. For the cores B36, B38, and DP7 the uppermost 1-2 (DP7 4) meter were sampled continuously. Below, 40 cm (approximately 16 samples) were sampled every meter. B26 is sampled every meter from the very surface. The Hercules Dome data set contains discontinues samples with non-equal steps throughout the firn core. The lowermost meter of B38 and B26 was sampled continuously again. In the following the data from single depth intervals will be compared as a measure of ongoing metamorphism. The absolute number of samples in each interval differ in a range between 16 and more than 20. Linear or exponential fits were applied at each depth interval to parameterize the variability due to the layering.

For image analysis the software MAVI, developed by the Fraunhofer Institute for Mathematics (Armbrecht and Sych, 2004)was used. The image stack is loaded into the software and treated as a 3-D object. After smoothing by applying a median 3x3x3 filter

the images were segmented. For estimation of the threshold value, two gaussian distribution functions were fitted to the grey value distribution (one for the pores and one for the ice phase) of three images of each stack. The arithmetic mean of the the maximim value of each of the gaussian distributions was taken as the threshold grey value for segmentation. After segmentation, an object filter was applied, to remove all objects adding less then 1 % to the pore or ice phase. From the 3-D binarized images, all relevant microstructure information of the sample volume can be obtained.

From the measured region a cube of 400 x 400 x 400 voxels (16 x 16 x 16 mm for B 26, B36, DP7, HD and FT, 6.3 x 6.3 x 6.3 mm for B 38) was extracted. This size is sufficiently large enough to be representative in volume for the firn properties considered (Coleou and others, 2001; Kaempfer and Schneebeli, 2007). Porosity is calculated from the size of the pore fraction compared to the whole volume of the sample. Density can be computed from the ice fraction times the density of ice (ρ_{ice} = 0.917 g/cm^3). The chord length l in 3 or more directions as a measure of the grain l_i and pore l_p size can be obtained. The specific surface area SSA represents the ice-air interface per unit mass:

$$SSA = \frac{S_d}{\rho} \tag{1}$$

with SSA = the specific surface area in cm^2/g and S_d the surface density - the ratio of total surface and the total volume of the sample and ρ the density of the sample (Domine and others, 2008). From that the effective radius R_{eff} - the radius of equivalent-sized spheres with the same SSA can be obtained by:

$$R_{eff} = \frac{3}{SSA \times \rho_{ice}} \tag{2}$$

The assumption is, that the ice phase of the snow and firn can be represented by ice spheres of the radius R_{eff}. If we plot the measured SSA versus the measured chord length, we derive a surprisingly clear relationship (Figure 2), supporting the assumption, that the snow grains can be represented by equal sized spheres with a similar SSA.

Additionally we computed the SSA from a sphere by:

$$SSA_{sphere} \sim \frac{3}{\frac{4}{3} \times r \times \rho} \tag{3}$$

with r the radius of the sphere = $\frac{4}{3} \times l_{sphere}$. The computed SSA_{sphere} is fairly well reproducing the measured values (Figure 2, red line).

The SSA and the chord length l are two independently obtained parameters. Plotting SSA_{sphere} over l_{sphere} of very different firn types shows a bijective relationship (Figure 2). Thus from geometry it is reasonable to represent the firn microstructure by the effective Radius R_{eff}. In the following the effective radius R_{eff} is used as grain size parameter.

All microstructure parameters obtained by MAVI represent values of the samples volume structure of each firn sample. For more details on microstructure analysis with MAVI, see (Ohser and Mücklich, 2000; Armbrecht and Sych, 2004)

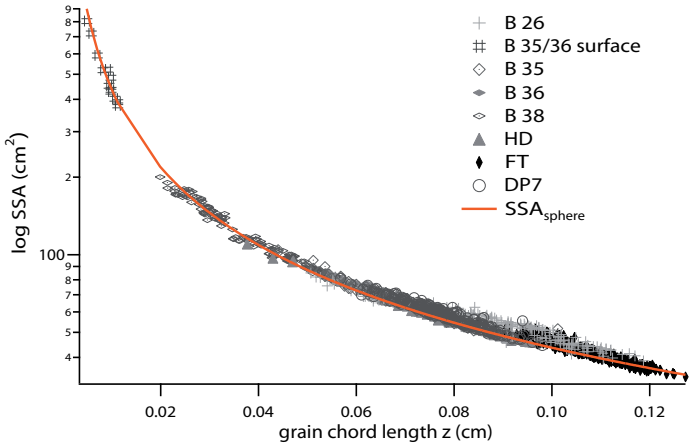

Fig. 2: The specific surface area SSA obtained from measured surface and density with the measured chord length of the different sites. In red the SSA, calculated from the measured chord length, assuming equal sized spheres, is shown. The results show, that using specific surface area under the assumption of equal sized spheres gives a surprisingly good approximation of the snow structure.

RESULTS

Density

The density profiles (smoothed by a running mean of 20 mm) of the firn cores show large fluctuations due to the layering of the firn (Figure 3) and differ in the densification rate. B 38 shows the highest density, followed by HD (density from CT-measurements). B 26 starts with lower density, but overcomes B 36 and DP7. Fire Track shows the lowest density.

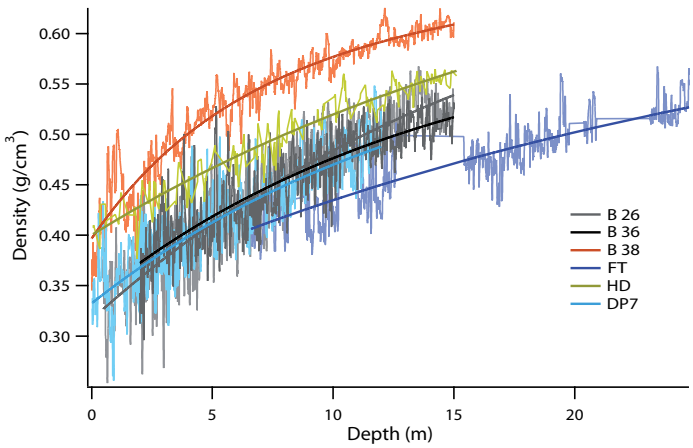

Fig. 3: Density Profiles of the firn cores

SSA and Grain Size

For all sites we find a rapid increase in grain size in the upper few meter (Figure 3A). The B38 site shows smallest grain sizes whereas the DP7 site and the B26 site show largest grain sizes. In greater depths the EDC site has largest grain sizes (Figure 3A). The *SSA* decreases rapidly in the uppermost meters. B38 shows highest values at the surface, DP7 and B26 lowest (Figure 3B). In greater depths the EDC site shows smallest values.

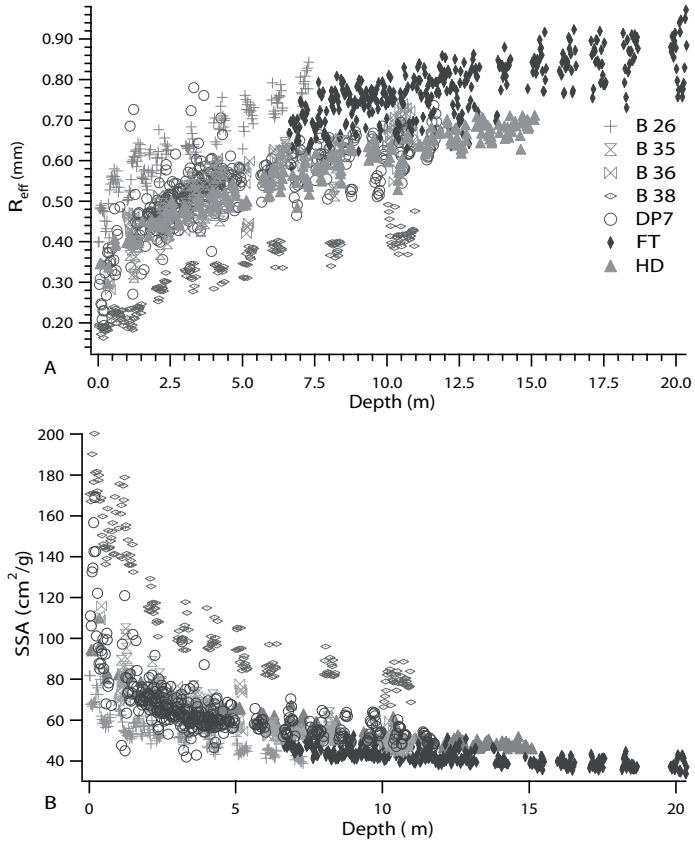

Fig. 4: The evolution of grain chord length with porosity (a), pore chord length and grain chord length (b), the specific surface area with porosity (c) and the anisotropy with grain size (d). The colors represent the evolution with depth and time - light grey from the near surface samples to black with the oldest and deepest samples

Both, *SSA* and grain size show large fluctuations. In order to compare the density variability with the grain size variability both were investigated in detail (Figure 4). Density and grain sizes for every single depth interval are compared. A linear fit is applied for each

depth interval. The evolution with depth is indicated by a stepwise shift in color from light grey (near-surface samples, youngest) to black (deepest and oldest samples).

B26

This firn core represents medium accumulation rate and temperatures of the Greenland ice sheet. On the inter-layer level the grain size shows a negative trend with density. Low density samples have large grain size and vive versa (Figure 4A). With increasing depth and age the slope increases. The slopes range from approximately -0.39 $mm/(g/cm^3)$ to 0.81 $mm/(g/cm^3)$. The overall trend of grain size and density is positive - with increasing density the grain size increases.

B35/36

This firn core site represents medium accumulation rates of the Antarctic Plateau from Dronning Maud Land, Antarctica. The grain sizes of B35 and B36 also show a negative trend with density within single depth intervals (Figure 4B). Only the surface sample and the uppermost depth interval of B35 show a positive trend (Figure 4B). At the very surface high density is associated with large grain size and vice versa. At all other depth intervals representing deeper and older firn, large density values correlate with small grain sizes. Again the slope increases from shallow to steep values with increasing depth and time. The B36 firn core shows trends from -0.8 to -2.4 $mm/(g/cm^3)$, the surface interval shows a much higher slope, whereas the bags from core B35 show values slightly less than B 36, ranging from approximately -0.33 to -1.44 $mm/(g/cm^3)$. The overall trend is again positive, with increasing density the grain size increases.

B38

The B38 firn core comes from the coastal region of Dronning Maud Land, Antarctica. It is not only characterized by very high annual mean temperature but also by a tremendous accumulation rate of 0.12 m w.e. per year. The grain size shows a positive trend with density for the single depth intervals (Figure 4C). Large grain size corresponds to high density and vice versa. The slope is not changing much with increasing depth. The slopes are positive, ranging from 0.35 $mm/(g/cm^3)$ at the surface to 0.54 $mm/(g/cm^3)$ at the lowermost depth interval. The overall trend is similar - with increasing density the grain size increases.

Depot700 (DP7)

The DP7 firn core comes from the high Antarctic Plateau with low accumulation rates. The grain size at DP7 site shows again a negative trend with density and the inter-layer level (Figure 4D). The slope is varying in the upper depth intervals, but is increasing with depth and time. The slope ranges approximately from -1.37 to -2.6 $mm/(g/cm^3)$, even though the surface bag shows a positive trend of 0.9 13 $mm/(g/cm^3)$ and some medium depth intervals values of approximately -0.6 $mm/(g/cm^3)$. Overall trend shows increasing grain size with increasing density. SSA shows a positive trend with density for the single depth intervals, and an overall negative trend (Figure 4D).

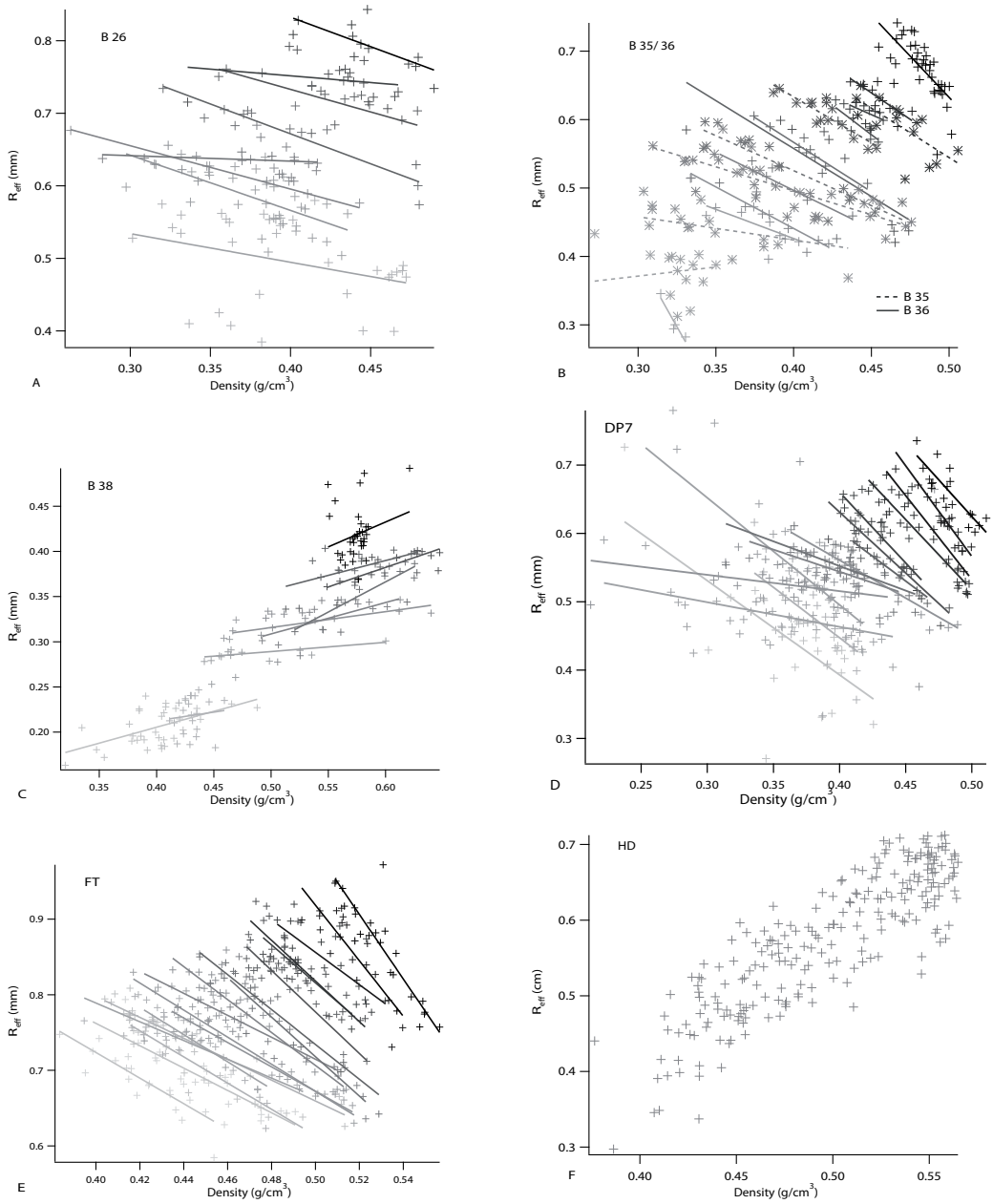

Fig. 5: Detailed grain size vs density profiles of the single depth intervals. Note the different scales. For each depth interval a linear relationship between density and grain size is apparent.

Fire Track (Dome C)

The Fire Track firn core from the Dome C vicinity represents the coldest site with lowermost accumulation rate of this study. The sampling and microstructure analysis starts at depths below 6 meter and an age of more than 100 years. On the inter-layer level the grain size shows a well pronounced negative trend with density (Figure 4E). The slope is increasing with depth and time. It ranges from -1.696 $mm/(g/cm^3)$ at uppermost interval to -4.2662 $mm/(g/cm^3)$ at the lowermost depth interval. The overall trend shows again increasing grain size with increasing density.

Hercules Dome (HD)

For the Hercules Dome (HD) site no detailed sampling for single depth intervals was conducted. Therefore it can only be used to study the overall trend of grain size with increasing density (figure 4F).

Whereas the overall trend shows the well known increase of grain size with increasing density, the inter-layer variability often shows an opposite trend. The firn cores B26, FT, DP7 and B35/ B36 show this behavior very well. Only the near-surface depth intervals (light grey lines) at the B35/36 site, as well as at the B26 site and all depth intervals of the B38 site show a positive trend - increasing grain size with increasing density.

The slope of the linear fit changes from site to site. It seems that firn cores with low accumulation rates and annual mean temperatures show the strongest negative trend (FT and DP77). With increasing temperature and accumulation rate the slope is decreasing (B35/36 and B26) and turns to positive values at the warmest site with extremely high accumulation rate (B38). The slope is also increasing (in negative direction) with increasing depth and age. Surface depth intervals show weak slopes, whereas the intervals deeper down show more steep gradients.

A simple model of grain growth

The Arrhenius equation assumes linear particle growth under isothermal conditions:

$$r^2(t) = Kt + r_0^2 \tag{4}$$

with

$$K = K_0 \exp(-E/RT) \tag{5}$$

The radius $r(t)$ of a particle is determined from an initial radius r_0 and growth rate K, which is a function of rate constant K_0, activation energy E, gas constant R and absolute temperature T. Values for E vary between 47.0×10^3 J/mol [Gow (1969)] and 42.4×10^3 J/mol [Paterson (1999)], while K_0 is on the order of 6.75×10^7 mm^2/a [Flach and others (2005)].

Growth rates calculated from the above range of parameters vary considerably. Budd and Jacka (1989) assumed E and K_0 to be temperature–dependent, and Jacka and Li (1994) supply parameters to fit activation energy E and growth rate K to temperature. The initial value r_0 is usually fixed at an arbitrary value, due to a lack of reference values obtained from the field.

Growth rates

From the measured grain size profiles we aim to find a parametrization of grain growth as a function of annual mean temperature $\bar{T}$, temperature gradient ∇T and accumulation rate A.

Effective radius measurements are available for each firn core in steps of 2.5 cm, with approximately 16 single measurements repeating in 1–meter intervals to capture grain size variability. To determine a mean grain size profile, effective radii are averaged over the measurement intervals. Firn age $t(z)$ corresponding to the mean radius at depth z can be estimated from the velocity $v(z) = A \cdot \rho_{ice} \cdot \rho(z)^{-1}$ at which a snow layer is buried below the surface.

$$t(z) = \int_0^z \frac{dz'}{v(z)} \tag{6}$$

Temperature propagation into the snow pack $T(z)$ is modeled as an exponentially decaying oscillation as described by Paterson (1999), depending on $\bar{T}$, amplitude of the seasonal temperature signal at the surface ΔT, thermal diffusivity of snow k, and frequency ω and phase φ of the seasonal signal. The phase value is fixed at the point of positive temperature amplitude.

$$T(z) = \bar{T} + \Delta T \exp\left(-z\sqrt{\omega/2k}\right) \cdot \sin\left(\omega\varphi - z\sqrt{\omega/2k}\right) \tag{7}$$

Annual mean temperature $\bar{T}$ and amplitude ΔT can be obtained from the MODIS Land Surface Temperature product. The thermal diffusivity is easily calculated from the measured firn core densities using the empirical approach developed by Sturm and others (1997).

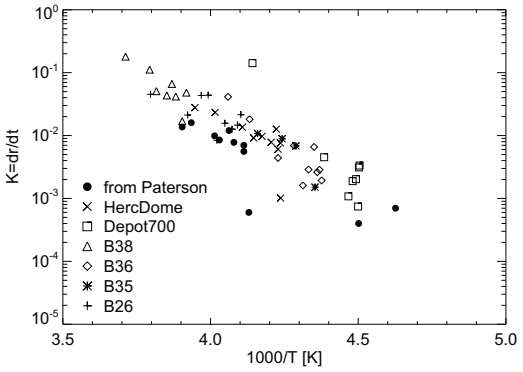

Fig. 6: Growth rates derived from profile data, and Paterson (1999)

Input data for the determination of the growth rate from radius measurements are mean grain size profiles with corresponding values for temperature, temperature gradient ∇T (derived from the temperature profile in equation (8)), density and firn age. The growth rate $K = dr/dt$ is determined numerically for every depth interval. We compare growth rates determined from our data set with values published by Paterson (1999) and find our values in good accordance (fig. 6), albeit systematically larger. A possible explanation for this effect lies in the use of different methods to determine grain size. The temperature-dependent activation energy E and rate constant K_0 are difficult to fit to parameters obtained from measurements, since they are very sensitive to noise in the data. For this reason, we chose to directly fit the growth rate K, and determine coefficients for equation (9):

calculated.

$$K(T) = a_0 \exp\left(a_1[1000/(\bar{T} + \nabla T)] + a_2\right) \tag{8}$$

We propose using the following parameter set to estimate the temperature–dependent growth rate:

$$\begin{aligned} a_0 &= 0.165 \\ a_1 &= -5.218 \\ a_2 &= -3.712 \end{aligned} \tag{9}$$

Surface grain size

The grain size of the near-surface layer r_0 depends on temperature and accumulation rate: high temperatures correspond to more water vapor transport and thus to faster grain growth [Domine and others (2008)]. Higher accumulation reduces the time the snow grains are subject to a strong temperature gradient and slows down the grain growth process.

To quantify the temperature and accumulation dependency of the surface grain size, initial radii r_0 and their standard deviation σ_{r_0} were estimated from the measured grain sizesof the upper 30 cm interval of each measured individual profile. This was done for all available grain size profiles except the FireTrack profile since it starts at a depth of 6m.

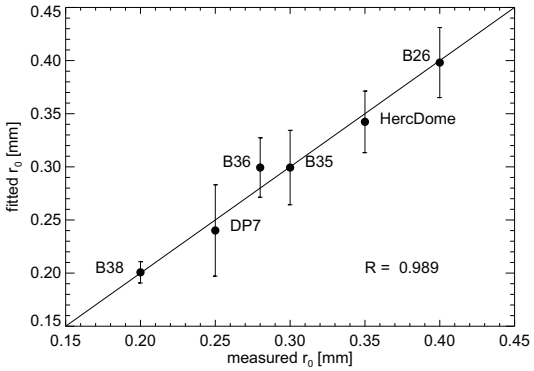

Fig. 7: Correlation between simulated and measured surface grain sizes

Table 3: Initial radii, radius standard deviation, temperatures, accumulation rates

Name	r_0	σ_{r_0}	$\bar{T}$ [^{o}C]	A [m w.e. $\cdot$ a^{-1}]
B26	0.40	$\pm$ 0.033	-31.60	0.180
B35	0.30	$\pm$ 0.035	-44.60	0.067
B36	0.28	$\pm$ 0.028	-44.60	0.067
B38	0.20	$\pm$ 0.010	-18.10	1.250
Depot700	0.25	$\pm$ 0.043	-51.00	0.045
Hercules Dome	0.35	$\pm$ 0.029	-37.00	0.180

A multiple linear regression applied to the data from table 3 yields the following relationship between initial grain radius r_0, mean annual temperature $\bar{T}$ [^{o}C] and accumulation rate A [m w.e. $\cdot$ a^{-1}].

$$r_0(\bar{T},A) = a_0 + a_1\bar{T} + a_2 A \tag{10}$$

with

$$\begin{aligned} a_0 &= 0.781 \pm 0.019 \\ a_1 &= 0.085 \pm 0.002 \\ a_2 &= -0.279 \pm 0.055 \end{aligned} \tag{11}$$

In order to test the accuracy of our fit, we compared initial radii determined from equation 10 with measured values. It can be seen that our multiple regression approach reproduces the measured values with sufficient accuracy.

Model results

Fig. 8 shows model results in comparison with grain size models from by Paterson Paterson (1999) and Zwally and Li (2002). We chose initial radii r_0 from equation (11) for better comparison and varied only the way of calculating k. It can be seen that the rapid grain growth in the upper layers influenced by a strong temperature gradient are represented more realistically by the new approach. Our approach overestimates grain growth for B38 , a site with an extremely high accumulation rate of 1.25 m water equivalent per year and a comparably high mean annual temperature of -18^{o}C. For the Depot700 core, the extreme growth caused by a very low accumulation of $\approx$ 0.045 m water equivalent per year and, in consequence, the long exposure time of snow layers to a large temperature gradient, is underestimated in our model. For intermediate polar climate conditions, the simulated grain size profiles closely fit the measurements.

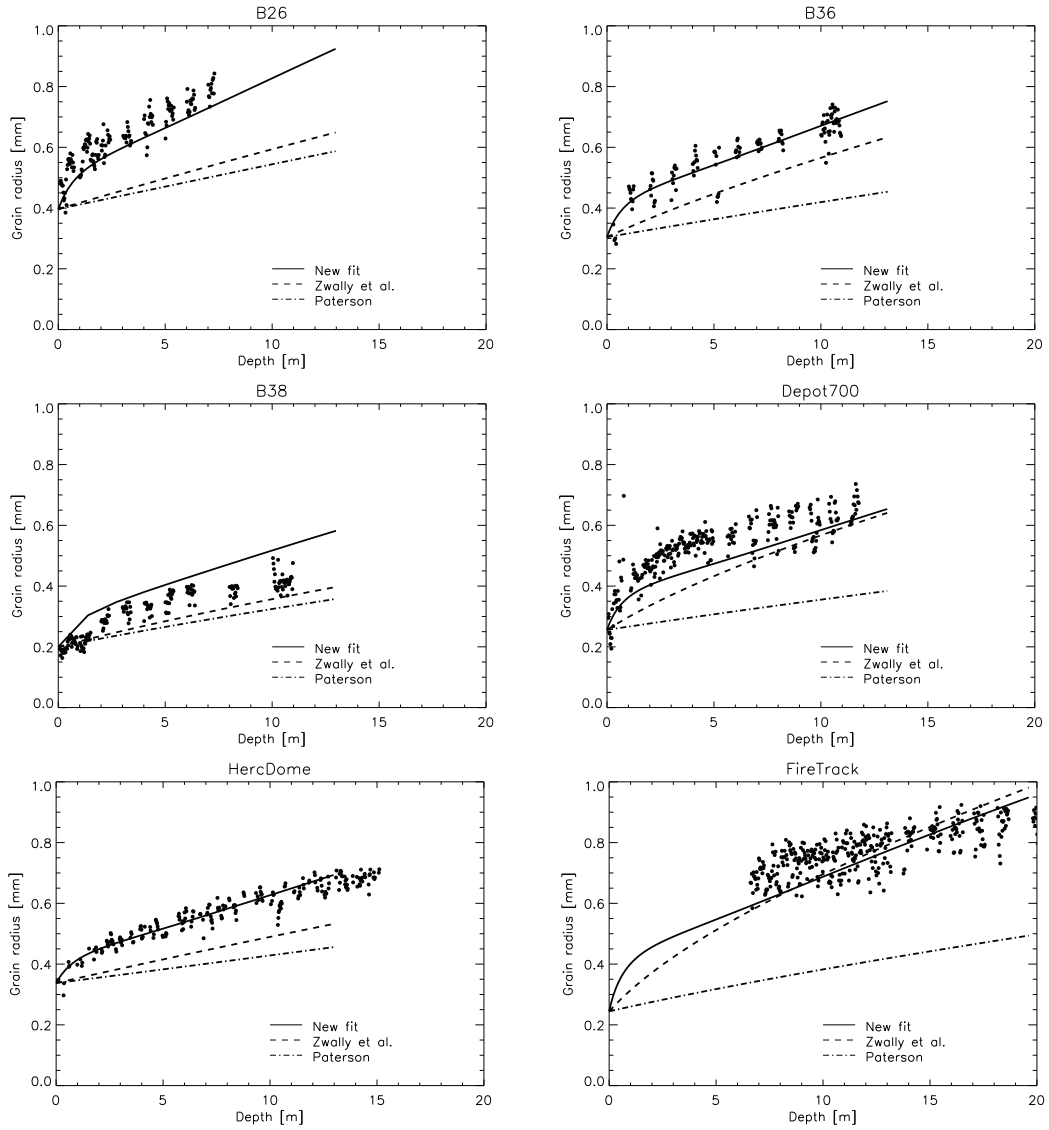

Fig. 8: Modeled grain size profiles for six polar firn cores

DISCUSSION

The sequence of unit layers in the firn is very important for the point of view of remote sensing, because the boundary of unit layers reacts as an interface between different dielectric materials. The main microstructural change at an interface occurs in the density and grain size of the firn layer. Often the density variability is taken as a proxy for stratigraphy and the total amount of layers is linked to backscatter signature (Flach and others, 2005; Rott and others, 1993). With our high resolution density data we can not define a

clear difference in variability in density or in the amount of layers between the different sites. Shiraiwa et al (1996) also compared the number of unit layers in 38 snow pits of 1 -2 meter depth from the coast up to the plateau. Their number of layers per meter was half as high as the number found in our study - ranging between 10 and 20, but a clear difference in the total amount of layers between sites at different local climate conditions was also not found (Shiraiwa and others, 1996). A slight trend for a higher amount of layers at higher altitude could be identified. The density variability in terms of layering can not be directly taken as a measure for number of layers and with that as a reason for different backscatter behavior.

Grain size seems to be strongly connected to density. The sites differ considerably in absolute values, as does the density. Shiraiwa et al. (1996) find non-linear altitudinal changes in grain size and strong variations in regions of katabatic wind. The alteration of grain size and types and the thickness of single layers vary characteristically for the different sites. This could be a hint for the different interaction of snow and microwave signatures. On the other hand Gay and others (2002) find large variations in grain size along their traverse from Terra Nova Bay to Dome C. The grain size is strongly linked to wind patterns of erosion, crust formation or calm conditions. The exposure of snow to temperature gradients on large time scales enables the formation of large grains and wind crusts, which in turn explain a particular behavior in microwave signature (Gay and others, 2002) for example at the Dome C vicinity. We find clearly different grain sizes at the different sites. B38 with shows the warmest temperature, however due to the extremely high accumulation rate the grain size is the smallest of all sites. The next warm site is the B 26 firn core and indeed we here find the largest grain sizes of all firn core sites. On the other hand the two coldest sites FT and DP7 show similar large grain sizes in greater depth. This is due to the very low accumulation rate and the long time, a snow layer is exposed to temperature gradients at the surface. The grain growth is not only temperature dependent. The grain size at a certain depth is the result of the competing influence of annual mean temperature and accumulation rate.

The grain growth at a single site is influenced by local climate factors such as temperature and accumulation rate and probably also by the initial grain size and grain size variability within the different layers. The overall trend for all sites is, that grain size increases and SSA decreases with increasing density. Nishimura and Maeno (1985) discussed the rounding and growth of ice particles as the main reason for the drastic decrease in specific surface area in the upper part (Nishimura and Maeno, 1985). The slower liner decrease in greater depth was attributed to the development of bonding and particles.

The trend within single depth intervals is opposite to the overall trend. In general grain size is decreasing with increasing density. Also Taylor (1971) observed the inverse variation of density with grain size. For grain size the slope of the linear fits is increasing with depth and age. As deeper in the firn column and as older the firn, as steeper the slope in the trend of grain size and density. The exception is found at B38. Here the trend within single depth intervals follows the overall trend. If we compare the trend of grain size and density at the different sites, we again find, that as older the snow as more pronounced is the negative trend. FT as the coldest site with lowest accumulation rate shows the highest slope, DP7, with similar climate conditions and with surface samples also shows

a high slope in greater depths. The slope is less strong at the surface, since it is developing with depth and time. B35/36 is the next warmer site with the next higher accumulation rate. Here we find a less strong slope and the surface samples show a weak or even positive slope. The same holds for B26. Finally at B38 with the warmest temperature and the highest accumulation rate shows positive values of the slope. Here the snow is moving down the firn column so fast, due to the extremely high accumulation rate, that the grains size has no time to adapt to density in the way than at the other sites.

So obviously the surface ”fresh” snow inhabits a positive trend - large grain size corresponds to high densities. As soon as the snow is exposed to metamorphism in the near surface area - this trend turns to negative. Further more it seems, that at the surface a broad range in density can be covered by small range in grain size. In greater depth and with increased age the range in density decreases, whereas the range in grain size stays the same or even increases.

Grain Growth Model

Discussion of the model

competing impact of temperature and accumulation rate - therefore overestimating B 38 samples and underestimating DP7 and FT samples

No physical approach, but since such a broad range of local climate conditions is used for parameterizing the values, good approximation for polar conditions.

Problems of the model approach: error sources

Advantage of the model approach: easy to apply; use for back-scatter models in Remote sensing.

Comparison of modeled grain radius with Flanner and Zenner (Flanner and Zender, 2006) for temperature gradient growth (their ”long-term” growth is 30 days. But one experimental set up is comparable to Dome C (temperature -50, temperature gradient 20.

Baunach (Baunach and others, 2001) has comparable temperature gradients (30 degree per meter)

discussion initial gain size and impact of grain growth (Flanner and Zender, 2006)

CONCLUSION

We present a simple model of snow grain growth that incorporates effects of the strong TG growth in the upper layers of the snowpack as well as ET growth at depths no longer influenced by the seasonal temperature gradient. Our approach uses the Arrhenius equation to model particle growth and derives an empirical fit of the temperature–dependent growth rate from firn core data. Additionally, a solution to the problem of finding a realistic initial radius for eqation 4 is presented.

Since the firn cores used to derive our model parameter set do not exceed a depth of $\approx$ 20 m, we cannot predict the accuracy of our model results for greater depths and recommend this model for remote sensing applications that to consider firn–microwave interactions in the upper layers of the snow pack only.

Using data from six firn cores from Greenland and Antarctica which represent a very heterogeneous set of environmental conditions to derive empirical parameters for our grain growth model, we can safely assume our model to be applicable to the entire polar regions. In order to further test the validity of our relation for estimating surface grain sizes, more data will be needed.

REFERENCES

Alley, R. B., J. F. Bolzan and I. M. Whillans, 1982. Polar firn densification and grain growth, *Annals of Glaciology*, **3**, 7–11.

Armbrecht, J. and T. Sych, 2004. MAVI - Modular Algorithms for Volume Images.

Baunach, T., C. Fierz, P.K. Satyawali and M. Schneebeli, 2001. A model for kinetic grain growth, *Annals of Glaciology*, **32**(1), 1–6.

Budd, W.F. and T.H. Jacka, 1989. A review of ice rheology for ice sheet modelling, *Cold Regions Science and Technology*, **16**(2), 107 – 144.

Colbeck, S.C., 1983. Theory of metamorphism of dry snow, *Journal of Geophysical Research*, **88**, 5475–5482.

Coleou, C., B. Lesaffe, J. B. Brzoska, W. Ludwig and E. Boller, 2001. Three-dimensional snow images by X-ray microtomogrpaphy, *Annals of Glaciology*, **32**, 75–81.

Courville, Z.R., M.R. Albert, M.A. Fahnestock, L.M. Cathles and C.A. Shuman, 2007. Impacts of an accumulation hiatus on the physical properties of firn at a low-accumulation polar site, *Journal of Geophysical Research*, **112**, 10.

Domine, F., M. Albert, Jacobi H.-W., A. A. Kokhanovsky, M. Lehning, G. Picard and W. R. Simpson, 2008. Snow physics as relevant to photochemistry, *Atmospheric Chemistry and Physics*, **8**, 171–208.

Flach, J.D., K.C. Partington, C. Ruiz, E. Jeansou and M.R. Drinkwater, 2005. Inversion of the Surface Properties of Ice Sheets From Satellite Microwave Data, *IEEE Transactions on Geoscience and Remote Sensing*, **43**(4), 743–752.

Flanner, M.G. and C.S. Zender, 2006. Linking snowpack microphysics and albedo evolution, *Journal of Geophysical Research*, **111**, D12208.

Flin, F., J.-B. Brzoska, B. Lesaffre, C. Coleou and R. A. Pieritz, 2004. Three-dimensional geometric measurements of snow microstructural evolution under isothermal conditions, *Annals of Glaciology*, **38**.

Freitag, J., F. Wilhelms and S. Kipfstuhl, 2004. Microstructure-dependent densification of polar firn derived from X-ray microtomography, *Journal of Glaciology*, **30**, 243–250.

Gay, M., M. Fily, C. Genthon, M. Frezzotti, H. Oerter and J.-G. Winther, 2002. Snow grain-size measurements in Antarctica, *Journal of Glaciology*, **48**, 527–535.

328 Gow, A.J., D.A. Meese and R.W. Bialas, 2004. Accumulation variability, density profiles and crystal growth trends in ITASE firn and
329 ice cores from West Antarctica, *Annals of Glaciology*, **39**, 101–109.

330 Gow, Anthony J., 1969. On the rates of growth of grains and crystals in South Polar firn, *Journal of Glaciology*, **8**(53), 241–252.

331 Isaksson, E., M. R. van den Broeke, J.-G. Winther, L. Karlf, J. F. Pinglot and N. Gundestrup, 1999. Accumulation and proxy-
332 temperature variabibility in Dronning Maud Land, Antarctica, determined from shallow firn cores, *Annals of Glaciology*, **29**, 17–22.

333 Jacka, T.H. and Jun Li, 1994. The steady-state crystal size of deforming ice, *Annals of Glaciology*, **20**, 13–18.

334 Jordan, R., 1991. A one-dimensional temperature model for a snow cover, *Special Report SR 91-16*, U.S. Army Cold Regions Research
335 and Engineering Laboratory.

336 Kaempfer, T.U. and M. Schneebeli, 2007. Observation of isothermal metamorphism of new snow and interpretation as a sintering
337 process, *Journal of Geophysical Research*, **112**, D24101.

338 Lacroix, P., M. Dechambre, B. Legresy, F. Blarel and F. Remy, 2008. On the use of the dual-frequency ENVISAT altimeter to determine
339 snowpack properties of the Antarctic ice sheet, *Remote sensing of environment*, **112**, 1712–1729.

340 Legresy, B. and F. Remy, 1998. Using the temporal variability of satellite radar altimetric observations to map surface properties of
341 the Antarctic ice sheet, *Journal of Glaciology*, **44**(147), 197–206.

342 Maeno, N. and T. Ebinuma, 1983. Pressure sintering of ice and its implication to the densification of snow at polar glaciers and ice
343 sheets, *Journal of Physical Chemistry*, **87**, 4103–4110.

344 Nishimura, H. and N. Maeno, 1985. Studies on structures and physical properties of snow on Mizuho Plateau, Antarctica, *Annals of*
345 *Glaciology*, **6**, 105–107.

346 Ohser, J. and F. Mücklich, 2000. Statistical Analysis of Microstructures in Materials Science, John Wiley and Sons, Ltd.

347 Paterson, W.S.B., 1999. Physics of Glaciers, Butterworth-Heinemann, 3 ed.

348 Rotschky, G., W. Rack, W. Dierking and H. Oerter, 2006. Retrieving Snowpack Properties and Accumulation Estimates From a
349 Combination of SAR and Scatterometer Measurements, *IEEE Transactions on Geoscience and Remote Sensing*, **44**(4), 943–956.

350 Rott, H., K. Sturm and H. Miller, 1993. Active and passive signatures of Antarctic firn by means of field measurements and satellite
351 data, *Annals of Glaciology*, **17**, 337–343.

352 Schneebeli, M. and S.A. Sokratov, 2004. Tomography of temperature gradient metamorphism of snow and associated changes in heat
353 conductivity, *Hydrological Processes*, **18**, 3655–3665.

354 Shi, J. and J. Dozier, 2000. Estimation of snow water equivalence using SIR-C/X-SAR. II. Inferring snow depth and particle size,
355 *Geoscience and Remote Sensing, IEEE Transactions on*, **38**(6), 2475–2488.

Shiraiwa, T., H. Shoji, T. Saito, K. Yokoyama and O. Watanabe, 1996. Structure and dielectrical properties of surface snow along the traverse route from coast to Dome Fuji Station, Queen Maud Land, Antarctica, *Proc. NIPR Symp. Polar Meteorolo. Glaciol.*, **10**, 1–12.

Srivastav, S. K. and R. P. Singh, 1991. Microwave radiometry of snow-covered terrains, *Int. J. Remote Sensing*, **12**, 2117–2131.

Sturm, M., J. Holmgren, M. Koenig and K. Morris, 1997. The thermal conductivity of seasonal snow, *Journal of Glaciology*, **43**(143), 26–41.

Taylor, L. D., 1971. Glaciological studies on the South Pole traverse, 1962-1963, *Antarctic Research Series, Antarctic Snow and Ice studies 2*, **16**, 209–224.

Tran, Ngan, F. Remy, Hui Feng and P. Femenias, 2008. Snow Facies Over Ice Sheets Derived From Envisat Active and Passive Observations, *IEEE Transactions on Geoscience and Remote Sensing*, **46**, 3694–3708.

Wilhelms, F., 1996. Measuring the Conductivity and Density of Ice Cores, *Berichte zur Polarforschung, Alfred Wegener Insititut für Polar- und Meeresforschung*, **191**.

Wilhelms, F., 2000. Measuring the Dieelectric Properties of Ice Cores, *Berichte zur Polarforschung, Alfred Wegener Insititut für Polar- und Meeresforschung*, **367**.

Zwally, H.J. and J. Li, 2002. Seasonal and interannual variations of firn densification and ice-sheet surface elevation at the Greenland summit, *Journal of Glaciology*, **48**, 199–207.

D Publication 4 - The impact of accumulation rate on the anisotropy and air permeability of polar firn at a high accumulation site

Hörhold, M. W., Albert, M. R., Freitag, J. (2009)

Journal of Glaciology, Vol.55, No. 192, pp.625-631.

The impact of accumulation rate on anisotropy and air permeability of polar firn at a high-accumulation site

Maria W. HÖRHOLD,[1] Mary R. ALBERT,[2] Johannes FREITAG[1]

[1]*Alfred Wegener Institute for Polar and Marine Research, Am Handelshafen 12, D-27570 Bremerhaven, Germany*
E-mail: Maria.Hoerhold@awi.de
[2]*US Army Cold Regions Research and Engineering Laboratory, 72 Lyme Road, Hanover, New Hampshire 03755-1290, USA*

ABSTRACT. The first three-dimensional properties of polar firn obtained by X-ray microtomography are used to study the microstructure of snow on a 15 m deep firn core from West Antarctica. The snow is found to undergo coarsening down to approximately 2.5 m depth before grain growth and densification become the prevalent mechanisms of microstructure change. In contrast to previous assumptions, distinct anisotropy of the ice and pore geometry is observed throughout the profile, with a maximum at 2.5 m depth. The air permeability and the degree of anisotropy vary with depth and can be linked to short-term changes in accumulation rate via the residence time for which a certain snow layer stays in the uppermost 2.5 m. Patterns of the degree of anisotropy and air permeability of buried polar firn are relative indicators of past accumulation rates.

INTRODUCTION

On polar ice sheets the surface snow and firn forms a layered and porous medium that remains permeable to gases over depths of many tens of meters. Local surface conditions affect the generation and transformation of the snow and firn column; the temperature by affecting the rate of densification, and the accumulation rate by forming the layering and determining the time the snow is exposed to insolation and temperature gradients at the surface. Single snow layers are created by depositional events and consist of very different snow types, leaving a highly stratified firn pack (Gow, 1965; Alley and others, 1982; Palais and others, 1982; Alley, 1988). Since the properties of the different snow layers are very distinct in grain and pore size, forming diverse stratigraphic horizons (Palais and others, 1982), they transform differently in applied temperature gradients and load (Alley and others, 1982).

The microstructure of surface snow and the stratigraphic and grain-scale characteristics vary spatially with varying accumulation rates on the East Antarctic ice sheet (Watanabe, 1978; Shiraiwa and others, 1996), as does the air permeability (Courville and others, 2007). However, it is not clear how short-term changes in temperature or accumulation rate are reflected in the firn properties over time, as subsequent burial moves layers down through the firn column. For a relatively high-accumulation site in West Antarctica, Rick and Albert (2004) discuss the impact of temperature and accumulation rate, on seasonal and decadal scales, on the permeability and microstructure of firn. Albert and others (2004) report that low accumulation rates, in areas like the East Antarctic plateau, cause extreme firn metamorphism, due to the length of time the snow is exposed to insolation and wind at the surface. Small differences in accumulation rate create very large differences in microstructure, permeability and thermal conductivity in the top meters of firn, which leave an enduring record as the firn becomes buried (Rick and Albert, 2004; Courville and others, 2007). The occurrence of highly permeable and porous layers at greater depths in the megadunes area documents that a change in climate conditions would influence both the microstructure and the permeability. At least at cold, low-accumulation sites, a signature of changing accumulation rate is maintained in the microstructure and air permeability of the firn column.

Earlier studies addressing polar snow microstructure used thin or thick sections from firn samples to obtain information about the microstructure (Gow, 1969; Alley and others, 1982; Rick and Albert, 2004). This technique enabled only a two-dimensional analysis, and the quantitative microscopy is limited (Davis and others, 1996). Recently, X-ray microtomography has been used to study alpine or artificial, sampled or sieved snow, observed for different time intervals in the laboratory (Flin and others, 2004; Schneebeli and Sokratov, 2004; Kaempfer and others, 2005; Kaempfer and Schneebeli, 2007). In experimental set-ups for isothermal metamorphism (Flin and others, 2004; Kaempfer and Schneebeli, 2007), temperature gradient metamorphism (Schneebeli and Sokratov, 2004) and micromechanical studies (Pieritz and others, 2004), it has been shown that snow can be correctly described using microtomography and image-analysis tools (Coléou and others, 2001).

In this study, for the first time, microtomography is used to profile polar firn with varying layers and properties. A 15 m long firn core drilled during the US ITASE (International Trans-Antarctic Scientific Expedition) campaign 2002 at Hercules Dome is used to investigate the snow and firn microstructure and air permeability. Hercules Dome is situated at 86° S, 105° W, with relatively high accumulation rates of 0.16–0.20 m w.e. a^{-1} over the last 300 years and low temperatures of –35 to –40°C (Jacobel and others, 2005). Permeability measurements and microtomography are used to describe the evolution of the microstructure with time and depth. We observe a stratigraphically induced high variability in microstructure and air permeability and a distinct anisotropy of the firn throughout the profile. In addition, influences that induce variations of the firn characteristics over a longer-term trend (and hence, across multiple layers) impact the anisotropy and air-permeability profile. These longer-term variations are superposed on the layering and the changes that occur with depth due simply to layer deposition, densification and other processes. By considering

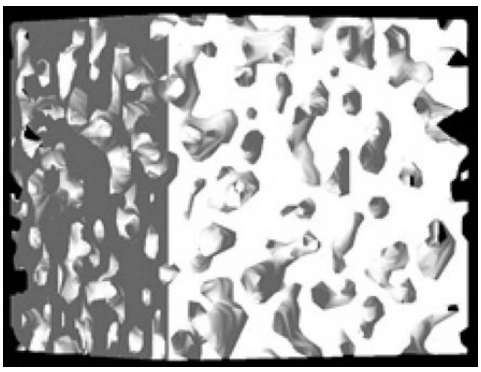

Fig. 1. A reconstructed firn cube with side length 16 mm showing the pore phase from 2.5 m depth. White is the pore phase; voids represent the ice grains.

the time the snow is exposed to near-surface conditions, we can link these variations to short-term changes in the accumulation rate. Our results confirm that changes in accumulation rate leave a signature in the firn permeability and microstructure as the firn becomes buried.

METHODS

The firn-core permeability was measured following the procedures described by Albert and others (2000), Rick and Albert (2004) and Courville (2007). The measurements were applied at 220 homogeneous firn-core sections, as identified on a light-table, of 3–10 cm length. Due to poor core quality, no permeability data were available in several intervals of the uppermost 2 m and at 8.5–9.5 m depth. Homogeneous coarse-, fine- and medium-grained layers, distinguished by visual inspection of the grain size relative to the surrounding layers, were sampled in every depth interval of the firn core for further analysis. Microstructural properties of the firn grain and pore space were obtained at –25°C by X-ray microtomography using a micro-CT (computed tomography) scanner (1074 SkyScan) inside a cold room. A charge-coupled device (CCD) camera of 768×512 pixels and 256 grey levels was used as an X-ray detector. Cylindrical snow and firn samples of 2 cm diameter and height were drilled out of the main core with a hole saw. The sample was placed on a turntable in front of the source, and was rotated in 0.9° intervals during scanning. A set of 210 shadow images was captured while the rotation completed a semicircle.

A convolution algorithm with a back projection for fan beams transformed the shadow images into a series of horizontal cross-sections representing the three-dimensional (3-D) structure of the snow. The resolution as well as the distance between adjacent reconstructed images was 40 µm, so the object was displayed by a 3-D grid of grey image values (voxels) with a spacing of 40 µm in the x, y and z directions. For digital image analysis a cubic region of 16 mm side length (leaving $400 \times 400 \times 400$ voxels) was chosen out of the cylindrical sample. A sample 3-D image is shown in Figure 1. The image size is large enough to sufficiently represent the firn properties (Hörhold, 2006; Freitag and others, 2008).

The image-processing and analysis procedures were conducted with *MAVI* (Modular Algorithm for Volume Images), a software for analyzing 3-D material, developed by the Fraunhofer Institute (Armbrecht and Sych, 2005). After application of filter and segmentation procedures, an additional object filter was used to remove all objects adding less than 1% to the total pore or ice volume.

All parameters were obtained and analyzed referring to the volume of the firn cube. The porosity of a sample is given by the ratio of void representing voxels to the total voxel number of the firn cube. A measure for grain and pore size is the grain- and pore-chord length, defined as the mean intersection of a line with the object being the void or the grain in different directions (Ohser and Mücklich, 2000). The measurement of the surface area and the integral of mean curvature is based on the application of the so-called Crofton's intersection formulae (Ohser and Mücklich, 2000; Armbrecht and Sych, 2005). The surface density represents the ratio of the ice–air surface and the corresponding volume of the ice phase. Small-grained snow from the near surface will have a larger surface density than sintered, well-rounded snow deeper down the firn column. The integral of mean curvature is defined as the mean of the minimum and maximum curvature at each surface element, integrated over the whole surface of the volume (Ohser and Mücklich, 2000). It therefore is a measure of the curvature of the ice phase's structure and displays the size and roundness of the ice matrix. Divided by the number of voxels of each sample, we obtain a mean value for the sample, so negative values represent a mean of concave forms, and positive values a mean of convex forms within the firn cube. Dendritic crystals will show negative values and large, smooth surfaces result in curvature values around zero.

The strength of *MAVI* is that it enables the 3-D study of structure characteristics related to the surface density. Each surface element of a microstructural component can be represented by a surface-normal vector with its specific direction. The surface-normal distribution displays the directional distribution of all surface-normal vectors. Apart from gravitational settling along the z axis in the snow, vertical temperature gradients result in vertical water-vapor transport within the snowpack. Thus a preferential direction of the texture is to be expected in the vertical direction, and isotropic behaviour in the horizontal direction. Therefore in this paper we study the fraction of surface-normal vectors orientated in two horizontal and the vertical directions with an apex angle of 30° (Armbrecht and Sych, 2005). We take the ratio of the fractions of the horizontal directions (the mean of the two horizontal fractions) and the vertical direction (s-n fraction). The ratio for an istotropic texture such as a sphere will be 1, whereas the ratio of a texture elongated within the horizontal plane will be >1, and a texture elongated in the vertical plane will be <1 (Ohser and Mücklich, 2000).

Depending on the length of the core pieces (3–10 cm, as designated on the light-table), two to five subsamples were analyzed by micro-CT and averaged, representing the microstructure of that specific layer. In order to study larger-scale features, a running mean was applied with a window length covering several layers and weighting the points by the number of measured subsamples.

Density measurements within the uppermost 2.5 m of firn were used to convert this to a water equivalent depth of 0.9 m. Measured accumulation rates (personal communication from D. Dixon, 2006) were then used to calculate the time taken for a snow layer to be buried to a depth of 2.5 m.

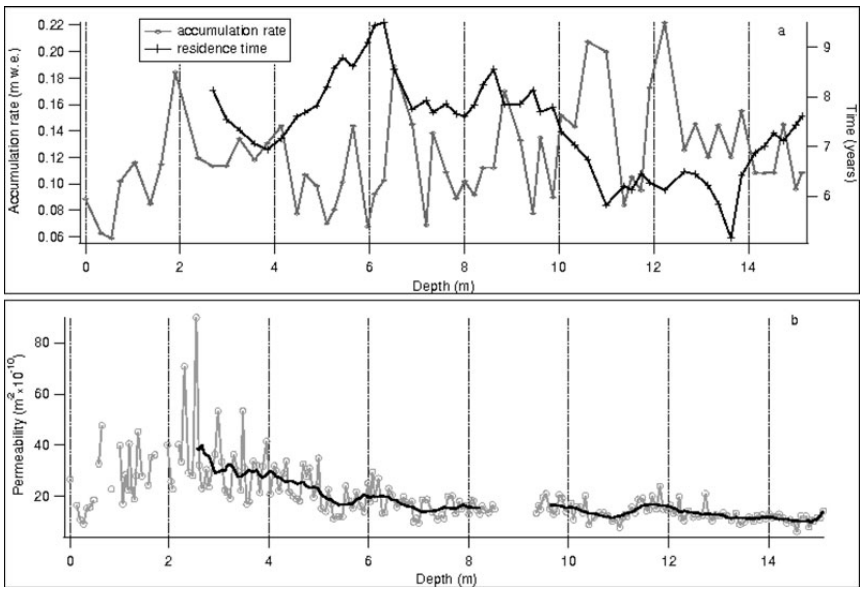

Fig. 2. (a) The accumulation rate as obtained by chemical analysis together with the calculated residence time in the uppermost 2.5 m and (b) the measured air permeability. The black curve is the running mean average over the different layers, starting from 2.5 m.

RESULTS

At Hercules Dome for the most recent 60 year accumulation estimates, based on chemical analysis and density measurements, a mean accumulation rate of approximately 0.12 m w.e. a^{-1} is observed (Fig. 2a). The calculated residence time within the uppermost 2.5 m shows a peak near 6 m depth, a local minimum below, a second peak near 8.5 m depth, and then generally decreases, with a local maximum near 12 m depth (Fig. 2a).

The results for permeability are shown in Figure 2b, and microstructural characteristics are shown in Figure 3. We observe a large variability of all parameters due to the layering of the firn. For the chord length in grain size and pore space (Fig. 3a and b) we find clearly larger values for the vertical than for the two horizontal directions. The ratio of the normal vector fractions is plotted in Figure 3f. A ratio of 1 indicates isotropy. Values less than 1, as found here, show that more surface-normal vectors point in the horizontal plane than in the vertical plane. The firn texture is vertically anisotropic.

In order to display the long-term trend, the running mean is calculated for all parameters (Figs 2b and 3). For the permeability we find an increase until 2.5 m depth. The permeability below is decreasing, but shows two local maxima near 6 and 12 m depth (Fig. 2b). Both the grain size and the pore size increase rapidly until 2–3 m depth. Below, the pore size decreases slowly (Fig. 3a and b). Whereas the porosity almost linearly decreases with depth (Fig. 3c), surface density and the mean of the integral of mean curvature rapidly decrease and increase respectively until 2 m depth, continuing their trend, but at more gradual rates, below this (Fig. 3d and e). For the anisotropy we find an increase until 2–3 m depth, and then a decrease, but with a region of low anisotropy between 7 and 8 m depth followed by a region of increased anisotropy near 10 m depth (Fig. 3f).

The increase in the chord lengths and the mean of the integral of mean curvature and the decrease of surface density imply coarsening of the texture until 2–3 m depth, accompanied not only by maximum permeability and pore size but also by maximum anisotropy. Here we refer to coarsening of firn as a general increase in both the grain size and the pore size. Below that, densification becomes significant, and continued gradual metamorphism decreases pore size and porosity while continuously increasing the grain size. At this site the firn is highly stratified, with each layer showing very different properties in terms of microstructure, permeability and development of anisotropy. The illustrated variation in the longer-term trends, particularly in the permeability and anisotropy profiles, is not related to the layering but to longer-term processes.

ANISOTROPY

At Hercules Dome the maximum degree of anisotropy is reached at approximately 2.5 m depth (Fig. 3d). However, in contrast to previous studies (Alley, 1987), we find that anisotropy does exist below that, though it tends to decrease with depth. Moreover, these data show that anisotropy does not decrease in monotonic fashion, but rather that there are depths at which anisotropy is strongly pronounced and other depths at which it is not.

Yosida and others (1955) and Colbeck (1983) introduced models of oriented crystal growth. In natural snow subjected to changes in weather, temperature gradients are mostly oriented in the vertical direction. The temperature gradients then induce gradients in water-vapor transport. Crystals grow by condensation of water vapor on their bottom portions, because the bottom of a growing particle is cold relative to the average snow temperature at its height (Colbeck, 1983). Alley and others (1982) found that crystals in coarse firn exhibit a strong vertical shape orientation near the surface, which can be attributed to the strong vertical water-vapor and heat transport.

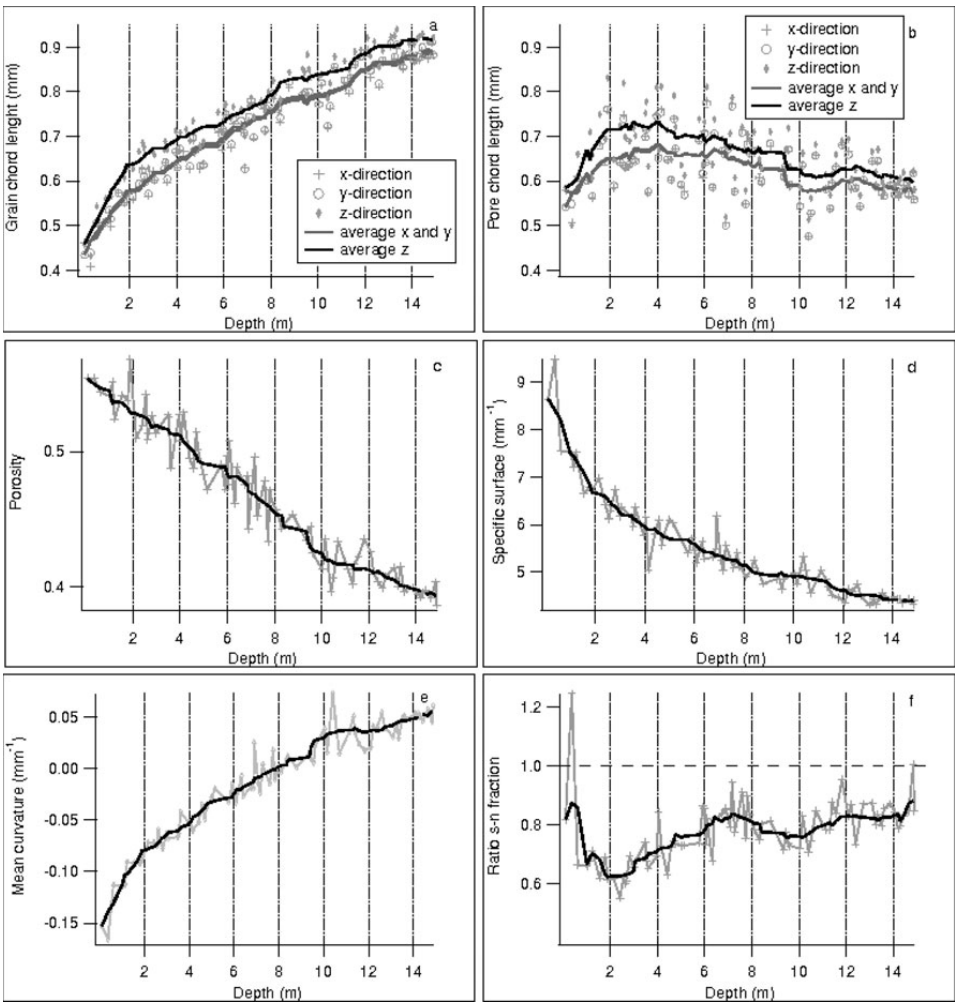

Fig. 3. (a, b) The mean grain (a) and pore (b) chord lengths in *x*, *y* and *z* directions. Dark curves represent the running mean (grey for horizontal; black for vertical). (c–f) The porosity (c), surface density (d), mean curvature (e) and ratio of the normal vector fractions s-n (f),

On the other hand, Schneebeli and Sokratov (2004) found in temperature gradient experiments with different snow layers that anisotropy occurred in dense, fine-grained layers, whereas low-density layers exposed to similar gradients did not show an anisotropy texture after the same time interval. Our data support these observations: we find highly porous layers to be less anisotropic than less porous layers in the same depth interval. The small-scale variability in the anisotropy profile is probably controlled by the different formation of anisotropy in the different layers.

ACCUMULATION RATE AND RESIDENCE TIME

From the microstructure and permeability data we can conclude that despite the very different properties of the different layers in terms of permeability and anisotropy, the larger-scale features shape the evolution with depth. These features are visible in both the low- and high-permeability layers and in the low- and high anisotropy layers respectively. The observed variability does not originate from the layering nor the linear compaction with depth. Changes in the metamorphic regime must be the basic cause. A major parameter determining the metamorphism is the impact of the accumulation rate, which, however, is difficult to parameterize since it superimposes the effects of the layering and densification.

The maximum in coarsening, permeability and anisotropy is obtained by 2.5 m depth, while below that, densification combined with slow grain growth appears to become important. It appears that, at this site, as long as a certain layer stays in the uppermost 2.5 m, it is exposed to significant temperature gradients, periodically higher annual temperatures and metamorphically induced coarsening. We hypothesize that the degree of coarsening, permeability and anisotropy of each layer deeper down the firn column is designated by the degree of these parameters at 2.5 m depth. In turn the degree at 2.5 m depth results from the history between 0 and 2.5 m depth, i.e. the time spent in the near-surface area. This residence time depends only on the accumulation rate.

We test the possibility that the time that snow spends in the near surface influences its permeability and anisotropy at

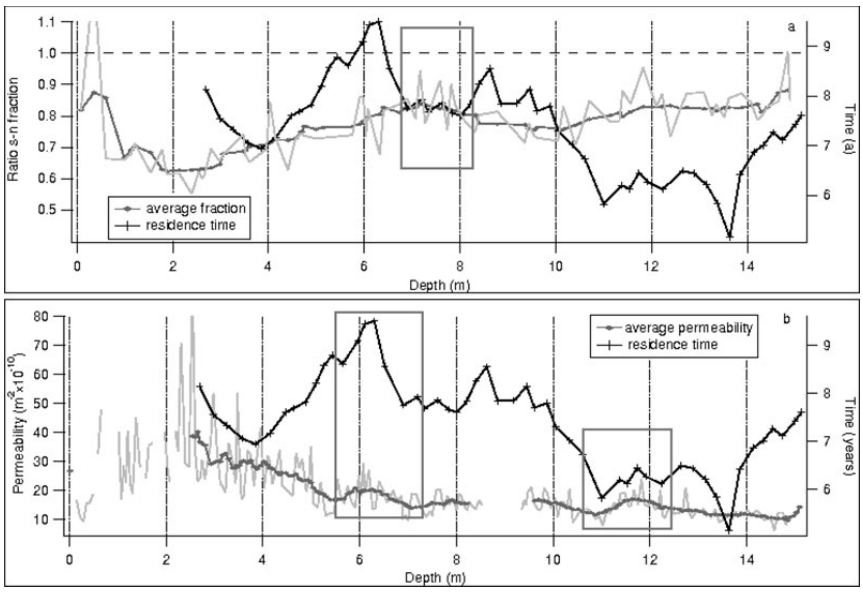

Fig. 4. The residence time with mean anisotropy (a) and air permeability (b).

depth, by using the density to calculate residence time in the near surface (Fig. 2a). Since the accumulation rate and thus the residence time were calculated on different scales and samples than the microstructure and permeability, here we can only compare the evolution with depth of these two different parameter sets (Fig. 4a and b).

An examination of the residence time in comparison with the average anisotropy in Figure 4a shows that it is the zone between 7 and 8 m where the surrounding long residence times are briefly interrupted by a phase of decreased residence time. When the firn at 7–8 m depth in this firn core was near-surface snow, it did indeed spend less time in the near surface. The shorter time that it spent in the near-surface region of higher temperature gradients means that it was less exposed to rapid metamorphic processes. The result is that the firn structure at 7–8 m shows low vertical anisotropy (Fig. 4a). As shown in Figure 4a, the residence time in the near-surface area decreases below 10 m depth and thus results in a less anisotropic character. The features of very short residence time around 11 m and at 13–14 m are not reflected in anisotropy.

In Figure 4b the measured air permeability is shown, together with the residence time. The peak in permeability at 2.5 m depth is due to the maximum of coarsening. Similar increases in permeability down to 2–4 m have been reported previously at different high-accumulation polar sites (Albert and others, 2000; Albert and Schulz, 2002; Rick and Albert, 2004). The second maximum around 6 m depth and at 11–12 m can again be linked to the residence time. Increased residence time strengthens the connectivity of the pore space and by that the air permeability of the firn. The residence-time minima at 7 and 11 m coincide with distinct permeability minima. Nevertheless there are areas where a correlation is not apparent, such as the decrease in permeability above 6 m, even though the residence time is increasing.

Not all changes in residence time are displayed in the analyzed microstructural parameters, especially at greater depths. Additionally the anisotropy and the air permeability of the firn clearly behave differently with regard to the residence time (Fig. 4a and b). Accordingly, other processes contribute to the evolution of firn properties with depth; the mechanisms for the genesis of anisotropy and permeability differ at depths below several meters in firn. Courville (2007) observed a much larger impact of small changes in accumulation pattern on microstructure and permeability in regions of very low accumulation than in regions of high accumulation. This might be one explanation for the less pronounced influence of changes in accumulation rate in the deeper firn layers, where the correlated accumulation rate was higher than in the uppermost meter. On the other hand, Rick and Albert (2004) show that the growth of necks between the grains is the dominant mechanism for permeability reduction at depths between approximately 2 and 10 m, and that a warming of temperatures over time would also impact metamorphism at this depth. Thus, the top ~10 m of firn is subject to a number of effects that would be reflected in the permeability of buried layers, including trends in surface temperature and accumulation rates. The calculated residence time is an integrated measure over the uppermost 2.5 m. We do not know the residence time of individual layers (e.g whether a certain layer has spent a certain fraction of the time in the very uppermost centimeters and might therefore be exposed to large temperature gradients, or whether it monotonically became buried below 2.5 m depth). Anisotropy is probably mainly generated within the upper few centimeters below the surface, where temperature gradients are largest. Permeability, on the other hand, could be the result of longer-term processes such as the interaction of air ventilation and coarsening, which increase the pore size or pore connectivity when densification does not overrule the effect. This seems to be the case in the upper 2.5 m at this site. Thus more differentiated residence times for different depth intervals need to be investigated.

CONCLUSION

The highly layered polar firn reflects the occurrence of metamorphism of different snow types at large timescales and under constantly changing environmental conditions. At Hercules Dome, the maximum in our permeability measurements from this site is consistent with measurements at other sites (Albert and others, 2000; Albert and Shultz, 2002; Rick and Albert, 2004) showing a permeability maximum near ~2.5 m depth. Our first results from 3-D microtomography scan imaging of polar firn show that this is accompanied by general firn coarsening (increase in both grain size and interstitial pore space) in this region. Below that, other processes including grain growth, necking and compaction influence the metamorphism of the microstructure. The texture of the firn shows distinct anisotropy throughout the profile, which is a result of vertical temperature gradients and subsequent water-vapor gradients. Short-term changes in accumulation rate affect the residence time of certain firn layers in the uppermost meter of the firn column, where rapid metamorphism takes place and the largest temperature gradients occur. We found a clear signature of changing accumulation rate in the firn-anisotropy and air-permeability profiles in the firn below approximately 5 m depth. Our data confirm that even though the effects of changes are most pronounced in the near surface, they remain evident through time as the firn becomes buried, even at this high-accumulation site.

ACKNOWLEDGEMENTS

We thank the US ITASE field team 2002 for drilling the core, and D. Dixon from University of Maine for providing the accumulation rate data of the site. This work was funded in part by German Science Foundation (DFG) grant FR2527/1-1 and supported by the German Academic Exchange Division (DAAD) and funded in part by US National Science Foundation grants NSF-OPP 0538492 and NSF-OPP 0229527 to M. Albert. We also thank the two anonymous reviewers for helpful comments.

REFERENCES

Albert, M.R. and E. Shultz. 2002. Snow and firn properties and air–snow transport processes at Summit, Greenland. *Atmos. Environ.,* **36**(15–16), 2789–2797.

Albert, M.R., E.F. Shultz and F.E. Perron, Jr. 2000. Snow and firn permeability at Siple Dome, Antarctica. *Ann. Glaciol.,* **31**, 353–356.

Albert, M., C. Shuman, Z. Courville, R. Bauer, M. Fahnestock and T. Scambos. 2004. Extreme firn metamorphism: impact of decades of vapor transport on near-surface firn at a low-accumulation glazed site on the East Antarctic plateau. *Ann. Glaciol.,* **39**, 73–78.

Alley, R.B. 1987. Texture of polar firn for remote sensing. *Ann. Glaciol.,* **9**, 1–4.

Alley, R.B. 1988. Concerning the deposition and diagenesis of strata in polar firn. *J. Glaciol.,* **34**(118), 283–290.

Alley, R.B., J.F. Bolzan and I.M. Whillans. 1982. Polar firn densification and grain growth. *Ann. Glaciol.,* **3**, 7–11.

Armbrecht, J. and T. Sych. 2005. *MAVI – Modular algorithms for volume images.* Kaiserslautern, Fraunhofer Institut für Techno- und Wirtschaftsmathematik.

Colbeck, S.C. 1983. Theory of metamorphism of dry snow. *J. Geophys. Res.,* **88**(C9), 5475–5482.

Coléou, C., B. Lesaffre, J.B. Brzoska, W. Ludwig and E. Boller. 2001. Three-dimensional snow images by X-ray microtomography. *Ann. Glaciol.,* **32**, 75–81.

Courville, Z.R. 2007. Gas diffusivity and air permeability of the firn from cold polar sites. (PhD thesis, Dartmouth College.)

Courville, Z.R., M.R. Albert, M.A. Fahnestock, L.M. Cathles and C.A. Shuman. 2007. Impacts of an accumulation hiatus on the physical properties of firn at a low-accumulation polar site. *J. Geophys. Res.,* **112**(F2), F02030. (10.1029/2005JF000429.)

Davis, R.E., E.M. Arons and M.R. Albert. 1996. Metamorphism of polar firn: significance of microstructure in energy, mass and chemical species transfer. *In* Wolff, E.W. and R.C. Bales, *eds. Chemical exchange between the atmosphere and polar snow.* Berlin, etc., Springer-Verlag, 379–401. (NATO ASI Series I: Global Environmental Change 43.)

Flin, F., J.-B. Brzoska, B. Lesaffre, C. Coléou and R.A. Pieritz. 2004. Three-dimensional geometric measurements of snow microstructural evolution under isothermal conditions. *Ann. Glaciol.,* **38**, 39–44.

Freitag, J., S. Kipstuhl and S.H. Faria. 2008. The connectivity of crystallite agglomerates in low-density firn at Kohnen station, Dronning Maud Land, Antarctica. *Ann. Glaciol.,* **49**, 114–120.

Gow, A.J. 1965. On the accumulation and seasonal stratification of snow at the South Pole. *J. Glaciol.,* **5**(40), 467–477.

Gow, A.J. 1969. On the rates of growth of grains and crystals in South Polar firn. *J. Glaciol.,* **8**(53), 241–252.

Hörhold, M.W. 2006. Microstructure and air transport properties of polar firn. (MS thesis, University of Bremen.)

Jacobel, R., B.C. Welch, E. Steig and D. Schneider. 2005. Glaciological and climatic significance of Hercules Dome, Antarctica – an optimal site for deep ice core drilling. *J. Geophys. Res.,* **110**(F1), F01015. (10.1029/2004JF000188.)

Kaempfer, T.U. and M. Schneebeli. 2007. Observation of isothermal metamorphism of new snow and interpretation as a sintering process. *J. Geophys. Res.,* **112**(D24), D24101. (10.1029/2007JD009047.)

Kaempfer, T.U., M. Schneebeli and S.A. Sokratov. 2005. A microstructural approach to model heat transfer in snow. *Geophys. Res. Lett.,* **32**(21), L21503. (10.1029/2005GL023873.)

Ohser, J. and F. Mücklich 2000. *Statistical analysis of microstructures in materials science.* Chichester, Wiley.

Palais, J.M., I.M. Whillans and C. Bull. 1982. Snow stratigraphic studies at Dome C, East Antarctica: an investigation of depositional and diagenetic processes. *Ann. Glaciol.,* **3**, 239–242.

Pieritz, R.A., J.B. Brzoska, F. Flin, B. Lesaffre and C. Coléou. 2004. From snow X-ray microtomograph raw volume data to micromechanics modeling: first results. *Ann. Glaciol.,* **38**, 52–58.

Rick, U.K. and M.R. Albert. 2004. Microstructure and permeability in the near-surface firn near a potential US deep-drilling site in West Antarctica. *Ann. Glaciol.,* **39**, 62–66.

Schneebeli, M. and S.A. Sokratov. 2004. Tomography of temperature gradient metamorphism of snow and associated changes in heat conductivity. *Hydrol. Process.,* **18**(18), 3655–3665.

Shiraiwa, T., H. Shoji, T. Saito, K. Yokoyama and O. Watanabe. 1996. Structure and dielectric properties of surface snow along the traverse route from coast to Dome Fuji Station, Queen Maud Land, Antarctica. *Proc. NIPR Symp. Polar Meteorol. Glaciol.,* **10**, 1–12.

Watanabe, O. 1978. Distribution of surface features of snow cover in Mizuho Plateau. *Mem. Natl Inst. Polar Res.,* Special Issue 7, 154–181.

Yosida, Z. *and 6 others.* 1955. Physical studies on deposited snow. I. Thermal properties. *Contrib. Inst. Low Temp. Sci. Ser. A* 7, 19–74.

MS received 18 February 2008 and accepted in revised form 27 January 2009

E Publication 5 - Lattice Boltzmann modeling of the air permeability of polar firn

Courville, Z., Hörhold, M. W., Hopkins, M., Albert, M.

Journal of Geophysical Research, Earth Surface, accepted.

Lattice-Boltzmann modeling of the air permeability of polar firn

Air permeability modeling of firn

Zoe Courville
Cold Regions Research and Engineering Laboratory
Hanover, NH USA

Maria Hörhold
Alfred Wegener Institute for Polar and Marine Sciences
Bremerhaven, Germany

Mark Hopkins
Cold Regions Research and Engineering Laboratory
Hanover, NH USA

Mary Albert
Thayer School of Engineering
Dartmouth College
Hanover, NH USA

Abstract

Recent advances in three-dimensional (3-D) imaging of snow and firn combined with numerical modeling of flow through complex geometries have greatly improved the ability to predict permeability values based on microstructure. In this work, we combined 3-D reconstructions of polar firn microstructure obtained from micro-computed tomography (micro-CT) reconstructions and a 3-D lattice-Boltzmann model of air flow. We compared the modeled results to measurements of permeability for polar firn with a wide range of grain and pore scale characteristics. The results show good agreement between permeability measurements and modeled permeability values from the lattice-Boltzmann model over a wide range of sample types. The lattice-Boltzmann model is better at predicting measured permeability values than traditional empirical equations for polar firn.

34 1. Introduction

35 Snow and firn properties influence the transport of gases between the atmosphere
36 and underlying snowpack and are thus important for understanding chemical transport
37 and interpreting ice cores [*Albert et al*., 2004]. Vapor transport, in particular, can be
38 enhanced by "wind-pumping," pressure driven ventilation in firn due to wind moving
39 over surface roughness [*Colbeck*, 1989]. This effect is especially amplified in areas of
40 high permeability, large grained (and large-pore-size) snow [*Albert*, 2002 and *Albert et*
41 *al.*, 2004]. Permeability is a material property that affects the ability of a fluid to move
42 through a porous material. Until recently, it has been impossible to calculate the detailed
43 flow field through a three dimensional (3-D) heterogeneous porous medium. Past efforts
44 to calculate transport through snow have used numerical solutions based on either
45 continuum theory or a simplified representation of the microstructure. Simplified snow
46 microstructures have been represented by either an assemblage of spherical grains or
47 bundles of capillaries, and transport equations have been developed according to
48 empirical formulas based on research in similar porous media such as soils and
49 sandstones [*Carman*, 1956; *Walsh and Brace*, 1984; *Costa*, 2006]. The advantage of this
50 approach is that the parameters utilized in the empirical formulas (e.g. porosity, volume-
51 to-surface ratio, grain size, pore size) are generally first-order and are relatively easily
52 and inexpensively obtained from two-dimensional (2-D) thin or thick sections as well as
53 newly developed optical techniques [e.g. *Dominé et al*., 2006; *Matzl and Schneebeli,*
54 2006; *Painter et al*., 2007; *Gallet et al*., 2009] for determining specific surface area.
55 Snow researchers have recently begun to employ more sophisticated and realistic models
56 of 3-D microstructural geometry in snow for use in heat transport models [*Arons and*

57 *Colbeck*, 1998] and 3-D data obtained from micro-computed tomography (micro-CT)
58 imaging of snow for use in densification and heat and gas transport models in snow
59 [*Lundy et al*., 2002; *Freitag et al*., 2004; *Kaempfer et al*., 2005]. *Hörhold et al*. [2009]
60 presented the first 3-D analysis of anisotropy and permeability of polar firn based on
61 micro-CT data using samples from Hercules Dome, Antarctica.

62 The permeability of a material can be expressed by Darcy's equation:

63 $$\frac{q}{A} = -\frac{k}{\mu}\nabla p\,, \qquad (1)$$

64 where k is the permeability of the medium, q is the volumetric flow rate, A is the
65 cross-sectional area of the material, ∇p is the pressure gradient through the material, and
66 μ is the fluid viscosity. The permeability of the medium can be expressed in terms of
67 porosity by equating Poiseuille's law with Darcy's equation. Poiseuille's law for a
68 conduit model of a porous medium comprised of cylindrical tubes of constant radius is:

69 $$\frac{q}{A} = -\frac{R^2\phi}{8\mu}\nabla p \qquad (2)$$

70 where R is the radius of the tubes making up the conduit model and ϕ is the total
71 porosity of a material, or the total open space of the material, as determined by:

72 $$\phi = 1 - \rho_{snow}/\rho_{ice} \qquad (3)$$

73 where ρ_{snow} is the density of the snow and ρ_{ice} is the density of ice. The total
74 porosity is easily determined from laboratory measurements of density. The open
75 porosity, or the porosity open to air flow throughout the sample without the contribution
76 of dead end or closed pores which do not contribute to air flow, is more germane to

77 determining the permeability, but also harder to determine. Solving for the permeability
78 produces the Kozeny-Carman equation [e.g. *Revil and Cathles*, 1999]:

79 $$k = \frac{\phi}{c}\left(\frac{V_p}{S}\right)^2 = \frac{\phi}{c}\left(\frac{R}{2}\right)^2, \qquad (4)$$

80 where V_p/S, is the ratio of the pore volume to surface area, which equals
81 $(\pi R^2 L)/(2\pi RL) = R/2$ when the pore geometry is assumed to be a bundle of cylindrical
82 tubes. R is the radius of the tubes, L is the length of the tubes, and c is dependent on the
83 cross-sectional area of the tubes that make up the microstructure model; $c = 2$ for circular
84 pores, 1.67 for equilateral triangles, 1.78 for squares. Empirically, c has been found to be
85 5 for many types of granular porous media [*Carman*, 1956; *Dullien*, 1992].
86 Snow, existing as a solid in a range of temperatures approaching its melting point,
87 is a unique porous medium in that surface layers undergo rapid metamorphism from
88 sublimation and condensation processes driven by diurnal and seasonal temperature
89 gradients [*Colbeck*, 1983; *Kaempfer et al*., 2005; *Pinzer and Schneebeli*, 2009]. Snow
90 exists naturally in several complex forms, ranging from those best modeled as random
91 assemblages of nearly spherical particles for newly fallen, wind blown snow, or as
92 conduit bundles for compacted firn. The microstructure of snow can be extremely
93 complex, as exhibited by faceted, cup-shaped depth hoar. Snow also exhibits a large
94 variability of site-to-site permeability values [*Rick and Albert*, 2004] correlated to
95 variations in conditions, as well as large temporal variability related to metamorphism
96 and seasonal variability in snow properties. Permeability of polar firn, snow more than
97 one year old, has been measured at a number of sites, e.g. *Albert et al.,* [2000], *Albert*

98 *and Shultz* [2002], *Rick and Albert* [2004], *Albert et al*., [2004], *Courville et al*., [2007],
99 *Hörhold et al*., [2009], and *Fujita et al*., [2009].

100 Until recently, the only technique for imaging the 3-D microstructure of snow was
101 to fill the pores with a fixative, perform serial thin sections of the encapsulated snow, and
102 reassemble the thin sections. In recent years, micro-CT techniques have been developed
103 that permit the nondestructive imaging of snow samples. The micro-CT uses sequential
104 x-ray scans of a material to recreate 3-D images of snow samples taken from the field. It
105 is a well-developed tool that has been used to examine the structure of a variety of porous
106 media by several researchers [e.g. *Auzerais et al*., 1996; *Coker et al*., 1996; and *Fredrich*
107 *et al*., 2006] and recently by investigators examining snow structure [*Coléou et al*., 2001;
108 *Flin et al*., 2001; *Lundy et al*., 2002; *Freitag et al*., 2004; *Pieritz et al.*, 2004; *Schneebeli*,
109 2004; *Kaempfer et al*., 2005; *Flin and Brzoska*, 2008; and *Hörhold et al.,* 2009].

110 In conjunction with the improved ability to image 3-D microstructures, numerical
111 techniques have been developed that use high resolution digital models to calculate heat
112 conduction and gas flow through 3-D microstructures. One of these is the lattice-
113 Boltzmann method (LBM), which is well suited to model viscous flow through porous
114 media. Lattice-Boltzmann models were developed from lattice gas models in which
115 discrete gas particles move on a lattice network. The particles are allowed to collide at
116 nodes, with collisions governed by a simplified collision operator. After collision, the
117 particles bounce back in the direction opposite the original path. The movement and
118 collision of the particles is governed by kinetic gas theory. After a collision, the
119 distribution is allowed to relax into equilibrium by one of several collision operators
120 which have been developed. The Navier-Stokes equations can be recovered from the

121 lattice-Boltzmann algorithm through the collision operator [*Succi*, 2002]. Lattice-
122 Boltzmann models using micro-CT 3-D data as input have been used to compute the
123 permeability of several types of porous media [*Chen and Doolen*, 1998] including
124 sandstone [e.g. *Auzerais et al*., 1996; *Manwart et al., 2002*; *Arns et al.*, 2004; *White et al*.,
125 2006; and *Kemeda et al*., 2006], sand [e.g. *Ahrenholz et al*., 2006; *Lehmann et al*., 2008],
126 and metallic foams [e.g. *Gerbaux et al*., 2010]. *Freitag et al*. [2002] used 3-D data
127 obtained from serial sectioning of snow samples in lattice-Boltzmann models of air
128 permeability and gas diffusivity. In this work, we combined 3-D micro-CT
129 reconstructions and a 3-D lattice-Boltzmann model of air flow and compared the modeled
130 results to measurements of permeability for polar firn with a wide range of grain and pore
131 scale characteristics.
132
133 2. Methods
134 2.1 Field sites and samples
135 We examined two sets of firn samples as part of this work. The first set of
136 samples is taken from the megadunes region of East Antarctica (81°S, 125°E). We chose
137 eight samples from two different megadunes areas, located within 3 km of one another,
138 with two different accumulation rates. Four samples were taken from the windward face
139 of a dune, in an area of low accumulation (2 to 3 cm w.e. a^{-1}) and four samples were
140 taken from the leeward face of the dune, in an area that experienced no snow
141 accumulation (hiatus) [*Courville et al*., 2007]. The samples were taken from depths of 0.1
142 m, 0.4 m, 8 m, 9 m, and 10 m. The different accumulation rates in the megadunes area
143 resulted in varying grain and pore sizes; in polar areas in general, low accumulation rates

144 result in large grains due to longer residence times spent in near-surface temperature
145 gradients. The second set of samples were taken from an area experiencing relatively
146 higher accumulation, Hercules Dome, Antarctica (86°S, 105°W), with an accumulation
147 rate estimated to be 18 to 22 cm w.e. a^{-1}.

148 We obtained the core samples from the megadunes area using both an
149 electromechanical drill and a hand drill. These samples were 8 cm in diameter and
150 nominally 1 m in length. The Hercules Dome firn cores were taken during the 2004 US
151 ITASE traverse using a smaller electromechanical drill and were 5 cm in diameter and 1
152 m in length.

153

154 2.2 Laboratory Methods

155 The core samples were shipped to CRREL in Hanover, NH, where stratigraphy,
156 density, permeability, grain size, gas diffusivity, and thermal conductivity measurements
157 were made in a cold room laboratory. From the 1-m long cores retrieved in the field, we
158 cut sections of relatively homogeneous layers based on visual stratigraphy. These
159 samples varied from 4- to 10-cm in length. The density of each sample was determined
160 from measurements of mass and volume.

161 The permeability is determined from pressure and flow rate measured with a
162 custom-designed permeameter [*Albert et al.,* 2000]. The permeameter is based on
163 *Shimizu* [1970]'s design, which incorporates a double-head flow sampler that eliminates
164 edge effects. The sampler has two concentric regions in which flow and pressure are
165 measured through the sample. The pressure in the two regions is matched to ensure that
166 the flow is the same, and measurements are read through the center of the sample. A

167 flexible rubber membrane is inflated around the core sample to create an air-tight seal.
168 The rubber membrane accommodates a wide range of sample diameters and lengths. We
169 make ten pressure measurements at incremental flow rates, and ensure that the pressure
170 versus flow rate measurements follow Darcy's equation, i.e. are linear. Any
171 measurement values that are not linear are repeated or discarded. The ten values of
172 permeability at the different flow rates for any given sample are generally within 3% of
173 one another. Replicate permeability values from tests on the same samples are on
174 average within 6% of one another. Permeability values from tests on samples from the
175 same layer in a snow pack vary less than 10% [*Albert and Perron*, 2000]. The minimum
176 length of a sample that can accurately be measured in the permeameter is 3 cm. It is
177 often the case that several stratigraphic layers are present in one bulk sample due to the
178 inhomogeneous nature of most firn, especially near-surface firn from high accumulation
179 areas.
180
181 2.3 Micro-tomography
182 We shipped the core samples in insulated boxes as received, with no pore-filler, to
183 the Alfred Wegener Institute (AWI) in Bremerhaven, Germany for micro-CT imaging.
184 The AWI micro-CT scanner is a commercially available Skyscan 1074SR modified to
185 operate in a -25°C cold room, as described in *Freitag et al.* [2002]. The CT scanner has
186 an integrated microfocus X-ray tube that operates at 40 kV and 1000 μA. A charge-
187 coupled device (CCD) camera is used as the X-ray detector with a total range of 256
188 greyscale units. The mean grey levels of ice and pore space differ by as many as 100
189 greyscale units, with a signal-to-noise ratio >120, which allows the two phases to be

190 distinguished from one another. The snow sample is placed on a turntable which rotates
191 at intervals of 0.9°. 210 shadow images make up one 180° rotation of the sample. A
192 digital convolution algorithm transforms the shadow images into a series of horizontal
193 cross-sectional images that are used to construct the 3-D structure of the final image. 490
194 horizontal scans at 40 micron spacing make up one three dimensional image. The
195 resolution of one voxel is 40 microns. The maximum size of sample that can fit in the
196 CT-scanner is 25 mm in diameter and 20 mm in height. Each original bulk sample was
197 cut into three to five subsamples 2 cm in length in order to fit in the CT-scanner. A hole
198 saw was used to cut a 2.5-cm diameter core out of the center of the original larger core
199 sample. The 2.5-cm diameter grey value images from the CT-scanner are then cropped to
200 a 1.6-cm cube, segmented and filtered, and used as the input in the lattice-Boltzmann
201 model.
202 We determined the threshold value between air (white) and ice (black) pixels for
203 each sample using two different methods. The first method involved choosing a
204 threshold value for each subsample so that the average overall porosity of the modeled
205 subsamples equaled the original measured sample porosity. The threshold for each of the
206 individual subsamples was chosen so that 2-D slices of the binary image matched the
207 geometry of the greyscale image based on visual inspection. The second method, as
208 outlined in *Freitag et al*., 2004 and *Hörhold et al., 2009*, is to choose the threshold value
209 as the mid-point of the maxima for the pore space and ice particle values in the greyscale
210 histogram from several of the 2-D slices. Threshold values for each individual subsample
211 were chosen in this manner, as opposed to picking a universal threshold value for all
212 samples. Both methods result in reconstructed digital samples with porosities near the

213 measured porosities of the original samples (see Table 2 for a summary of the porosity
214 values). *Freitag et al*., 2004 compare the density calculated from the micro-CT data to
215 high-resolution density measured by gamma absorption and found that they agreed well.
216 The sample images were processed either using a 3x3x3 Gaussian filter with $\sigma = 1.2$
217 (megadunes samples) or a 3-D median filter with a 3x3x3 mask (Hercules Dome
218 samples) in order to remove image artifacts. The binary, filtered images were
219 reassembled into a 3-D reconstruction and used as input for the 3-D LBM permeability
220 model. Samples of the 3-D micro-CT digital reconstructions of firn from each megadunes
221 area are shown in Figure 1. Microstructural characterization from the 3-D
222 reconstructions of the micro-CT data for the samples was determined using MAVI
223 (Modulated Algorithms for Volume Images), a specialized, commercially-available,
224 micro-CT software package. Microstructure data represent mean values of a volume of
225 ~4.096 cm^3 of firn. Porosity, ϕ, is the fraction of air voxels in the volume, or the total
226 porosity. The density of the snow sample is calculated from the micro-CT data as $(1-\phi)\rho_{ice}$, where ρ_{ice} is the density of ice, equal to 0.917 g/cm^3. The specific surface of the
228 snow matrix, SSA, is defined as the surface density per mass, and is determined from the
229 micro-CT data as:

230 $$\text{SSA} = \text{total surface area of snow/ total unit volume} \quad (5)$$

231 The effective diameter, d_{eff}, or optical grain size is then calculated from the SSA [*Warren*,
232 1982, *Nolin and Dozier*, 1993*, Nolin and Dozier*, 2000]:

233 $$d_{eff} = 6/\text{SSA} \quad (6)$$

234 We report the effective grain diameter, d_{eff}, as proposed by *Dominé et al*., 2008 and
235 others. The volume-to-surface-ratio of the pores, V_p/S, is calculated by dividing the total

236 volume of the pores (air fraction) by the total surface. The tortuosity factor can be
237 calculated by MAVI geometrically. The value is obtained by an arithmetic mean of all
238 pathways.
239
240 2.4 Lattice-Boltzmann Model
241 The LB model uses a 19-direction D3Q19 lattice [*Succi*, 2002]. The middle node
242 represents the rest particle, with the remaining nodes representing 18 possible non-zero
243 velocities. The 3-D data from micro-CT scans are used as the input geometry for the
244 model. Each voxel in the 3-D image represents one node in the lattice-Boltzmann model
245 so that the resolution of the model is also 40 microns. The model uses a force at each
246 pore node to drive the flow that approximates the pressure gradient across the sample.
247 The model utilizes the Bhatnagar-Gross-Krook (BGK) collision operator which employs
248 a single relaxation time parameter. The 3-D cubic model snow samples have a 40 micron
249 resolution that results in 320x320x320 nodes. To make the sample periodic in the flow
250 direction a cubic sample is reflected about the plane perpendicular to the flow and joined
251 to its mirror image. The final sample has 320x320x640 nodes. Simple on-site bounce-
252 back is used at pore-solid interfaces as well as at the solid boundary at the sample sides.
253 The flow through the model sample reaches reasonable convergence in about 5000 time
254 steps, which takes approximately 10 hours to run on a PC. Low Reynolds numbers, less
255 than 0.1, were used in order to insure laminar flow. The Reynolds number is determined
256 by VL/ν, where V is the fluid velocity per unit cross-sectional area, as calculated by the
257 LBM; L is an arbitrary length, equal to 10 lattice units; and ν is the kinematic viscosity,
258 which is set to a constant value. The permeability of the sample is computed from

259 Darcy's equation. The model was validated by testing flow around consolidated periodic
260 arrays of spheres compared to published results [*dos Santos et al*., 2005; *Larson and*
261 *Higdon*, 1989]. The results of the test of Stokes flow around consolidated spheres (i.e.
262 spheres with non-zero contact area between spheres) are shown in Table 1, the
263 dimensions are in lattice units.

264 For the megadunes samples, the LBM composite permeability, k_{COMP}, for three to
265 five subsamples were combined by adding the reciprocal of each subsample weighted by
266 the subsample length to estimate the bulk permeability of the original sample:

267

268 $$k_{COMP} = \frac{L}{\sum_{i}^{m} \frac{L_i}{(k)_i}} \qquad (7)$$

269

270 where L is the total length of the sample, L_i is the length of the subsample, i, and
271 $(k)_i$ is the permeability of the *ith* subsample. For the Hercules Dome samples, we chose
272 one representative subsample to model permeability using the LBM.

273 The REV (representative elementary volume) of the both coarse and fine grained
274 sample types was determined by running the LB model for cubic volumes of
275 100x100x100 voxels at 125 different starting voxel locations, 150x150x150 at 27
276 different starting locations, 200x200x200 at eight different starting locations and
277 250x250x250 at eight starting locations. The results for two different types of samples are
278 shown in Figure 2. For the fine-grained sample, the 200 unit voxel cube (0.5 cm^3) is a
279 stable result, with the permeability values calculated for the 250 unit cube (1 cm^3) having
280 a standard deviation of +/-7%. For the course-grained sample, the 250 unit cube (1 cm^3)

281 gives a reasonable result, with the average deviation from the result of the model using
282 the entire 320 cubic volume +/-5%, and the standard deviation of the results of the eight
283 250 cubic units being +/-7%. This is within the limit of the error of our permeability
284 measurements. Examination of the REV model runs for the coarse-grained samples
285 reveal that some of these subsample were stratified, with top and bottom portions having
286 different permeability values, i.e. volumes sampled from different portions of the entire
287 sample revealed systematic, geometrically based differences. The result of the
288 stratification of the coarse-grained subsample is that a larger REV is required to produce
289 a reasonable permeability value.
290
291 3. Model and Measurement Validation
292 We determined the permeability of a 10-cm diameter, 10-cm height cylinder
293 randomly packed with 4-mm diameter glass beads using the permeameter [*Albert et al.*,
294 2007]. The measured permeability for the beads was $k = 9.97 \times 10^{-9}$ m^2 +/- 0.50×10^{-9} m^2
295 for 20 replicate tests, which compares well to the Kozeny-Carman (KC), $k_{KC} = 10.12 \times$
296 10^{-9} m^2, and the Kozeny-Blake (KB), $k_{KB} = 12.15 \times 10^{-9}$ m^2, predictions for
297 unconsolidated granular media of the same diameter and porosity. The lattice-Boltzmann
298 model value of a computer generated sample of glass beads with the same geometry was
299 10.70×10^{-9} m^2, with a relative error of 7% compared to the average measured value for
300 the bead packs, and reasonably close to the precision of the permeameter, approximately
301 5%.
302 4. Results for Firn Samples
303 4.1 Microstructure characterization

304 Results for the microstuctural properties of the micro-CT data are summarized in
305 Table 2. *Hörhold et al*., [2009] presents many more details on the Hercules Dome data.
306 The near surface snow grains at the hiatus site were large, with an effective grain
307 diameter of 1.5 mm on average, compared to the accumulation site, with an effective
308 grain diameter of 1.0 mm in the near surface, as determined from micro-CT data. The
309 average effective grain diameter of the Hercules Dome samples in the near surface was
310 1.5 mm. The porosities of the samples, determined from density measurements, vary
311 from 0.4 to 0.6. The average pore sizes, determined from the micro-CT data, vary from
312 0.86 mm for the fine-grained, accumulation samples to 1.12-1.39 mm for the coarse-
313 grained, samples from the megadunes region and 0.6 mm for the Hercules Dome
314 samples. This allows a minimum of 15 nodes per pore, above the 4 nodes per pore needed
315 to insure that the LBM produces Poiseuille flow in the pores [*Succi*, 2002].
316
317 4.2 Lattice-Boltzmann model
318 For the megadunes samples, the comparison between the calculated permeability
319 values from the LBM and the original measured permeability values is shown in Figure
320 3. The composite permeability calculated from the subsample permeabilities, determined
321 using Equation 7, is indicated by the open circles in the figure. The results are
322 summarized in Table 2. For the Hercules Dome modeling runs, one representative
323 subsample of each sample was modeled and used to represent the composite value of the
324 original sample, as the Hercules Dome samples tended to be shorter, more homogeneous,
325 and less layered than the megadunes samples. These results are shown in Figure 4 along
326 with the composite values of permeability for the megadunes samples. In order to

examine the performance of the model in comparison to the experimental results, we examined the variability of the permeability values from modeled megadunes subsamples in comparison to the composite value, as well as the error between the modeled and measured results. For the Hercules Dome samples, only one subsample was taken from each bulk original sample, and only the total error between measured and modeled results is reported in Table 2.

4.3 Variability of megadunes subsamples

The stratigraphy of the megadunes site is quite complex, with areas experiencing hiatus having coarse bands of large-grained, highly metamorphosed firn [*Albert et al*., 2004] alternating with accumulation areas with near-surface layering as seen in other polar regions, and the beginning of a paleo-dune hiatus surface at depth. This variability in the firn structure is seen in our measurements of both permeability and microstructure. For three of the megadunes samples, the modeled subsamples show considerable spread in permeability values, caused by inhomogeneous layering within the samples. The individual subsamples for Sample C, for instance, had values of volume-to-surface ratio (V_p/S) of the pore space varying from 0.14 mm to 0.22 mm. Sample G had individual subsample V_p/S values varying between 0.27 mm and 0.40 mm. Samples A and B, in comparison, had subsample V_p/S values which had no significant variation and variation in the range between 0.18 and 0.21 mm, respectively, and also smaller variability in the permeability values. The largest variability occurs in samples near the surface (C and F) where more natural layering occurs, and consequently the original samples would not be as homogeneous. Coarse-grained samples from the accumulation area at depth (D and

350 G) also have high variability. This depth (approximately 10 m) at the accumulation site
351 marked a transition between snow that had been accumulating and a hiatus dune surface
352 buried below, which accounts for some of the variability in permeability and V_p/S ratio
353 between subsamples. The rest of the samples, smaller grained and with less layering,
354 have coefficient of variation (CV) values of calculated permeability between subsamples
355 that range from 8 to 13%.
356
357 4.4 Error
358 The average composite modeled permeability values are within 25% (average
359 absolute relative error of modeled values compared to measured values) of the measured
360 bulk values. The 25% error has a large uncertainty of 18%, and is not normally
361 distributed. About half of the simulations showed a relatively small error around +/- 0.3 x
362 10^{-9} m^2, Figure 5. The other half showed much larger errors, up to +/- minus 2 x 10^{-9} m^2,
363 almost a factor of ten. We could not find a sufficient explanation of this large variation.
364 The large errors may be partially explained by larger grain size. The samples which have
365 the greatest error between the modeled and measured results are in general coarse-
366 grained, deeper samples (samples B, D, and G) from the megadunes site, or shallow
367 samples (sample K and M) from Hercules Dome. The higher error in the Hercules Dome
368 samples compared to measured results can be attributed to the use of one subsample to
369 represent the original sample instead of finding a composite model result. The high
370 errors from the megadunes site may be partly due to metamorphic changes induced in
371 transport, which is supported by the general trend of the modeled megadunes
372 permeability values to be higher than the measured results. It is likely that some

373 metamorphism of the snow samples from the megadunes occurred during shipment of the
374 samples to Germany from the U.S., as evidenced by condensation on the inside of the
375 plastic bags used to ship the samples and the disappearance of markings made on the
376 samples before shipment. No temperature data-loggers had been placed with the
377 shipment to determine if the temperatures during transport were high enough (i.e. greater
378 than -10ºC) to induce changes as was done with all later shipments, including the
379 Hercules Dome samples. The temperature logs during the Hercules Dome shipment
380 show that temperatures stayed below -20°C, and metamorphism was likely minimized.
381 Other methodological errors are 1) the reduced size of the CT samples, as
382 compared to the measured sample size; 2) the destruction of the interface between
383 subsamples caused by cutting the sample, which we are not able to reconstruct in the
384 modeling; 3) errors introduced by the segmentation process and filtering; and 4) error due
385 to the volume modeled for the coarse-grained subsamples being close to the REV. This
386 last effect is observable in a plot of the statistical error of the measured permeability
387 values compared to the modeled permeability values versus the effective grain diameter
388 of the sample in Figure 5. There is an observable increase in error as the grain size for
389 the sample increases.
390 It should be noted that the coarse-grained samples examined are end-members in
391 terms of both grain sizes as well as permeability for polar firn, due to the fact that they
392 are from an accumulation hiatus region. For most types of firn will have REV's for the
393 LBM on the smaller end of the REV values determined here of ~1 to 1.5 cm^3.
394
395 4.5 Comparison to traditional permeability correlations

396 We compared the results from the LBM to empirical relationships for
397 permeability (Figure 6). *Shimizu* (1970) related permeability to grain size, d_{grain}, for
398 several types of season snow:

399 $$k_{shimizu} = 0.077 d_{grain}^2 e^{(-7.8\rho^*)} \quad (8)$$

400 where ρ^* is the specific gravity of snow. For comparison, we calculated ρ^* for
401 each sample based on density measurements. We compared the LBM results to the
402 Kozeny-Carman (KC) relationship (Equation 4) with $c = 5$.

403 In previous work examining the permeability of polar firn, *Rick and Albert* [2004]
404 and *Hörhold* [2006] developed relationships for permeability following *Revil and Cathles*
405 (1999) utilizing the concept of the formation factor, F, which is equal to ϕ^{-m} according the
406 empirically based Archie relationship, where ϕ is porosity and m is the "cementation
407 exponent." *Rick and Albert* (2004) modified the Kozeny-Carman relationship to include
408 a pore size term:

409 $$k_{RA} = (d_{pore}/4)(V_p/S)^2 \phi \quad (9)$$

410 Here we use the pore size as determined from micro-CT data for d_{pore}. *Hörhold*
411 [2006] further added a term for the tortuosity of the firn, τ, following *Walsh and Brace*
412 [1984], as well as a term defining the anisotropy, dl, as described in *Hörhold et al*.,
413 [2009]:

414 $$k_{hörhold} = (d_{pore}/4)(V_p/S)^2(\phi/\tau)dl \quad (10)$$

415 Here we use the geometrical tortuosity, τ, as determined by the micro-CT, and
416 computed as the deviation of the flow pathway to that of a straight line. It should be
417 noted that this tortuosity is not the same as the tortuosity factor, which relates such

418 material properties of the porous medium as electrical conductivity, diffusivity, etc. to
419 those in free air.

420 As can be seen in Figure 6, the LBM is much better at determining the
421 permeability than the Shimizu's relationship and the KC equation, which are traditionally
422 used to predict snow permeability. The model does moderately better at predicting the
423 permeability than the newer formulations of *Rick and Albert* [2004] and *Hörhold* [2006]
424 which incorporate more details on the microstructure of snow. These microstructural
425 details, namely the pore size, tortuosity, and anisotropy, require data from the micro-CT
426 that are not as easily determined as porosity, grain size, and SSA. The microstructural
427 values used in these relationships are based on the micro-CT data and are subject to many
428 of the same errors and uncertainties as underlying structure for the LBM.

429

430 5. Conclusions

431 Lattice-Boltzmann modeling of flow through 3-D micro-CT reconstructions
432 shows great promise in understanding microscale details of pressure-driven air flow
433 through firn. The lattice-Boltzmann model is a useful tool for determining snow
434 permeability, reproducing measured results and able to model permeability values at a
435 much smaller scale than is possible with measurements. This will be especially useful
436 when examining the permeability of single stratigraphic layers on the order of 1 cm.
437 Measured results across a range of porosities and grain sizes are reproduced by the
438 model, and the model is better at predicting permeability than traditional permeability
439 relationships for snow. While computationally intensive, lattice-Boltzmann modeling
440 can provide insight, by modeling the entire flow field in the snow matrix, into the nature

441 of the flow around the complex microstructure of the firn, without having to make
442 simplifications to the snow or firn geometry.

443 Acknowledgements

444 This work was supported by NSF OPP grants 0125276 and 9814676. The authors
445 would also like to thank Johannes Freitag of the Alfred Wegener Institute for help with
446 the modeling, and Heinz Miller of the Alfred Wegener Institute for helping to fund some
447 of the work. The helpful comments of the anonymous reviewers were greatly
448 appreciated.

449 Reference List

450
451 Albert, M.R. (2002), Effects of snow and firn ventilation on sublimation rates, *Ann.*
452 *Glaciol., 35*, 52-56.

453
454
455 Albert, M.R. and F.E. Perron, Jr. (2000), Ice layer and surface crust permeability in a
456 seasonal snow pack, *Hydrol. Process., 14*, 3207-3214.

457

458 Albert, M.R., E.F. Shultz, and F.E. Perron, Jr. (2000), Snow and firn permeability at Siple
459 Dome, Antarctica, *Ann. Glaciol., 31*(1), 353-356.

460

461 Albert, M.R., C. Shuman, Z. Courville, R. Bauer, M. Fahnestock, and T. Scambos
462 (2004), Extreme firn metamorphism: impact of decades of vapor transport on near-
463 surface firn at a low-accumulation glazed site on the East Antarctic Plateau, *Ann.*
464 *Glaciol*., 39, 73-78.

465

466 Arns, C.H., M.A. Knackstedt, W.V. Pinczewski, and N.S. Martys (2004), Virtual
467 permeametry on microtomographic images, *J. Petroleum Sci. Eng., 45*, 41-46.

468

469 Arons, E.M. and S.C. Colbeck (1998), Effective medium approximation for the
470 conductivity of sensible heat in dry snow, *Int. J. Heat Mass Transfer, 41*(17), 2653-2666.

471

472 Ahrenholz, B., J. Tölke, and M. Krafczyk (2006), Lattice-Boltzmann simulations in
473 reconstructed parameterized porous media, *Int. J. Comp. Fluid Dyn., 20*(6), 369-377.

474

475 Auzerais, F.M., J. Dunsmuir, B.B. Ferréol, N. Martys, J. Olson, T.S. Ramakrishnan, D.H.
476 Rothman, and L.M. Schwartz (1996), Transport in sandstone: A study based on three
477 dimensional microtomography, *Geophys. Res. Lett., 23*(7), 705-708.

478

479 Carman, P.C. (1956), *Flow of Gases Through Porous Media*, Academic Press Inc., New
480 York, 182 pp.

481

482 Chen, S., and G.D. Doolen (1998), Lattice-Boltzmann method for fluid flows, *Ann. Rev.*
483 *Fluid Mech., 30*, 329-364.

484

485 Colbeck, S.C. (1983), Theory of metamorphism of dry snow, *J. Geophys. Res. 88*, 5475-
486 5482.

487

488 Colbeck, S.C. (1989), Air movement in snow due to wind pumping, *J. Glaciol., 35*(120),
489 209-213.

490

491 Coléou, C., B. Lesaffre, J.-B. Brzoska, W. Ludwig, and E. Boller (2001), Three-
492 dimensional snow images by X-ray microtomography, *Ann. Glaciol*., *32*, 75-81.

493

494 Coker, D.A., S. Torquato, and J.H. Dunsmuir (1996), Morphology and physical
495 properties of Fontainbleau sandstone via a tomographic analysis, *J. Geophys. Res.,*
496 *101*(B8), 17,497-17,506.

497

498 Costa, A. (2006), Permeability-porosity relationship: A reexamination of the Kozeny-
499 Carman equation based on a fractal pore-space geometry assumption, *Geophys. Res.*
500 *Lett., 30*, L02318, doi:10.1029/2005GR025134.
501
502 Courville, Z.R., M.R. Albert, M.A. Fahnestock, L.M. Cathles IV, and C.A. Shuman
503 (2007), Impacts of an accumulation hiatus on the physical properties of firn at a low-
504 accumulation polar site, *J. Geophys. Res., 112*, F02030, doi:10.1029/2005JF000429.
505
506 Dominé, F., R. Salvatori, L. Legagneux, R. Salzano, M. Fily, and R. Casacchia (2006),
507 Correlation between the specific surface area and the short wave infrared (SWIR)
508 reflectance of snow, *Cold Reg. Sci. Tech., 46*, 60-68.
509
510 Dominé, F., M. R. Albert, T. Huthwelker, H.-W. Jacobi, A.A. Kokhanovsky, M. Lehning,
511 G. Picard, and W.R. Simpson (2008), Snow physics as relevant to photochemistry,
512 *Atmos. Chem. Phys., 8*, 171-208.
513
514 dos Santos, L.O.E., C.E.P Ortiz, H.C. de Gaspari, G.E. Haverroth, and P.C. Philippi
515 (2005), Prediction of intrinsic permeabilities with lattice-Boltzmann method, *18th Int.*
516 *Conf. Mech. Eng. Proc*., Nov. 6-11, Ouro Preto, MG.
517
518 Dullien, F.A.L. (1992), Porous Media: fluid transport and pore structure, second edition,
519 Academic Press, Inc., 574 pp.

520

521 Flin, F., J.-B. Brzoska, B. Lesaffre, C. Cloléou, and P. Lamboley (2001), Computation of
522 normal vectors of discrete 3D objects: application to natural snow images from X-ray
523 tomography, *Image Anal. Stereol., 20*, 187-191.

524

525 Flin, F., and J.-B. Brzoska (2008), The temperature-gradient metamorphism of snow:
526 vapor diffusion model and application to tomographic images, *Ann. Glaciol. 49*, 17-21.

527

528 Fredrich, J.T., A.A. DiGiovanni, and D.R. Noble (2006), Predicting macroscopic
529 transport properties using microscopic image data, *J. Geophys. Res*., 111, B03201,
530 doi:10.1029/2005JB003774.

531

532 Freitag, J., U. Dobrindt, and J. Kipfstuhl (2002), A new method for predicting transport
533 properties of polar firn with respect to gases on the pore-space scale, *Ann. Glaciol., 35*,
534 538-544.

535

536 Freitag, J., F. Wilhelms, and S. Kipfstuhl (2004), Microstructure-dependent densification
537 of polar firn derived from X-ray microtomography, *J. Glaciol., 50*(169) 243-250.

538

539 Fujita, S., J. Okuyama, A. Hori, and T. Hondoh (2009), Metamorphism of stratified firn
540 at Dome Fuji, Antarctica: A mechanism for local insolation modulation of gas transport
541 conditions during bubble close off*, J. Geophys. Res*., *114*, F03023,
542 doi:10.1029/2008JF001143.

543

544 Gallet, J.C., F. Dominé, C.S. Zender and G. Picard (2009), Measurement of the specific
545 surface area of snow using infrared reflectance in an integrating sphere at 1310 nm and
546 1550 nm, *The Cryosphere, 3*, 167-182.

547

548 Gerbaux, O. F. Buyens, V.V. Mourzenko, A. Memponteil, A. Vabre, J.-F. Thovert, and
549 P.M. Adler (2010), Transport properties of real metallic foams, *J. Colloid Int. Sci., 342*,
550 155-165.

551

552 Hörhold, M. (2006), Microstructure and air transport properties of polar firn. MS thesis,
553 University of Bremen, Bremen, Germany, 77 pp.

554

555 Hörhold, M., M.R. Albert, and J. Freitag (2009), The impact of accumulation rate on
556 anisotropy and air permeability of polar firn at a high-accumulation site, *J. Glaciol.,*
557 *55*(192) 625-630.

558

559 Larson, R.E., and J.J.L. Higdon (1989), A periodic grain consolidation model of porous
560 media, *Phys. Fluids A, 1*(1), 38-46.

561

562 Lehmann, P., M. Berchtold, B. Ahrenholz, J. Tölke, A. Kaestner, M. Krafczyk, H.
563 Flühler, and H.R. Künsch (2008), Impact of geometrical properties on permeability and
564 fluid phase distribution in porous media, *Adv. Water Res., 31*, 1188-1204.

565

566 Lundy, C.C., M.Q. Edens, and R.L. Brown (2002), Measurement of snow density and
567 microstructure using computed tomography, *J. Glaciol., 48*(161), 312-316.
568
569 Kaempfer, T., M. Schneebeli, and S.A. Sokratov (2005), A microstructural approach to
570 model heat transfer in snow, *Geophys. Res. Lett., 32*, L21503,
571 doi:10.1029/2005GL023873.
572
573 Kameda, A., J. Dvorkin, Y. Keehm, A. Nur, and W. Bosl (2006), Permeability-porosity
574 transforms from small sandstone fragments, *Geophys., 71*(1), N11-N19.
575
576 Manwart, C., U. Aaltosalmi, A. Koponen, R. Hilfer, and J. Timonen (2002), Lattice-
577 Boltzmann and finite-difference simulations for the permeability of three-dimensional
578 porous media, *Phys. Rev. E, 66*, 016702.
579
580 Matzl, M., and M. Schneebeli (2006), Measuring specific surface area of snow by near-
581 infrared photography, *J. Glaciol., 52*(179), 558-564.
582
583 Nolin, A., and J. Dozier (1993), Estimating snow grain size using AVIRIS data, *Remote*
584 *Sens. Environ., 44*(2-3), 231-238.
585
586 Nolin, A., and J. Dozier (2000), A hyperspectral method for remotely sensing the grain
587 size of snow, *Remote Sens. Environ., 74*(2), 207-216.
588

589 Painter, T.H., N.P. Molotch, M. Cassidy, M. Flanner, and K. Steffen (2007), Instruments
590 and methods: Contact spectroscopy for determination of stratigraphy of snow optical
591 grain size, *J. Glaciol., 53*(180), 121-127.
592
593 Pieritz, R.A., J.-B. Brzoska, F. Flin, B. Lesafre, C. Coléou (2004), From snow X-ray
594 microtomography raw volume data to micromechanics modeling: first results, *Ann.*
595 *Glaciol*., *38*, 52-58.
596
597 Pinzer, B.R. and M. Schneebeli (2009), Snow metamorphism under alternating
598 temperature gradients: Morphology and recrystallization in surface snow*, Geophys. Res.*
599 *Lett*., *36*, L23503, doi: 10.1029/2009GL039618.
600
601 Revil, A., and L.M. Cathles III, (1999), Permeability of shaly sands, *Water Res. Res.,*
602 *35*(3), 651-662.
603
604 Rick, U.K., and M.R. Albert (2004), Microstructure and permeability in the near-surface
605 firn near a potential US deep-drilling site in West Antarctica, *Ann. Glaciol*., 39(1), 62-66.
606
607 Schneebeli, M. (2004), Numerical simulation of elastic stress in the microstructure of
608 snow, *Ann. Glaciol., 38*, 339-342.
609
610 Shi, J., R.E. Davis, and J. Dozier (1993), Stereological determination of dry snow
611 parameters for discrete microwave modeling, *Ann Glaciol*., *17*, 295-299.

612

613 Shimizu, H. (1970), Air permeability of deposited snow, *Contributions from the Institute*

614 *of Low Temperature Science, Series A*, 22, 1-32.

615

616 Succi, S. (2002), *The Lattice-Boltzmann Equation for Fluid Dynamics and Beyond,*

617 *Oxford University Press,* Oxford. 288 pp.

618

619 Walsh, J.B. and W.F. Brace (1984), The effect of pressure on porosity and the transport

620 properties of rock, *J. Geophys. Res., 89*(B11), 9425-9431.

621

622 Warren, S.G. (1982), Optical properties of snow, *Rev. Geophys. Space Phys*., *20*,

623 1R1505, 67.

624

625 White, J.A., R.I. Borja, and J.T. Fredrich (2006), Calculating the effective permeability of

626 sandstone with multiscale lattice-Boltzmann/finite element simulations, *Acta Geotech*., 1,

627 195-209, doi: 10.1007/s11440-006-0018-4.

628

629 Table Captions

630 Table 1. Results of Stokes flow around periodic array of consolidated spheres for the
631 lattice-Boltzmann model compared to the empirical results of *Larson and Higdon* [1989].
632 Units are lattice units and model time step.

633

634 Table 2. Results and errors for the modeled samples. V_p/S is the volume-to-surface ratio
635 of the pore space (mm); ϕ is the porosity, comparing the measured bulk porosity (meas)
636 to the average porosity from the micro-CT data (CT) obtained for the individual
637 subsamples as well as the total sample (in bold); for length, we report the total length of
638 the original bulk sample (cm) in bold, as well as the length for the subsamples (2 cm); k
639 is permeability (m^2); σ is the standard deviation of the permeability values for the
640 subsamples; CV is the coefficient of variation of the subsamples permeability for each
641 bulk sample, defined as the standard deviation divided by the mean of the observations;
642 and the relative error is the percent value of the modeled composite results as obtained
643 using Equation 7 (in bold) compared to the bulk measured result (in bold) shown with the
644 individual results for the subsamples. Note that this is not the error of the individual
645 subsamples compared to the measured result. Samples A-H are samples from a
646 megadune accumulation area (MD a) and a megadune hiatus area (MD h). Samples I-M
647 are from Hercules Dome (HD a). For these samples, we chose one subsample to run in
648 the lattice-Boltzmann, as indicated in the table, and present the microstructural data from
649 the micro-CT of the other subsamples for comparison.

650

651

652 Figure Captions

653

654 Figure 1. Firn samples from high accumulation megadunes site, left, at 0.4 m (top) and 9
655 m (bottom) depths, compared to coarse-grained firn from accumulation hiatus site, right,
656 at the same depths. White is snow and black is pore space.

657

658 Figure 2. Determination of the REV of a coarse-grained sample (diamonds) and a fine-
659 grained sample (crosses). The average values of the REV runs for a given volume are
660 shown as open circles.

661

662 Figure 3. Lattice-Boltzmann model versus measured results from different types of snow
663 at a megadunes site; subsample permeabilities modeled by the LBM are compared to the
664 bulk sample permeability, not permeability measurements for those subsamples.
665 Different colors represent the individual samples, with the subsamples from each sample
666 represented in the same color. Open circles represent the bulk permeability values of the
667 original samples. Closed diamonds represent the subsections modeled from micro-CT 3-
668 D imaging. Letters refer to different types of snow. A, B, F, and H are snow samples
669 from megadunes areas experiencing hiatus in snow accumulation. C, D, E, and G are
670 from a megadunes area experiencing low accumulation. See Table 2 for a more complete
671 description. The straight line marks the value of the modeled permeability vs. measured
672 permeability.

673

674 Figure 4. Modeled permeability results versus measured results for megadunes and
675 Hercules Dome samples. The composite modeled result for the megadunes samples is
676 compared to the measured result. The modeled result from one representative subsample
677 from the Hercules Dome samples is presented. The straight line marks the value of the
678 modeled permeability vs. measured permeability.
679
680 Figure 5. Statistical error (modeled permeability minus measured permeability) vs.
681 effective grain diameter.
682
683 Figure 6. Comparison of LBM to empirical relationships for permeability of snow from
684 *Shimizu* [1970], the Kozeny-Carman relationship (with $c = 5$), *Rick and Albert* [2004],
685 and *Hörhold* [2006]. The straight line marks the value of the measured permeability.
686
687
688
689
690
691

692 Table 1

diameter	cell length	k theoretical	k modeled	error (%)
22	21	0.671	0.663	1.20
44	42	2.7763	2.7699	0.23
66	63	6.1671	6.1427	0.40
112	107	17.978	17.9515	0.15
138	131	25.114	25.0336	0.32

693 Table 2.

sample	site	depth (m)	V_p/S (mm)	ϕ (meas)	ϕ (calc)	length (cm)	d_{eff} (mm)	k, calc. (m^2) $x10^{-9}$	k, meas. (m^2) $x10^{-9}$	variability, k_{sub}		rel. err.
										σ (m^2)$x10^{-9}$	CV %	%
A	**MD h**	**9.7**	**0.16**	**0.40**	**0.40**	**8.3**	**1.71**	**1.79**	**1.59**	**2**	**12**	**12.6**
A1			0.16		0.40	2	1.81	1.84		0.5	2.6	
A2			0.16		0.39	2	1.67	2.02		2.2	12.4	
A3			0.16		0.40	2	1.64	1.58		2.1	12	
B	**MD h**	**8.5**	**0.20**	**0.41**	**0.41**	**7.2**	**1.73**	**2.46**	**1.66**	**3**	**13**	**48.2**
B1			0.21		0.41	2	1.74	2.73		2.6	10.7	
B2			0.21		0.41	2	1.75	2.63		1.7	6.9	
B3			0.18		0.41	2	1.71	2.12		3.4	13.9	
C	**MD a**	**0.1**	**0.19**	**0.56**	**0.56**	**12.7**	**0.93**	**3.02**	**2.69**	**39**	**86**	**12.3**
C1			0.14		0.56	2	0.76	2.33		6.9	22.9	
C2			0.15		0.56	2	0.89	1.95		10.7	35.5	
C3			0.26		0.56	2	1.03	3.52		50.1	16.6	
C4			0.22		0.56	2	0.98	1.02		7.2	239	
D	**MD a**	**9.2**	**0.26**	**0.51**	**0.51**	**10.4**	**1.42**	**6.04**	**4.18**	**15**	**23**	**44.5**
D2			0.27		0.51	2	1.34	5.91		1.3	2.2	
D3			0.28		0.51	2	1.48	7.86		18.2	30.1	
D4			0.23		0.51	2	1.49	4.99		10.5	17.3	
E	**MD a**	**0.4**	**0.22**	**0.59**	**0.59**	**11.1**	**1.00**	**5.88**	**5.93**	**6**	**11**	**-0.8**
E1			0.22		0.60	2	1.02	6.46		5.8	9.9	
E2			0.18		0.58	2	0.98	5.26		6.2	10.5	
E3			0.22		0.62	2	1.01	6.50		6.2	10.6	
E4			0.25		0.57	2	1.04	5.50		3.8	6.4	
F	**MD h**	**0.4**	**0.28**	**0.52**	**0.52**	**12.6**	**1.70**	**5.41**	**6.29**	**22**	**34**	**-14.0**
F1			0.33		0.52	2	1.80	6.83		14.2	26.2	
F2			0.27		0.52	2	1.43	2.62		27.9	52.5	
F3			0.29		0.53	2	1.52	7.74		23.2	43	
F4			0.26		0.52	2	1.85	7.78		23.7	43.8	
F5			0.26		0.52	2	1.88	7.21		18	33.3	
G	**MD a**	**10.4**	**0.34**	**0.51**	**0.50**	**9.5**	**1.72**	**10.24**	**7.94**	**29**	**27**	**29.0**
G2			0.34		0.52	2	1.84	7.54		27	26.4	
G3			0.40		0.48	2	1.66	13.10		28.5	27.9	
G4			0.27		0.51	2	1.70	11.90		16.8	16.4	
H	**MD h**	**0.2**	**0.24**	**0.58**	**0.58**	**11.5**	**1.71**	**8.04**	**9.70**	**7**	**8**	**-17.1**
H1			0.27		0.58	2	1.55	8.42		3.8	4.8	
H2			0.23		0.57	2	1.58	7.15		8.9	11.1	
H3			0.22		0.58	2	1.69	8.59		5.4	6.8	
H4			0.25		0.58	2	2.01	8.18		1.3	1.7	
I	**HD a**	**10.0**	**0.14**	**0.43**	**0.43**	**4.1**	**1.20**	**1.19**	**1.09**			**9.2**
J	**HD a**	**10.7**	**0.17**	**0.45**	**0.43**	**6.0**	**1.32**		**1.36**			**22.8**
J1			0.17		0.43	2	1.31					
J2			0.17		0.43	2	1.31	**1.67**				
J3			0.17		0.44	2	1.33					
K	**HD a**	**0.3**	**0.13**	**0.57**	**0.56**	**5.7**	**0.63**		**1.54**			**-26.6**
K1			0.14		0.58	2	0.59	**1.13**				
K2			0.13		0.53	2	0.67					
L	**HD a**	**1.1**	**0.17**	**0.59**	**0.57**	**3.8**	**0.83**	**2.60**	**2.84**			**-8.5**
M	**HD a**	**1.2**	**0.15**	**0.53**	**0.52**	**3.9**	**0.80**		**4.06**			**-59.1**
M1			0.15		0.53	2	0.79	**1.66**				
M2			0.14		0.51	2	0.81					

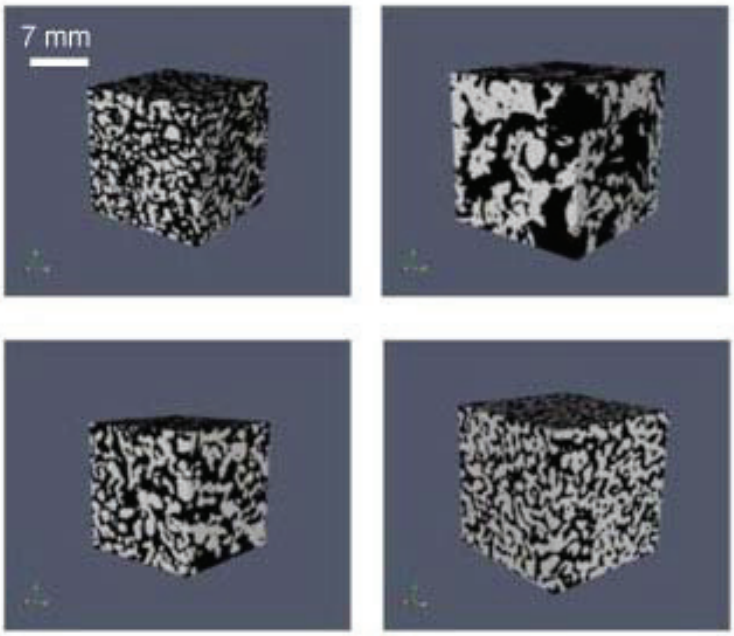

694
695 Figure 1. Firn samples from high accumulation megadunes site, left, at 0.4 m (top) and 9
696 m (bottom) depths, compared to coarse-grained firn from accumulation hiatus site, right,
697 at the same depths. White is snow and black is pore space.

698

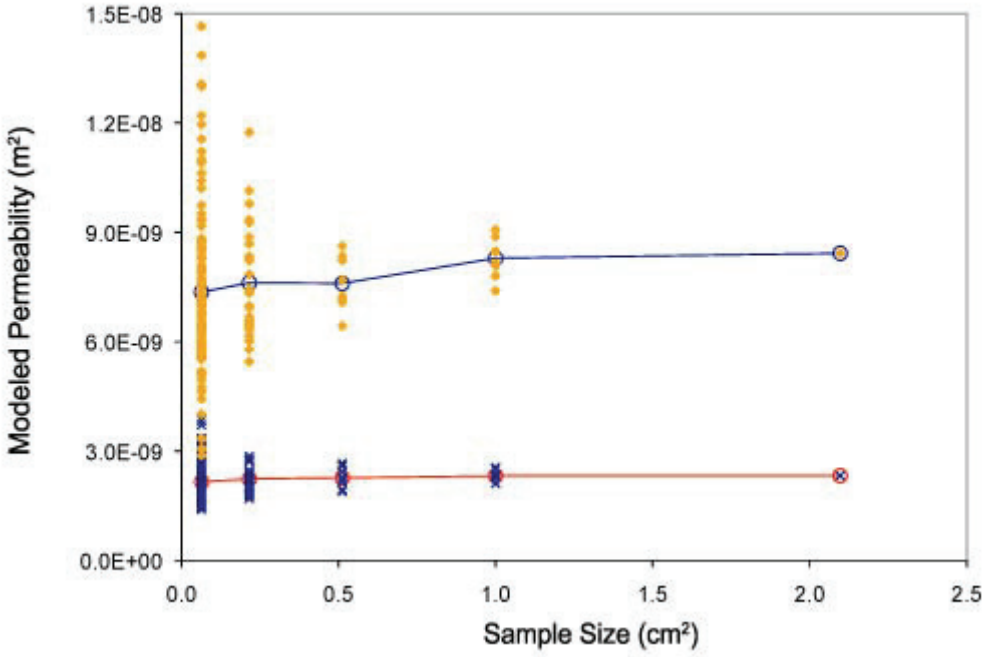

699 Figure 2. Determination of the REV of a coarse-grained sample (diamonds) and a fine-
700 grained sample (crosses). The average values of the REV runs for a given volume are
701 shown as open circles.

702
703
704

705

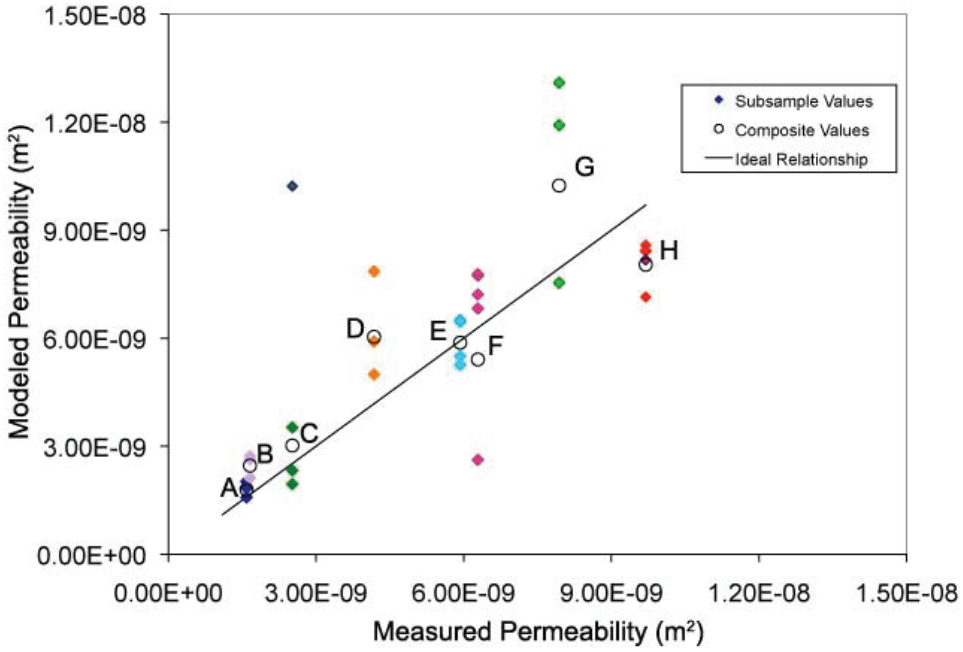

706

707 Figure 3. Lattice-Boltzmann model versus measured results from different types of snow
708 at a megadunes site; subsample permeabilities modeled by the LBM are compared to the
709 bulk sample permeability, not permeability measurements for those subsamples.
710 Different colors represent the individual samples, with the subsamples from each sample
711 represented in the same color. Open circles represent the bulk permeability values of the
712 original samples. Closed diamonds represent the subsections modeled from micro-CT 3-
713 D imaging. Letters refer to different types of snow. A, B, F, and H are snow samples
714 from megadunes areas experiencing hiatus in snow accumulation. C, D, E, and G are
715 from a megadunes area experiencing low accumulation. See Table 2 for a more complete
716 description. The straight line marks the value of the modeled permeability vs. measured
717 permeability.

718

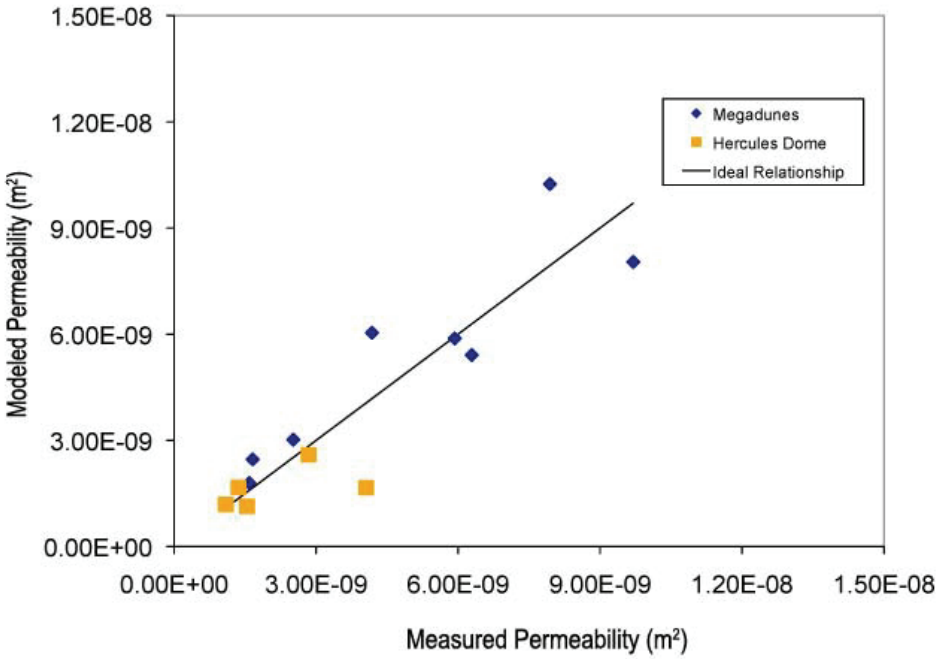

719
720 Figure 4. Modeled permeability results versus measured results for megadunes and
721 Hercules Dome samples. The composite modeled result for the megadunes samples is
722 compared to the measured result. The modeled result from one representative subsample
723 from the Hercules Dome samples is presented. The straight line marks the value of the
724 modeled permeability vs. measured permeability.

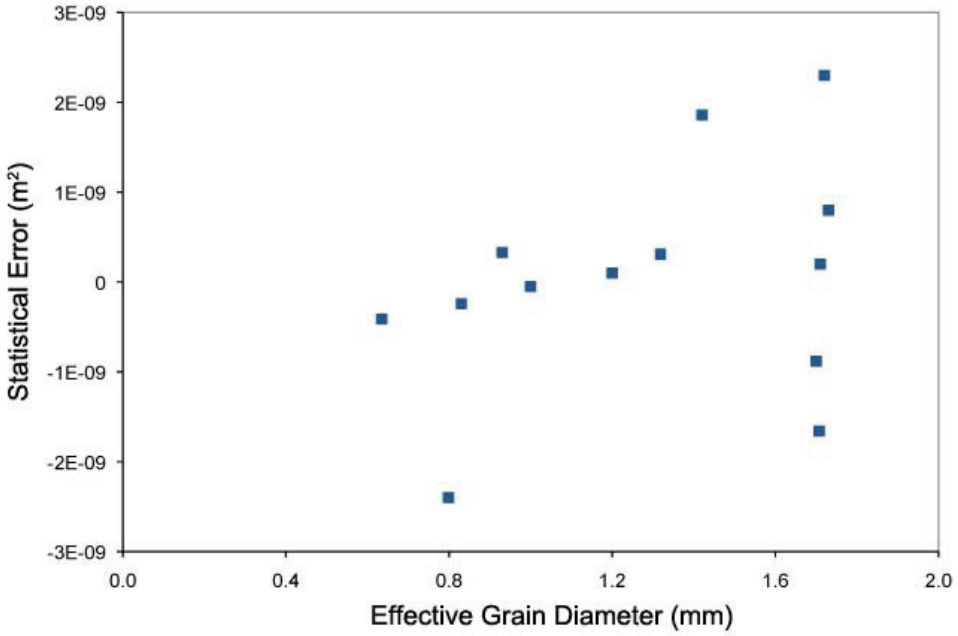

725
726 Figure 5. Statistical error (modeled permeability minus measured permeability) vs.

727 effective grain diameter.

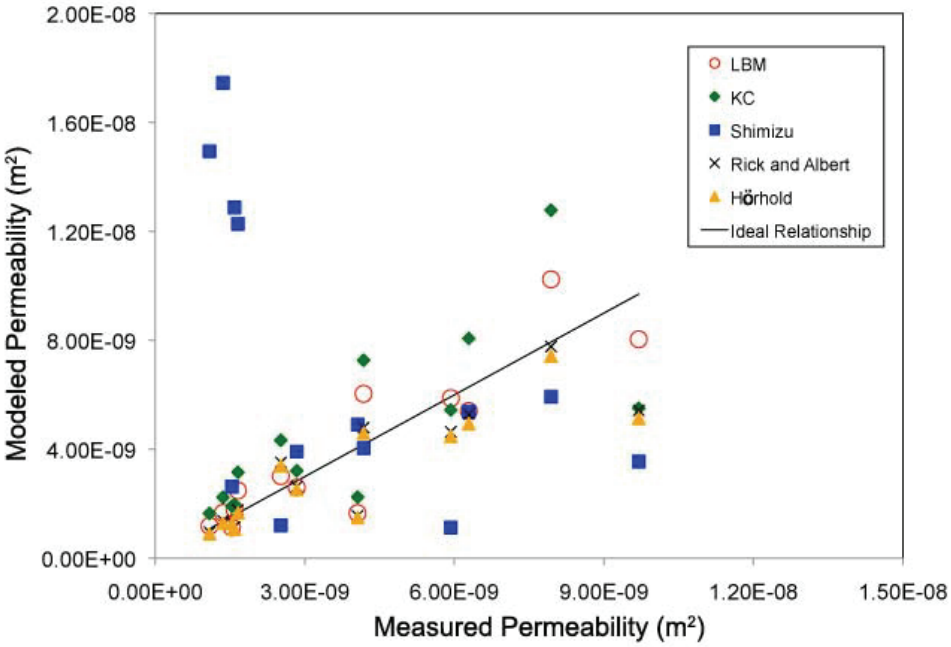

728 Figure 6. Comparison of LBM to empirical relationships for permeability of snow from
729 *Shimizu* [1970], the Kozeny-Carman relationship (with $c = 5$), *Rick and Albert* [2004],
730 and *Hörhold* [2006]. The straight line marks the value of the measured permeability.
731
732